WAVE PROPAGATION AND IMAGING IN RANDOM WAVEGUIDES

by

Liliana Borcea

Contents

1. Introduction

Array imaging is an important technology with a wide range of applications in underwater acoustics, seismology, non-destructive evaluation of materials, medical ultrasound, and elsewhere. It is concerned with locating remote, compactly supported sources and/or scatterers from measurements at arrays of sensors. The sensors are devices that transform one form of energy into another. Depending on the application they may be antennas that convert electromagnetic waves to/from electric signals, hydrophones that convert changes in water pressure to electrical signals, ultrasonic transducers that transmit and receive ultrasound waves, and so on. When the sensors are located sufficiently close together, they behave as a collective entity, called the array. The sensors in passive arrays are receivers of the waves generated by unknown remote sources. Active arrays have sensors that play the dual role of sources and receivers. The sources emit waves that propagate through the medium and are scattered back to the array, where they are captured by the receivers.

The recordings at the receivers are called the array data. The coherent imaging process seeks to transform the data into an imaging function that peaks in the support of the unknown sources or scatterers. The key data processing step in the image formation is the synchronization of the received signals using a mathematical model of wave back-propagation from the array to a search (imaging) location $\vec{\mathbf{r}}_s$. The expectation is that when $\vec{\mathbf{r}}_s$ lies in the support of the unknown sources or scatterers, the recordings are synchronized and add up over the sensors to give a peak value of the imaging function. Indeed, this happens if we have an accurate model of wave propagation between the array and the imaging region.

Image formation is somewhat similar to the time reversal process. Time reversal is an experiment that uses an active array to first receive the waves from a remote source, and then re-emit the time-reversed recordings back in the medium. The wave equation is time reversible if the medium is non-dissipative, so the waves are expected to propagate back to the source and focus near it. The focusing resolution in the range direction is mostly affected by the bandwidth of the emitted signals. The focusing in cross-range (i.e., in the plane orthogonal to the range) depends on many factors, such as how large the array is, how far the source is, and how much scattering occurs between the source and receiver. The focusing is never perfect, because the array cannot capture the whole wave field emitted from the source. Thus, the time reversal process is not exactly like solving the wave equation backward in time to recover the initial source. The expectation is that the larger the array is, the better the focus, because more of the waves are captured and turned back. But no matter how large the array is, even if it surrounds the source, the evanescent waves cannot reach it, and the focusing resolution is limited by diffraction. For example, the resolution of refocusing of time harmonic waves cannot exceed the Abbe diffraction limit of $\lambda/2$, where λ is the wavelength [**9**]. In most applications the array

is supported in a set of small diameter (aperture) $|\mathcal{A}|$ with respect to the distance L of propagation, and the expected resolution of refocusing in cross-range is given by the Rayleigh formula $\lambda L/|\mathcal{A}|$ if there is no scattering in the medium. The interesting property of time reversal, known as *super-resolution*, is that scattering may improve the cross-range focusing. This is demonstrated and explained in [**12, 13, 20**], and it is analyzed theoretically and numerically in [**3, 2, 25**]. The latter studies are based on random models of the scattering medium, and introduce the important concept of *statistical stability*. Stability means that the focusing is robust, it is independent of the realization of the random medium, it is observable and reproducible. Stability is guaranteed in general only for sources emitting broad-band signals, as pointed out in [**3**], although there are regimes where it holds for narrowband signals as long as the sources and arrays have sufficiently large support [**25**].

The super-resolution and robustness of time reversal are due entirely to the waves propagating back in exactly the same medium they came from. The observer has access to the vicinity of the source and can see the focus there, whereas in imaging the access is limited to the array. Moreover, the medium is not known in detail in many imaging applications. For example, in underwater acoustics, the smooth part of the wave speed is known, but there are small scale fluctuations due to internal waves [**14**] that cannot be known, and are not even of interest in imaging. It is the uncertainty about such small scale inhomogeneities that we model with random spatial processes, and thus speak of imaging in random media.

The array data processing for image formation may appear to mimic the back-propagation of the waves in the time reversal process, but there is a fundamental difference. While in time reversal the waves go back in the same medium, the back-propagation in imaging is done mathematically, using a fictitious medium model that incorporates the large scale features of the wave speed, but not its fluctuations, which are unknown. This difference is essential in regimes with strong cumulative scattering of the waves by the random inhomogeneities. The longer the waves travel in the random medium, the stronger the scattering, which leads to loss of coherence of the wave field. The coherent waves are useful in imaging because we can relate the locations of the sought-after sources or scatterers to their arrival time. Multiple scattering by the inhomogeneities transfers energy to the incoherent part of the waves, the random fluctuations which are unwanted reverberations. We may think of the reverberations as *noise*, but we should remember that they are not ordinary additive, uncorrelated noise. They have complicated statistical structure, with correlations across the array and in the bandwidth, and are difficult to mitigate. Our goal is to quantify the deterioration of resolution and robustness of images in random media, and to propose efficient methods for mitigating cumulative scattering effects.

The data processing in image formation must take into account the presence of scattering boundaries, because they create multiple traveling paths of the waves received at the array. This happens in waveguides, where boundaries trap the waves and guide the energy in a preferred direction, the waveguide axis, along which the medium is unbounded. To analyze the wave field in waveguides, we may decompose it mathematically in an infinite, countable set of monochromatic waves called *waveguide modes*. In ideal waveguides, with flat boundaries and wave-speed that is constant or varies smoothly in the waveguide cross-section, the modes are uncoupled. Finitely many of them propagate along the waveguide axis at different speeds, and we may associate them to plane waves with different angles of incidence at the boundary. The slower modes correspond to nearly normal incidence. They bounce off the boundaries many times, thus taking a long path from the source to the array. The faster modes correspond to small grazing angles at the boundary, and shorter paths to the array. The remaining infinitely many modes are evanescent, with amplitudes decaying exponentially with the distance along the waveguide axis.

We are concerned with waveguides that are randomly perturbed versions of the ideal ones. They may have boundaries with small random fluctuations, and/or internal inhomogeneities that cause small fluctuations of the wave speed. We present a rigorous asymptotic theory of wave propagation in such waveguides, where the asymptotics is in the small parameter that measures the magnitude of the fluctuations. We show that when the waves travel sufficiently far from the source, the small fluctuations cause significant cumulative scattering. It amounts to coupling of the waveguide modes, and gradual loss of coherence of their amplitudes. We give a detailed analysis of mode coupling and quantify the net scattering via three important length scales: the *scattering mean free path*, the *transport mean free path* and the *equipartition distance*. The mode dependent scattering mean free path is the distance over which the mode loses its coherence, meaning that its random fluctuations dominate its statistical mean. The transport mean free path is classically defined as the distance beyond which the waves forget their initial direction [**26**]. Because the modes are associated to directions of incidence at the boundary, we define the mode dependent transport mean free path as the length scale over which the mode exchanges energy with the other modes. The equipartition distance is the longest of the three length scales, and it gives the distance over which scattering distributes the energy uniformly among the modes, independent of the initial source excitation.

The three length scales are important for understanding the limitations of imaging. For example, coherent imaging cannot work for arrays that are farther from the source than the scattering mean free path of all the modes, because there is no coherence left in the data. The recordings are just random medium reverberation. But if the array is not beyond the equipartition distance, we can still track how energy is transported in the waveguide by the modes, and thus localize sources or scatterers with

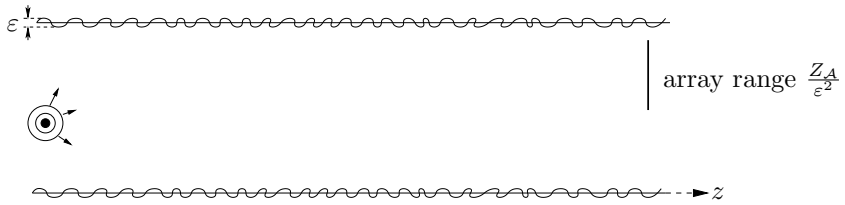

FIGURE 1. Schematic of the problem setup. The source emits a signal in a waveguide and the wave field is recorded at a remote array. The waveguide has fluctuating boundaries around the values $y = 0$ and $y = \mathfrak{D}$ and the medium may have fluctuating wave speed.

a more involved, incoherent parameter estimation approach. Beyond the equipartition distance imaging is impossible, because the waves lose all the information about their initial state, due to scattering.

We present an explicit analysis of imaging in random waveguides and contrast it with time reversal. For simplicity, we consider only the problem of imaging sources with passive arrays. Extensions to imaging with active arrays are straightforward if we use the Born approximation at the scatterers. Our study is for scalar (acoustic) waves in two dimensions. The three-dimensional waveguides are very similar to the two-dimensional ones if they have a bounded cross-section. We refer to [**4**] for a study of wave propagation in three-dimensional waveguides with unbounded cross-sections, in a set-up motivated by applications in underwater acoustics. The waves are trapped there by top and bottom boundaries, but the medium is unbounded in the remaining two directions.

The outline is as follows: We begin in section 2 with the set-up of the problem. The analysis of the wave field in ideal waveguides is in section 3, and in random waveguides in sections 4 and 5. The results are summarized in section 6. The model of the data measured at the array is in section 7. We use it in sections 8 and 9 to study time reversal and imaging. The analysis is illustrated with numerical simulations in section 10.

2. Set-up

Consider a two dimensional waveguide with range axis denoted by $z \in \mathbb{R}$ and transverse coordinate (cross-range) y belonging to a bounded interval, the waveguide cross-section. In ideal waveguides $y \in (0, \mathfrak{D})$. In perturbed waveguides the top and bottom boundaries $\mathcal{Y}(z)$ and $\mathcal{Y}_b(z)$ may fluctuate as illustrated in Figure 1. The acoustic pressure field $p(t, y, z)$ satisfies the wave equation

$$\left(\partial_y^2 + \partial_z^2 - c^{-2}\partial_t^2\right) p(t, y, z) = F(t, y)\delta(z), \tag{2.1}$$

where F models the source distribution at the origin of range, and c is the wave speed. Equation (2.1) holds for $y \in (\mathcal{Y}_b(z), \mathcal{Y}(z))$, $z \in \mathbb{R}$ and $t > 0$. It is complemented with

the pressure-release boundary conditions

$$p(t, y = \mathcal{Y}_b(z), z) = p(t, y = \mathcal{Y}(z), z) = 0, \tag{2.2}$$

and the initial condition

$$p(t, y, z) = 0, \quad t \ll 0. \tag{2.3}$$

Ideally, the wave speed c is constant or smoothly varying in the cross-section. But in media with numerous small, and typically weak inhomogeneities, c has rapid fluctuations. We neglect large scale variations of c for simplicity, but take into account small scale fluctuations.

We study wave propagation in perturbed waveguides with either randomly fluctuating boundaries (section 4), or randomly fluctuating wave speed (section 5) around the mean constant value c_o. We separate the fluctuations in order to compare their net scattering effects, but the results extend easily to waveguides with both interior inhomogeneities and perturbed boundaries. The analysis is asymptotic, in the limit $\varepsilon \to 0$, where ε is the small parameter that quantifies the magnitude of the fluctuations. In the waveguides with fluctuating boundaries we have (see Figure 1),

$$\frac{|\mathcal{Y}_b(z)|}{\mathfrak{D}} = O(\varepsilon) \quad \text{and/or} \quad \frac{|\mathcal{Y}(z) - \mathfrak{D}|}{\mathfrak{D}} = O(\varepsilon), \tag{2.4}$$

and similarly, in the waveguides with internal inhomogeneities,

$$\frac{|c(y, z) - c_o|}{c_o} = O(\varepsilon). \tag{2.5}$$

In either case, the fluctuations occur on a length scale ℓ, called correlation length, which is of the same order as the central wavelength λ_o.

To define λ_o let us denote by

$$\widehat{F}(\omega, y) = \int_{-\infty}^{\infty} dt\, F(t, y) e^{i\omega t} \tag{2.6}$$

the Fourier transform of the signal emitted from the source point y. We assume that it is supported in the frequency interval centered at ω_o, of length $2\pi\mathcal{B}$, where $\mathcal{B}$ is the bandwidth. The central wavelength λ_o is defined by

$$\lambda_o = \frac{2\pi c_o}{\omega_o}. \tag{2.7}$$

We use it throughout as the reference, order one length scale. See section 2.1 for more details on the source, and an example used in the analysis of time reversal and imaging.

Because the fluctuations are weak, the net scattering effects are negligible unless the waves travel a long distance in the waveguide. We will see that for both types of fluctuations, which we model with mean zero random processes, this means scaling the range as $z = O(\lambda_o/\varepsilon^2)$. This is why the array is at range $Z_{\mathcal{A}}/\varepsilon^2$ in Figure 1.

Before considering the problem in random waveguides, it is useful to describe the wave field $p_o(t,y,z)$ in ideal waveguides. It satisfies the wave equation

$$\left(\partial_y^2+\partial_z^2-c_o^{-2}\partial_t^2\right)p_o(t,y,z)=F(t,y)\delta(z),\quad z\in\mathbb{R},\ y\in(0,\mathfrak{D}), \tag{2.8}$$

with boundary conditions

$$p_o(t,0,z)=p_o(t,\mathfrak{D},z)=0, \tag{2.9}$$

and initial condition

$$p_o(t,y,z)=0,\quad t\ll 0. \tag{2.10}$$

The solution $p_o(t,y,z)$ can be modeled as a superposition of monochromatic waves, called waveguide modes. The mode decomposition is based on the eigenfunctions of the Sturm-Liouville operator

$$\mathcal{L}_y=\partial_y^2+\left(\frac{\omega}{c_o}\right)^2 \tag{2.11}$$

defined on the vector space $C_0^2(0,\mathfrak{D})$ of functions that are twice continuously differentiable in $(0,\mathfrak{D})$, and vanish at $y=0$ and $y=\mathfrak{D}$. There are infinitely many modes. Finitely many propagate to the right and left of the source, and we can associate them to plane waves that strike the boundaries at different angles of incidence. Their amplitudes are completely determined by the source excitation and do not change with range. Since problem (2.8)-(2.10) is separable, the modes are not coupled.

The wave field $p(t,y,z)$ in the randomly perturbed waveguides can also be decomposed into propagating and evanescent modes, as shown in sections 4 and 5. The key point in the decomposition is that the perturbation effects are mapped only to the mode amplitudes, which are coupled and vary with range because of scattering. The analysis in 4 and 5 gives a detailed characterization of the random mode amplitudes. We are especially interested in their first and second moments, which allow us to quantify the range scales over which the waves lose coherence and decorrelate due to scattering. We summarize and compare the net scattering effects of random boundaries and interior random inhomogeneities in section 6. These are the main results of the analysis, and we use them in sections 8 and 9 to analyze time reversal and imaging.

2.1. Narrowband and broadband sources. — We describe here a source that emits the same signal from all the points in its support. We use it in the analysis of sections 8 and 9.

The source $F(t,y)$ has the separable form

$$F(t,y)=\varphi(t)\frac{1}{\Delta_y}\rho\left(\frac{y-y^\star}{\Delta_y}\right), \tag{2.12}$$

with non-negative source density ρ compactly supported in the interval of length Δ_y centered at $y^\star \in (0, \mathfrak{D})$. We assume that

$$\left[y^\star - \frac{\Delta_y}{2}, y^\star + \frac{\Delta_y}{2}\right] \subset (0, \mathfrak{D}),$$

and normalize ρ by

$$\int_0^{\mathfrak{D}} \frac{dy}{\Delta_y} \rho\left(\frac{y - y^\star}{\Delta_y}\right) = 1.$$

If $\Delta_y \ll \mathfrak{D}$ we have a point-like source at $y^\star$.

The source emits the signal

$$\varphi(t) = e^{-i\omega_o t} f(\mathcal{B}t), \tag{2.13}$$

defined by the function f of dimensionless arguments, with Fourier transform $\widehat{f}$ supported in the interval $[-\pi, \pi]$. The temporal duration of $f(\mathcal{B}t)$ and therefore of $\varphi(t)$ is of order $1/\mathcal{B}$. The Fourier transform of the emitted signal is given by

$$\widehat{\varphi}(\omega) = \int_{-\infty}^{\infty} dt\, \varphi(t) e^{i\omega t} = \int_{-\infty}^{\infty} dt\, f(\mathcal{B}t) e^{i(\omega-\omega_o)t} = \frac{1}{\mathcal{B}} \widehat{f}\left(\frac{\omega - \omega_o}{\mathcal{B}}\right), \tag{2.14}$$

and it is supported at frequencies $\omega \in [\omega_o - \pi\mathcal{B}, \omega_o + \pi\mathcal{B}]$.

To study wave propagation to an array at long range $Z_{\mathcal{A}}/\varepsilon^2$ from the source, we observe the waves on a time scale

$$t = \frac{T}{\varepsilon^2}. \tag{2.15}$$

We distinguish between two regimes: *narrowband* and *broadband*. In the narrowband regime the bandwidth $\mathcal{B}$ is related to the central frequency by

$$\mathcal{B} = \varepsilon^2 \Omega_{\mathcal{B}}, \quad \frac{\Omega_{\mathcal{B}}}{\omega_o} = O(1), \tag{2.16}$$

and the emitted signal

$$\varphi\left(t = \frac{T}{\varepsilon^2}\right) = e^{-i\omega_o T/\varepsilon^2} f\left(\Omega_{\mathcal{B}} T\right) \tag{2.17}$$

has large temporal support, of the order of the travel time from the source to the array. In the broadband regime

$$\mathcal{B} = \varepsilon^q \Omega_{\mathcal{B}}, \quad q < 2,$$

and the signal

$$\varphi\left(t = \frac{T}{\varepsilon^2}\right) = e^{-i\omega_o T/\varepsilon^2} f\left(\varepsilon^{2-q} \Omega_{\mathcal{B}} T\right) \tag{2.18}$$

has temporal support that is smaller by a factor of ε^{2-q} than the travel time. We call such a signal a *pulse*.

Obviously, the larger $\mathcal{B}$ is, the smaller the pulse duration. For our analysis, it suffices to consider $q = 1$, so we define the broadband regime by

$$B = \varepsilon\Omega_{\mathcal{B}}, \quad \frac{\Omega_{\mathcal{B}}}{\omega_o} = O(1). \tag{2.19}$$

3. Ideal waveguides

A waveguide mode is a monochromatic wave $\widehat{P}(\omega, y, z)e^{-i\omega t}$ with $\widehat{P}(\omega, y, z)$ solving the Helmholtz equation

$$\left(\partial_y^2 + \partial_z^2 + k^2\right)\widehat{P}(\omega, y, z) = 0 \tag{3.1}$$

for $y \in (0, \mathfrak{D})$ and $z \in \mathbb{R}$, with homogeneous Dirichlet boundary conditions at $y = 0$ and $y = \mathfrak{D}$. Here k is the wavenumber, defined by

$$k = \frac{\omega}{c_o} = \frac{2\pi}{\lambda}.$$

At the central frequency ω_o we call it k_o.

We decompose the solution $p_o(t, y, z)$ of (2.8)-(2.10) in modes using the eigenfunctions $\phi_j(y)$ of the operator $\mathcal{L}_y$ defined in (2.11). This operator is self-adjoint, with real and simple eigenvalues $\lambda_j(\omega)$, and the set $\{\phi_j\}_{j\geq 1}$ of orthonormal eigenfunctions is complete in $L^2(0, \mathfrak{D})$. See for example [**27**]. The eigenfunctions are independent of the frequency because the wave speed is constant. They would depend on ω otherwise, but the analysis below would remain the same in all essential aspects. We have explicitly

$$\mathcal{L}_y\phi_j(y) = \lambda_j(\omega)\phi_j(y), \quad j = 1, 2, \ldots, \tag{3.2}$$

where

$$\phi_j(y) = \sqrt{\frac{2}{\mathfrak{D}}}\sin\left(\frac{\pi j y}{\mathfrak{D}}\right), \tag{3.3}$$

and

$$\lambda_j(\omega) = \left(\frac{\pi}{\mathfrak{D}}\right)^2\left[\left(\frac{k\mathfrak{D}}{\pi}\right)^2 - j^2\right]. \tag{3.4}$$

Because only the first $N(\omega)$ eigenvalues are positive, where

$$N(\omega) = \left\lfloor \frac{k\mathfrak{D}}{\pi} \right\rfloor \tag{3.5}$$

and $\lfloor\ \rfloor$ denotes the integer part, we write

$$\lambda_j(\omega) = \begin{cases} \beta_j^2(\omega) & \text{if } j = 1, \ldots, N(\omega) \\ -\beta_j^2(\omega) & \text{if } j > N(\omega). \end{cases} \tag{3.6}$$

The solution of (2.8)-(2.10) is given by

$$p_o(t,y,z) = \int_{-\infty}^{\infty} \frac{d\omega}{2\pi} \widehat{p}_o(\omega,y,z) e^{-i\omega t}, \tag{3.7}$$

with

$$\begin{aligned} \widehat{p}_o(\omega,y,z) = 1_{(0,\infty)}(z) \left[\sum_{j=1}^{N(\omega)} \phi_j(y)\, u^+_{j,o}(\omega,z) + \sum_{j=N(\omega)+1}^{\infty} \phi_j(y)\, v^+_{j,o}(\omega,z) \right] \\ +1_{(-\infty,0)}(z) \left[\sum_{j=1}^{N(\omega)} \phi_j(y)\, u^-_{j,o}(\omega,z) + \sum_{j=N(\omega)+1}^{\infty} \phi_j(y)\, v^-_{j,o}(\omega,z) \right]. \end{aligned} \tag{3.8}$$

The indicator function

$$1_{(a,b)}(z) = \begin{cases} 1 & \text{if } z \in (a,b) \\ 0 & \text{otherwise} \end{cases}$$

allows us to write $\widehat{p}_o$ to the right and left of the source. The first $N(\omega)$ components $u^{\pm}_{j,o}$ of the solution are propagating waves satisfying one dimensional Helmholtz equations with wavenumber $\beta_j(\omega)$

$$\left[\partial_z^2 + \beta_j^2(\omega)\right] u^{\pm}_{j,o}(\omega,z) = 0, \quad z \neq 0, \tag{3.9}$$

outgoing (radiation) conditions at $|z| \to \infty$, and source jump conditions at $z = 0$

$$\begin{aligned} u^+_{j,o}(\omega,0+) - u^-_{j,o}(\omega,0-) = 0, \\ \partial_z u^+_{j,o}(\omega,0+) - \partial_z u^-_{j,o}(\omega,0-) = \widehat{F}_j(\omega) := \int_0^{\mathfrak{D}} dy\, \phi_j(y) \widehat{F}(\omega,y). \end{aligned} \tag{3.10}$$

Explicitly, they are given by right and left going waves

$$u^+_{j,o}(\omega,z) = a_{j,o}(\omega) e^{i\beta_j(\omega)z}, \quad u^-_{j,o}(\omega,z) = b_{j,o}(\omega) e^{-i\beta_j(\omega)z}, \tag{3.11}$$

with amplitudes

$$a_{j,o}(\omega) = b_{j,o}(\omega) = \frac{\widehat{F}_j(\omega)}{2i\beta_j(\omega)}, \quad j = 1, \ldots, N(\omega). \tag{3.12}$$

The components $v^{\pm}_{j,o}(\omega,z)$ solve the equations

$$\left[\partial_z^2 - \beta_j^2(\omega)\right] v^{\pm}_{j,o}(\omega,z) = 0, \quad z \neq 0, \tag{3.13}$$

with decay condition $\lim_{|z|\to\infty} v^{\pm}_{j,o}(\omega,z) = 0$, and source jump conditions similar to (3.10). They are the evanescent waves given by

$$v^{\pm}_{j,o}(\omega,z) = e_{j,o}(\omega) e^{-\beta_j(\omega)|z|}, \quad e_{j,o} = -\frac{\widehat{F}_j(\omega)}{2\beta_j(\omega)}, \quad j > N(\omega). \tag{3.14}$$

We assume throughout that none of the mode wavenumbers β_j are zero in the bandwidth, meaning that there are no standing waves. We also suppose that $N(\omega)$

does not vary in the bandwidth, and we drop its dependence on ω. This amounts to having

$$\frac{k\mathfrak{D}}{\pi} = N + \vartheta(\omega), \quad \vartheta(\omega) \in (0,1), \quad \forall\, \omega \in [\omega_o - \pi\mathcal{B}, \omega_o + \pi\mathcal{B}]. \tag{3.15}$$

The wave field to the right of the source becomes

$$\widehat{p}_o(\omega, y, z) = \sum_{j=1}^{N} a_{j,o}(\omega)\phi_j(y)e^{i\beta_j(\omega)z} + \sum_{j=N+1}^{\infty} e_{j,o}(\omega)\phi_j(y)e^{-\beta_j(\omega)z}, \quad z > 0, \tag{3.16}$$

with negligible evanescent part at long ranges.

3.1. Plane waves interpretation. — Recalling definition (3.3) of ϕ_j, we can write the propagating part of (3.16) as a superposition of plane waves

$$\pm\frac{a_{j,o}(\omega)}{i\sqrt{2\mathfrak{D}}} \exp\left[i\left(\pm\frac{\pi j}{\mathfrak{D}}, \beta_j\right)\cdot(y,z)\right], \quad j = 1, \ldots, N.$$

We need both signs in the phases so that when we add the waves together, we satisfy the boundary conditions. The waves travel in the direction of the slowness vectors

$$\mathbf{K}_j^{\pm} = \left(\pm\frac{\pi j}{\mathfrak{D}}, \beta_j\right)$$

and strike the boundaries, where they are reflected.

Suppose that the waveguide supports many propagating modes, that is $N \gg 1$. Because the wavenumbers decrease with the index j, we see that the higher indexed modes have slowness vector that is almost orthogonal to the boundaries. Indeed, for the last mode we have

$$\mathbf{K}_N^{\pm} = \left(\pm\frac{\pi N}{\mathfrak{D}}, \beta_N\right)$$

with

$$\frac{\pi N}{\mathfrak{D}} \approx k, \quad \beta_N = \frac{\pi}{\mathfrak{D}}\sqrt{2\vartheta N} \approx k\sqrt{\frac{2\vartheta}{N}} \ll k,$$

so the slowness vector is almost parallel to the y axis. These waves strike the boundary many times and thus take a very long path from the source to the array. The mode propagates slowly at group speed

$$\frac{1}{\beta_N'(\omega)} = c_o\frac{\beta_N(\omega)}{k} \approx c_o\sqrt{\frac{2\vartheta(\omega)}{N}} \ll c_o.$$

The fastest mode is indexed by 1. It gives the slowness vector

$$\mathbf{K}_1^{\pm} = \left(\pm\frac{\pi}{\mathfrak{D}}, \beta_1\right) \approx \left(\pm\frac{k}{N}, k\right)$$

that is almost parallel to the range axis. This mode barely sees the boundaries, and travels quickly to the array with speed

$$\frac{1}{\beta_1'(\omega)} = c_o \frac{\beta_1(\omega)}{k} \approx c_o.$$

3.2. Long range pulse propagation. — Neglecting the evanescent part in (3.16) and using equation (3.12), we obtain that the pressure field measured at the range $Z_{\mathcal{A}}/\varepsilon^2$ of the array is

$$p_o\left(t, y, \frac{Z_{\mathcal{A}}}{\varepsilon^2}\right) \approx \sum_{j=1}^{N} \phi_j(y) \int_{-\infty}^{\infty} \frac{d\omega}{2\pi} \frac{\widehat{F}_j(\omega)}{2i\beta_j(\omega)} e^{i\beta_j(\omega) Z_{\mathcal{A}}/\varepsilon^2 - i\omega t}. \tag{3.17}$$

We describe it here for the separable source density (2.12), emitting the signal $\varphi(t)$ given by (2.13), and for the time $t = T/\varepsilon^2$. Since

$$\widehat{F}_j(\omega) = \int_0^{\mathfrak{D}} dy\, \phi_j(y) \int_{-\infty}^{\infty} dt\, F(t,y) e^{i\omega t}, \tag{3.18}$$

we obtain that

$$p_o\left(t = \frac{T}{\varepsilon^2}, y, \frac{Z_{\mathcal{A}}}{\varepsilon^2}\right) \approx \sum_{j=1}^{N} \phi_j(y)\, \mathfrak{f}_j^{\varepsilon}(T) \int_0^{\mathfrak{D}} \frac{dy'}{\Delta_y} \rho\left(\frac{y' - y^\star}{\Delta_y}\right) \phi_j(y'), \tag{3.19}$$

where we denote by $\mathfrak{f}_j^{\varepsilon}(T)$ the signals propagated by the modes,

$$\mathfrak{f}_j^{\varepsilon}(T) = \int_{-\infty}^{\infty} \frac{d\omega}{2\pi\mathcal{B}} \widehat{f}\left(\frac{\omega - \omega_o}{\mathcal{B}}\right) \frac{e^{i[\beta_j(\omega) Z_{\mathcal{A}} - \omega T]/\varepsilon^2}}{2i\beta_j(\omega)}. \tag{3.20}$$

In the narrowband regime defined by (2.16), we can change variables as

$$\omega = \omega_o + \varepsilon^2 w,$$

and obtain that

$$\begin{aligned} \mathfrak{f}_j^{\varepsilon}(T) &= \frac{e^{i[\beta_j(\omega_o) Z_{\mathcal{A}} - \omega_o T]/\varepsilon^2}}{2i\beta_j(\omega_o)} \int_{-\infty}^{\infty} \frac{dw}{2\pi\Omega_{\mathcal{B}}} \widehat{f}\left(\frac{w}{\Omega_{\mathcal{B}}}\right) e^{i\beta_j'(\omega_o) w Z_{\mathcal{A}} - iwT} + O(\varepsilon^2) \\ &= \frac{e^{i[\beta_j(\omega_o) Z_{\mathcal{A}} - \omega_o T]/\varepsilon^2}}{2i\beta_j(\omega_o)} f\left[\Omega_{\mathcal{B}}\left(T - \beta_j'(\omega_o) Z_{\mathcal{A}}\right)\right] + O(\varepsilon^2). \end{aligned} \tag{3.21}$$

Thus, the modes propagate the emitted signal at the group velocity

$$\frac{1}{\beta_j'(\omega_o)} = c_o \frac{\beta_j(\omega_o)}{k_o} \approx c_o \sqrt{1 - \frac{j^2}{N^2}}, \tag{3.22}$$

which varies with the mode index. The first arrival is for mode $j = 1$, with speed

$$\frac{1}{\beta_1'(\omega_o)} \approx c_o.$$

The other modes follow, with the latter ones traveling at much smaller speed than c_o. Since φ has long temporal support, of the same order as the travel time, it is not possible to distinguish the arrival of the modes. The array records the superposition of signals that are mixed together.

In the broadband regime defined by (2.19) we let

$$\omega = \omega_o + \varepsilon w,$$

and obtain from (3.20) that

$$\begin{aligned} \mathfrak{f}_j^\varepsilon(T) &= \frac{e^{i[\beta_j(\omega_o)Z_{\mathcal{A}}-\omega_o T]/\varepsilon^2}}{2i\beta_j(\omega_o)} \int_{-\infty}^{\infty} \frac{dw}{2\pi\Omega_{\mathcal{B}}} \widehat{f}\left(\frac{w}{\Omega_{\mathcal{B}}}\right) e^{i\frac{w}{\varepsilon}\left(\beta_j'(\omega_o)Z_{\mathcal{A}}-T\right)+i\frac{\beta_j''(\omega_o)w^2 Z_{\mathcal{A}}}{2}} \\ &= \frac{e^{i[\beta_j(\omega_o)Z_{\mathcal{A}}-\omega_o T]/\varepsilon^2}}{2i\beta_j(\omega_o)} f \star \mathfrak{d}_j\left[\frac{\Omega_{\mathcal{B}}\left(T-\beta_j'(\omega_o)Z_{\mathcal{A}}\right)}{\varepsilon}\right], \end{aligned} \tag{3.23}$$

where the star denotes convolution and $\mathfrak{d}_j$ is the dispersion kernel

$$\mathfrak{d}_j(\Omega_{\mathcal{B}}t) = \int_{-\infty}^{\infty} \frac{dw}{2\pi\Omega_{\mathcal{B}}} e^{i\beta_j''(\omega_o)w^2 Z_{\mathcal{A}}/2-iwt}. \tag{3.24}$$

The modes travel with speed $1/\beta_j'(\omega_o)$ as before, but now the array receives a train of pulses[(1)], which are well separated because their temporal support is small with respect to the travel time. The pulse shapes are affected by dispersion, due to the quadratic phase term proportional to

$$|\beta_j''(\omega_o)| = \frac{(\pi j/\mathfrak{D})^2}{c_o^2\beta_j^3(\omega_o)}.$$

It increases monotonically with the mode index, so we can expect that the late arrivals have significant pulse shape alteration due to dispersion.

4. Waveguides with random boundaries

The asymptotic analysis presented here is essentially the same if one or both boundaries of the waveguide have fluctuations. For simplicity, we assume that the top boundary $\mathcal{Y}(z)$ fluctuates about the mean value $\mathfrak{D}$, but set the bottom boundary to

$$\mathcal{Y}_b(z) = 0.$$

Waveguides with random $\mathcal{Y}_b(z)$ and $\mathcal{Y}(z)$ are studied in detail in [**1**] for both Dirichlet and Neumann boundary conditions. See also the studies [**17, 18**] for random waveguides with unbounded cross-section that support radiative modes in addition to the propagating and evanescent ones.

(1) See the top left picture in Figure 4 for an illustration of a train of pulses received at the array.

4.1. Model of the fluctuations. — We model the fluctuations of the top boundary with a random process $\mu(z)$

$$\mathcal{Y}(z) = \mathfrak{D}\left[1 + \varepsilon\mu(z)\right], \quad \varepsilon \ll 1. \tag{4.1}$$

We assume that $\mu(z)$ is bounded, stationary, with mean zero

$$\mathbb{E}[\mu(z)] = 0 \tag{4.2}$$

and mixing, i.e., with enough decorrelation[(2)]. Its covariance

$$\mathcal{R}_\mu(z) = \mathbb{E}[\mu(z+s)\mu(s)] \tag{4.3}$$

is integrable, and we normalize it by

$$\mathcal{R}_\mu(0) = 1. \tag{4.4}$$

We use the dimensionless parameter $\varepsilon \ll 1$ to model the small amplitude of the fluctuations.

Our method of solution is based on a coordinate change that straightens the boundary and maps the fluctuations inside the domain. It requires that $\mu(z)$ be twice differentiable, with almost surely bounded derivatives. This implies that $\mathcal{R}_\mu(z)$ has at least four derivatives. If $\mu(z)$ is not differentiable, another approach based on conformal mappings may be used, as explained in [**18**]. In the end, the results should not be that different.

The covariance $\mathcal{R}_\mu(z)$ is an even function, with maximum at $z = 0$. It decays to zero as $|z| \to \infty$, on a length scale called the *correlation length* ℓ. It is the range offset over which the fluctuations become statistically decorrelated. We define it using an auxiliary even, integrable and four times differentiable function $\mathcal{R}$ of dimensionless argument, satisfying $\mathcal{R}(0) = -\mathcal{R}''(0) = 1$. We let

$$\mathcal{R}_\mu(z) = \mathcal{R}\left(\frac{z}{\ell}\right), \tag{4.5}$$

and therefore

$$\ell = \sqrt{-\frac{\mathcal{R}_\mu(0)}{\mathcal{R}''_\mu(0)}} = \sqrt{-\frac{1}{\mathcal{R}''_\mu(0)}}. \tag{4.6}$$

An alternative definition of ℓ is given by the integral of $\mathcal{R}_\mu(z)$. It agrees with (4.6) up to an order one constant, because equation (4.5) gives

$$\int_{-\infty}^{\infty} dz\, \mathcal{R}_\mu(z) = \ell \int_{-\infty}^{\infty} du\, \mathcal{R}(u) = \ell\, O(1).$$

As an illustration, consider the Gaussian

$$\mathcal{R}_\mu(z) = e^{-\frac{z^2}{2\ell^2}}.$$

(2) Explicitly, $\mu(z)$ is a φ-mixing process, with $\varphi \in L^{1/2}(\mathbb{R}^+)$, as stated in [**21**, Section 4.6.2].

Its integral is

$$\int_{-\infty}^{\infty} dz\, \mathcal{R}_\mu(z) = \sqrt{2\pi}\ell$$

and the fluctuations are uncorrelated for range offsets exceeding 3ℓ, because

$$\mathcal{R}_\mu(z) \approx 0 \quad \text{if } |z| \geq 3\ell.$$

In the analysis we suppose that the boundary fluctuates only in the range interval $z \in [0, \bar{L}^\varepsilon]$,

$$\mathcal{Y}(z) = \mathfrak{D}, \quad z \in (-\infty, 0) \cup (\bar{L}^\varepsilon, \infty), \tag{4.7}$$

so we can specify outgoing boundary conditions on the Fourier coefficients $\widehat{p}(\omega, y, z)$ of the wave field. The confinement of the fluctuations to $z \leq \bar{L}^\varepsilon$ can be motivated by the hyperbolicity of the time-domain problem. If we wish to study wave propagation to a maximum range L^ε that is large and depends on ε in our case, we observe the field $p(t, y, z)$ in a time window supported at $t \lesssim L^\varepsilon/c_o$. In this window the waves are not affected by the medium beyond a range $\bar{L}^\varepsilon \gtrsim L^\varepsilon$, so we may set the fluctuation to zero for $z > \bar{L}^\varepsilon$. Here the symbols $\lesssim$ (and $\gtrsim$) mean less or equal (and larger or equal) up to an order one constant.

The truncation of the fluctuations at negative ranges can be justified under the *forward scattering approximation*, which says that when the correlation length is large enough, we can neglect the backscattered field. In this approximation the medium on the left of the source has little influence on the wave field at positive ranges, so we can discard the fluctuations at $z < 0$. We refer to [**16**] for a study of wave propagation in random waveguides with forward and backward wave coupling. The analysis is more complicated, and it accounts for important phenomena, such as enhanced backscattering, that cannot be analyzed under the forward scattering approximation. The results relevant to imaging are not that different, so we will consider regimes where the forward scattering approximation applies.

4.2. Change of coordinates. — To analyze the wave field in the random waveguide, we reformulate the problem with a change of coordinates that flatten the boundary

$$y = \mathcal{Y}(z)\frac{Y}{\mathfrak{D}}, \quad Y \in [0, \mathfrak{D}]. \tag{4.8}$$

We could use many other coordinate changes, but we prefer (4.8) because it is simple. Clearly, if the method is any good, the result should be independent of the choice that we make. This turns out to be the case, as shown in detail in [**1**].

Let the wave field in the new coordinate system be $P(t, Y, z)$. It is defined by

$$P(t, Y, z) = p\left(t, \mathcal{Y}(z)\frac{Y}{\mathfrak{D}}, z\right), \quad z \in \mathbb{R},\ Y \in [0, \mathfrak{D}], \tag{4.9}$$

and it satisfies the boundary conditions

$$P(t,0,z) = P(t,\mathfrak{D},z) = 0. \tag{4.10}$$

In the original coordinates we have

$$p(t,y,z) = P\left(t, \frac{y\mathfrak{D}}{\mathcal{Y}(z)}, z\right), \quad z \in \mathbb{R},\ y \in [0,\mathcal{Y}(z)]. \tag{4.11}$$

After Fourier transforming in t and using the chain rule, we obtain that the Fourier coefficients of (4.9) satisfy

$$\mathcal{L}^\varepsilon \widehat{P}(\omega,Y,z) = 0, \tag{4.12}$$

for $z \in (0,\bar{L}^\varepsilon)$ and $Y \in (0,\mathfrak{D})$. The partial differential operator $\mathcal{L}^\varepsilon$ is given by

$$\begin{aligned}\mathcal{L}^\varepsilon = \partial_z^2 + \frac{\left[\mathfrak{D}^2 + (Y\mathcal{Y}'(z))^2\right]}{\mathcal{Y}^2(z)}\partial_Y^2 - \frac{2Y\mathcal{Y}'(z)}{\mathcal{Y}(z)}\partial_{Yz}^2 \\ +Y\left[2\left(\frac{\mathcal{Y}'(z)}{\mathcal{Y}(z)}\right)^2 - \frac{\mathcal{Y}''(z)}{\mathcal{Y}(z)}\right]\partial_Y + k^2.\end{aligned} \tag{4.13}$$

Its dependence on the small parameter ε follows from the definition (4.1) of $\mathcal{Y}(z)$, and we can write it as a perturbation series of operators

$$\mathcal{L}^\varepsilon = \mathcal{L}_o + \varepsilon\mathcal{L}_1 + \varepsilon^2\mathcal{L}_2 + \varepsilon^3\mathcal{L}_3 + \dots \tag{4.14}$$

The leading order operator corresponds to the ideal waveguide

$$\mathcal{L}_o = \partial_z^2 + \partial_Y^2 + k^2. \tag{4.15}$$

The next two operators are given by

$$\begin{aligned}\mathcal{L}_1 + \varepsilon\mathcal{L}_2 = -2Y\mu'(z)[1-\varepsilon\mu(z)]\partial_{Yz}^2 + \left[-2\mu(z) + 3\varepsilon\mu^2(z) + \varepsilon(Y\mu'(z))^2\right]\partial_Y^2 \\ + \left[-\mu''(z) + \varepsilon\mu(z)\mu''(z) + 2\varepsilon(\mu'(z))^2\right]Y\partial_Y,\end{aligned} \tag{4.16}$$

and the remainder in (4.14) is an operator with $O(\varepsilon^3)$ random coefficients that depend on Y and z,

$$\varepsilon^3\mathcal{L}_3 + \dots = O(\varepsilon^3)\partial_{Yz}^2 + O(\varepsilon^3)\partial_Y^2 + O(\varepsilon^3)\partial_Y. \tag{4.17}$$

We do not write it explicitly, because it is negligible in our asymptotic analysis.

The boundary is flat for $z \in (-\infty,0)\cup(\bar{L}^\varepsilon,\infty)$ by assumption (4.7), so the change of variables (4.8) is trivial in this range domain

$$Y = y, \quad z \in (-\infty,0)\cup(\bar{L}^\varepsilon,\infty), \tag{4.18}$$

and $\widehat{P}$ satisfies the same equation as in the ideal waveguide

$$\mathcal{L}_o\widehat{P}(\omega,Y,z) = 0, \quad z \in (-\infty,0)\cup(\bar{L}^\varepsilon,\infty). \tag{4.19}$$

4.3. Mode decomposition. — We ensure that the boundary conditions (4.13) are satisfied exactly by decomposing $\widehat{P}(\omega, Y, z)$ in the $L^2(0, \mathfrak{D})$ basis of orthonormal eigenfunctions $\{\phi_j(Y)\}_{j\geq 1}$,

$$\widehat{P}(\omega, Y, z) = \sum_{j=1}^{N} \phi_j(Y) u_j(\omega, z) + \sum_{j=N+1}^{\infty} \phi_j(Y) v_j(\omega, z). \tag{4.20}$$

This looks similar to the decomposition (3.8) in ideal waveguides, but the problem is no longer separable, and the propagating and evanescent components u_j and v_j are random functions accounting for scattering at the random boundary.

The propagating components satisfy the differential equations

$$\begin{aligned}\left[\partial_z^2 + \beta_j^2(\omega)\right] u_j(\omega, z) = \widehat{F}_j(\omega)\delta(z) \\ - 1_{(0,\bar{L}^\varepsilon)}(z)\, \varepsilon \sum_{l=1}^{N} \left[Q_{jl}^\varepsilon(\mu(z))\, \partial_z + M_{jl}^\varepsilon(\mu(z))\right] u_l(\omega, z) \\ - 1_{(0,\bar{L}^\varepsilon)}(z)\, \varepsilon \sum_{l=N+1}^{\infty} \left[Q_{jl}^\varepsilon(\mu(z))\, \partial_z + M_{jl}^\varepsilon(\mu(z))\right] v_l(\omega, z) + O(\varepsilon^3)\,,\end{aligned} \tag{4.21}$$

for $j = 1, \ldots, N$, with outgoing conditions at $|z| \to \infty$, Similarly, the evanescent components satisfy

$$\begin{aligned}\left[\partial_z^2 - \beta_j^2(\omega)\right] v_j(\omega, z) = \widehat{F}_j(\omega)\delta(z) \\ - 1_{(0,\bar{L}^\varepsilon)}(z)\, \varepsilon \sum_{l=1}^{N} \left[Q_{jl}^\varepsilon(\mu(z))\, \partial_z + M_{jl}^\varepsilon(\mu(z))\right] u_l(\omega, z) \\ - 1_{(0,\bar{L}^\varepsilon)}(z)\, \varepsilon \sum_{l=N+1}^{\infty} \left[Q_{jl}^\varepsilon(\mu(z))\, \partial_z + M_{jl}^\varepsilon(\mu(z))\right] v_l(\omega, z) + O(\varepsilon^3)\end{aligned} \tag{4.22}$$

for $j > N$, with decay conditions $\lim_{|z|\to\infty} v_j(\omega, z) = 0$. The matrices Q_{jl}^ε and M_{jl}^ε couple the propagating and evanescent components, and are given by

$$Q_{jl}^\varepsilon(\mu(z)) = -2\mu'(z)[1 - \varepsilon\mu(z)] \int_0^{\mathfrak{D}} dy\, y\, \phi_j(y)\phi_l'(y), \tag{4.23}$$

and

$$\begin{aligned}M_{jl}^\varepsilon(\mu(z)) =& [-2\mu(z) + 3\varepsilon\mu^2(z)] \int_0^{\mathfrak{D}} dy\, \phi_j(y)\phi_l''(y) \\ &+ \varepsilon[\mu'(z)]^2 \int_0^{\mathfrak{D}} dy\, y^2 \phi_j(y)\phi_l''(y) \\ &+ \left[-\mu''(z) + \varepsilon\mu(z)\mu''(z) + 2\varepsilon(\mu'(z))^2\right] \int_0^{\mathfrak{D}} dy\, y\, \phi_j(y)\phi_l'(y).\end{aligned} \tag{4.24}$$

The characteristic function $1_{[0,\bar{L}^\varepsilon]}(z)$ in equations (4.21)-(4.22) indicates that the fluctuations are supported in the range interval $z \in [0, \bar{L}^\varepsilon]$.

We begin with the study of the propagating modes. The evanescent ones are analyzed in section 4.6.

4.4. The forward and backward going waves. — Note that equations (4.21) are the same as in the ideal waveguide in the range interval $z \in (-\infty, 0) \cup (\bar{L}^\varepsilon, \infty)$. Therefore, we write directly the solution as a backward going wave to the left of the source

$$u_j(\omega, z) = b_j^-(\omega) e^{-i\beta_j(\omega) z}, \quad z < 0, \tag{4.25}$$

and a forward going wave beyond the range of the fluctuations

$$u_j(\omega, z) = a_j^+(\omega) e^{i\beta_j(\omega) z}, \quad z > \bar{L}^\varepsilon. \tag{4.26}$$

Here $b_j^-(\omega)$, $a_j^+(\omega)$ are constant mode amplitudes that remain to be determined from the continuity conditions at $z = \bar{L}^\varepsilon$

$$\begin{aligned} a_j^+(\omega) &= u_j(\omega, \bar{L}^\varepsilon) e^{-i\beta_j(\omega)\bar{L}^\varepsilon} \\ i\beta_j(\omega) a_j^+(\omega) &= \partial_z u_j(\omega, \bar{L}^\varepsilon) e^{-i\beta_j(\omega)\bar{L}^\varepsilon}, \end{aligned} \tag{4.27}$$

and the source jump conditions at $z = 0$

$$\begin{aligned} u_j(\omega, 0+) - b_j^-(\omega) &= 0, \\ \partial_z u_j(\omega, 0+) + i\beta_j(\omega) b_j^-(\omega) &= \widehat{F}_j(\omega). \end{aligned} \tag{4.28}$$

The solution of (4.21) in the range interval $z \in (0, \bar{L}^\varepsilon)$ is a superposition of forward and backward going waves, with amplitudes a_j and b_j,

$$u_j(\omega, z) = a_j(\omega, z) e^{i\beta_j(\omega) z} + b_j(\omega, z) e^{-i\beta_j(\omega) z}, \quad j = 1, \ldots, N. \tag{4.29}$$

Because the fluctuations end at $z = \bar{L}^\varepsilon$, there should be no backward going wave there, so we ask that

$$b_j(\omega, \bar{L}^\varepsilon) = 0, \tag{4.30}$$

and rewrite the continuity conditions (4.27) as

$$\begin{aligned} a_j(\omega, \bar{L}^\varepsilon) &= a_j^+(\omega), \\ e^{i\beta_j(\omega)\bar{L}^\varepsilon} \partial_z a_j(\omega, \bar{L}^\varepsilon) + e^{-i\beta_j(\omega)\bar{L}^\varepsilon} \partial_z b_j(\omega, \bar{L}^\varepsilon) &= 0. \end{aligned} \tag{4.31}$$

The source jump conditions at $z = 0$ are

$$\begin{aligned} a_j(\omega,0+) + b_j(\omega,0+) &= b_j^-(\omega), \\ i\beta_j(\omega)\left[a_j(\omega,0+) - b_j(\omega,0+)\right] &= \widehat{F}_j(\omega) - i\beta_j(\omega) b_j^-(\omega) \\ &\quad - \left[\partial_z a_j(\omega,0+) + \partial_z b_j(\omega,0+)\right]. \end{aligned} \tag{4.32}$$

Moreover, substituting (4.29) in (4.21) we obtain

$$\begin{aligned} i\beta_j(\omega) &\left[e^{i\beta_j(\omega)z}\partial_z a_j(\omega,z) - e^{-i\beta_j(\omega)z}\partial_z b_j(\omega,z)\right] = \\ &- \partial_z\left[e^{i\beta_j(\omega)z}\partial_z a_j(\omega,z) + e^{-i\beta_j(\omega)z}\partial_z b_j(\omega,z)\right] \\ &- \varepsilon\sum_{l=1}^{N}\left[Q_{jl}^{\varepsilon}(\mu(z))\,\partial_z + M_{jl}^{\varepsilon}(\mu(z))\right]\left(a_l(\omega,z)e^{i\beta_l(\omega)z} + b_l(\omega,z)e^{-i\beta_l(\omega)z}\right) \\ &- \varepsilon\sum_{l=N+1}^{\infty}\left[Q_{jl}^{\varepsilon}(\mu(z))\,\partial_z + M_{jl}^{\varepsilon}(\mu(z))\right] v_l(\omega,z) + O(\varepsilon^3), \qquad z\in(0,\bar{L}^{\varepsilon}). \end{aligned} \tag{4.33}$$

Equations (4.30)-(4.33) do not define uniquely the amplitudes a_j and b_j. We need an extra equation to close the system. To derive it, we note that because we have a perturbation problem, the solution should behave like in the ideal waveguide in the proximity of the source. This happens when we ask that

$$e^{i\beta_j(\omega)z}\partial_z a_j(\omega,z) + e^{-i\beta_j(\omega)z}\partial_z b_j(\omega,z) = 0, \quad \forall\ z\in(0,\bar{L}^{\varepsilon}). \tag{4.34}$$

This equation is consistent with (4.31), and when combined with (4.33) it gives first order evolution equations for a_j and b_j. These equations, with the initial conditions

$$a_j(\omega,0+) = \frac{\widehat{F}_j(\omega)}{2i\beta_j(\omega)} = a_{j,o}(\omega) \tag{4.35}$$

derived from (4.32), and the outgoing conditions (4.30), determine $a_j(\omega,z)$ and $b_j(\omega,z)$. The waves on the left of the source are determined by

$$b_j^-(\omega) = \frac{\widehat{F}_j(\omega)}{2i\beta_j(\omega)} + b_j(\omega,0+), \tag{4.36}$$

and the waves at ranges $z > \bar{L}^{\varepsilon}$ follow from the continuity conditions (4.27).

We write next the infinite system of differential equations that describe the evolution and coupling of the modes.

4.5. Mode coupling. — The forward going wave amplitudes satisfy

$$\begin{aligned}\partial_z \widehat{a}_j(\omega,z) &= i\varepsilon \sum_{l=1}^{N} C^{\varepsilon}_{jl}(\omega,\mu(z))\, \widehat{a}_l(\omega,z) e^{i[\beta_l(\omega)-\beta_j(\omega)]z} \\ &\quad + i\varepsilon \sum_{l=1}^{N} \overline{C^{\varepsilon}_{jl}}(\omega,\mu(z))\, \widehat{b}_l(\omega,z) e^{-i[\beta_l(\omega)+\beta_j(\omega)]z} \\ &\quad + \frac{i\varepsilon}{2\beta_j(\omega)} \sum_{l=N+1}^{\infty} e^{-i\beta_j(\omega)z} \left[Q^{\varepsilon}_{jl}(\mu(z))\, \partial_z + M^{\varepsilon}_{jl}(\mu(z)) \right] \widehat{v}_l(\omega,z) + O(\varepsilon^3) \end{aligned} \tag{4.37}$$

for $z \in (0, \bar{L}^{\varepsilon})$, with initial condition (4.35). Here the bar denotes complex conjugation. Similarly, the backward going wave amplitudes satisfy

$$\begin{aligned}\partial_z \widehat{b}_j(\omega,z) &= -i\varepsilon \sum_{l=1}^{N} C^{\varepsilon}_{jl}(\omega,\mu(z))\, \widehat{a}_l(\omega,z) e^{i[\beta_l(\omega)+\beta_j(\omega)]z} \\ &\quad - i\varepsilon \sum_{l=1}^{N} \overline{C^{\varepsilon}_{jl}}(\omega,\mu(z))\, \widehat{b}_l(\omega,z) e^{-i[\beta_l(\omega)-\beta_j(\omega)]z} \\ &\quad - \frac{i\varepsilon}{2\beta_j(\omega)} \sum_{l=N+1}^{\infty} e^{i\beta_j(\omega)z} \left[Q^{\varepsilon}_{jl}(\mu(z))\partial_z + M^{\varepsilon}_{jl}(\mu(z)) \right] \widehat{v}_l(\omega,z) + O(\varepsilon^3)\,, \end{aligned} \tag{4.38}$$

for $z \in (0, \bar{L}^{\varepsilon})$, with end condition (4.30). The amplitudes are coupled directly by the coefficients

$$C^{\varepsilon}_{jl}(\omega,\mu(z)) = \frac{1}{2\beta_j(\omega)} \left[M^{\varepsilon}_{jl}(\mu(z)) + i\beta_l(\omega) Q^{\varepsilon}_{jl}(\mu(z)) \right] \quad j,l = 1,\ldots,N, \tag{4.39}$$

with Q^{ε}_{jl} and M^{ε}_{jl} defined in (4.23)-(4.24), and indirectly through the evanescent modes. We show next that the evanescent components $\{v_j(\omega,z)\}_{j>N}$ can be written in terms of the propagating amplitudes, and thus obtain a closed system for $\{a_j(\omega,z), b_j(\omega,z)\}_{j=1,\ldots,N}$.

4.6. Analysis of the evanescent modes. — When substituting (4.29) in (4.22), we obtain that $\{v_j(\omega,z)\}_{j>N}$ satisfy the equations

$$\begin{aligned}\left[\partial_z^2 - \beta_j^2(\omega)\right] v_j(\omega,z) &= \widehat{F}_j(\omega)\delta(z) - 2\varepsilon w^{\varepsilon}_j(\omega,z) \\ &\quad - 1_{(0,\bar{L}^{\varepsilon})}(z)\, \varepsilon \sum_{l=N+1}^{\infty} \left[Q^{\varepsilon}_{jl}(\mu(z))\, \partial_z + M^{\varepsilon}_{jl}(\mu(z)) \right] v_l(\omega,z) + O(\varepsilon^3)\,, \end{aligned} \tag{4.40}$$

with decay conditions

$$\lim_{|z|\to\infty} v_j(\omega,z) = 0, \tag{4.41}$$

where we let

$$w_j^\varepsilon(\omega,z) = 1_{(0,\bar{L}^\varepsilon)}(z) 2\beta_j(\omega) \sum_{l=1}^{N} \Big[C_{jl}^\varepsilon(\omega,\mu(z))\, a_l(\omega,z) e^{i\beta_l(\omega)z} + \overline{C_{jl}^\varepsilon}(\omega,\mu(z))\, b_l(\omega,z) e^{-i\beta_l(\omega)z} \Big].$$

To solve these equations, we begin by inverting the leading differential operator, using the Green's function

$$G_j(\omega,z) = \frac{e^{-\beta_j(\omega)|z|}}{2\beta_j(\omega)},$$

satisfying

$$\left(\partial_z^2 - \beta_j^2(\omega)\right) G_j(\omega,z) = -\delta(z), \quad \text{and} \quad \lim_{|z|\to\infty} G_j(\omega,z) = 0.$$

We obtain a system of integral equations for the infinite vector $\mathbf{v} = (v_{N+1}, \ldots)$,

$$\left[(\mathbf{I} - \varepsilon\mathbf{H})\,\mathbf{v}\right]_j(\omega,z) = -\frac{\widehat{F}_j(\omega) e^{-\beta_j(\omega)|z|}}{2\beta_j(\omega,z)} + \varepsilon \int_{-\infty}^{\infty} ds\, e^{-\beta_j(\omega)|s|} w_j^\varepsilon(\omega, z+s),$$

where $\mathbf{I}$ is the identity and $\mathbf{H}$ is the linear integral operator

$$\left[\mathbf{H}\mathbf{v}\right]_j(\omega,z) = \sum_{l=N+1}^{\infty} \int_{-\infty}^{\infty} ds\, e^{-\beta_j(\omega)|s|} \mathcal{H}_{jl}^\varepsilon(\omega, z+s) v_l(\omega, z+s),$$

with kernel

$$\mathcal{H}_{jl}^\varepsilon(\omega,z) = \frac{1_{(0,\bar{L}^\varepsilon)}(z)}{2\beta_j(\omega)} \left(Q_{jl}^\varepsilon(\mu(z))\,\partial_z + M_{jl}^\varepsilon(\mu(z)) \right) + O(\varepsilon^2).$$

It is shown in [**1**, Lemma 3.1] that $\mathbf{H}$ is a bounded operator on the space of square summable sequences of $L^2(\mathbb{R})$ functions with weights, equipped with the norm

$$\|\mathbf{v}\| = \left[\sum_{j=N+1}^{\infty} \left(j \|v_j\|_{L^2(\mathbb{R})} \right)^2 \right]^{\frac{1}{2}}.$$

Thus, we can invert the operator $\mathbf{I} - \varepsilon\mathbf{H}$ with the Neumann series

$$(\mathbf{I} - \varepsilon\mathbf{H})^{-1} = \mathbf{I} + \varepsilon\mathbf{H} + \varepsilon^2\mathbf{H}^2 + \ldots,$$

and write explicitly the evanescent waves in terms of the propagating ones.

The solution is

$$
\begin{aligned}
v_j(\omega,z) = & -\frac{\widehat{F}_j(\omega)}{2\beta_j(\omega,z)} e^{-\beta_j(\omega)|z|} \\
& + \varepsilon \sum_{l=1}^{N} a_l(\omega,z) e^{i\beta_l(\omega)z} \int_{-\infty}^{\infty} ds\, e^{-\beta_j(\omega)|s|+i\beta_l(\omega)s} C_{jl}(\omega,\mu(z+s)) \\
& + \varepsilon \sum_{l=1}^{N} b_l(\omega,z) e^{-i\beta_l(\omega)z} \int_{-\infty}^{\infty} ds\, e^{-\beta_j(\omega)|s|-i\beta_l(\omega)s} \overline{C_{jl}}(\omega,\mu(z+s)) + O(\varepsilon^2),
\end{aligned} \tag{4.42}
$$

because equations (4.37)-(4.38) give

$$
a_l(\omega,z+s) = a_l(\omega,z) + O(\varepsilon), \quad b_l(\omega,z+s) = b_l(\omega,z) + O(\varepsilon)
$$

for $s = O(1)$, where the decaying exponential in (4.42) is not negligible. We neglected the term

$$
\begin{aligned}
\left[\mathbf{H} \left(\frac{\widehat{F}_{N+1} e^{-\beta_{N+1}|z|}}{2\beta_{N+1}}, \dots \right) \right]_j (\omega,z) = & \sum_{l=N+1}^{\infty} \frac{\widehat{F}_l(\omega)}{2\beta_l(\omega)} \\
& \times \int_{-\infty}^{\infty} ds\, e^{-\beta_j(\omega)|s|} \mathcal{H}^{\varepsilon}_{jl}(\omega,z+s) e^{-\beta_l(\omega)|s+z|},
\end{aligned}
$$

because it is smaller than the residual at long ranges, due to the exponential decay in z. We also let $C_{jl}(\omega,\mu(z))$ be the leading (order one) part of the coupling matrices defined in (4.39), which we rewrite as

$$
C^{\varepsilon}_{jl}(\omega,\mu(z)) = C_{jl}(\omega,\mu(z)) + \varepsilon c_{jl}(\omega,\mu(z)). \tag{4.43}
$$

Note that the first term in (4.42) is precisely the solution in the ideal waveguide. It is exponentially small at long ranges, so we neglect it in the calculations below.

4.7. Closed system for the propagating modes. — The substitution of (4.42) in equations (4.37)-(4.38) gives a closed system of equations for the amplitudes of the propagating modes. We write it in compact form as

$$
\partial_z \begin{bmatrix} \mathbf{a}(\omega,z) \\ \mathbf{b}(\omega,z) \end{bmatrix} = \left[\varepsilon \boldsymbol{\Upsilon}(\omega,\mu(z),z) + \varepsilon^2 \boldsymbol{\gamma}(\omega,\mu(z),z) + O(\varepsilon^3) \right] \begin{bmatrix} \mathbf{a}(\omega,z) \\ \mathbf{b}(\omega,z) \end{bmatrix}, \tag{4.44}
$$

for the vectors $\mathbf{a}$ and $\mathbf{b}$ with components a_j and b_j, for $j = 1,\dots,N$, and matrices $\boldsymbol{\Upsilon}$ and $\boldsymbol{\gamma}$ with block structure

$$
\boldsymbol{\Upsilon}(\omega,\mu(z),z) = \begin{bmatrix} \boldsymbol{\Upsilon}^{(a)}(\omega,\mu(z),z) & \boldsymbol{\Upsilon}^{(b)}(\omega,(\mu(z),z) \\ \overline{\boldsymbol{\Upsilon}^{(b)}}(\omega,\mu(z),z) & \overline{\boldsymbol{\Upsilon}^{(a)}}(\omega,\mu(z),z) \end{bmatrix}, \tag{4.45}
$$

and

$$
\boldsymbol{\gamma}(\omega,\mu(z),z) = \begin{bmatrix} \boldsymbol{\gamma}^{(a)}(\omega,\mu(z),z) & \boldsymbol{\gamma}^{(b)}(\omega,\mu(z),z) \\ \overline{\boldsymbol{\gamma}^{(b)}}(\omega,\mu(z),z) & \overline{\boldsymbol{\gamma}^{(a)}}(\omega,\mu(z),z) \end{bmatrix}. \tag{4.46}
$$

The leading order $N \times N$ coupling matrices $\boldsymbol{\Upsilon}^{(a,b)}$ have the entries

$$\boldsymbol{\Upsilon}^{(a)}_{jl}(\omega, \mu(z), z) = iC_{jl}(\omega, \mu(z))e^{i[\beta_l(\omega)-\beta_j(\omega)]z}, \tag{4.47}$$

and

$$\boldsymbol{\Upsilon}^{(b)}_{jl}(\omega, \mu(z), z) = i\overline{C_{jl}}(\omega, \mu(z))e^{-i[\beta_l(\omega)+\beta_j(\omega)]z}, \tag{4.48}$$

and the second order coupling matrices are given by

$$\begin{aligned}\boldsymbol{\gamma}^{(a)}_{jl}(\omega, \mu(z), z) = ie^{i[\beta_l(\omega)-\beta_j(\omega)]z}\Big\{c_{jl}(\omega, \mu(z)) + \frac{1}{2\beta_j(\omega)}\sum_{l'>N}\int_{-\infty}^{\infty} ds\, e^{-\beta_{l'}|s|+i\beta_l(\omega)s} \\ \times \left[\beta_{l'}(\omega)Q_{jl'}(\omega, \mu(z))\mathrm{sgn}(s) + M_{jl'}(\omega, \mu(z))\right] C_{l'l}(\omega, \mu(z+s))\Big\},\end{aligned} \tag{4.49}$$

and

$$\begin{aligned}\boldsymbol{\gamma}^{(b)}_{jl}(\omega, \mu(z), z) = -ie^{-i[\beta_l(\omega)+\beta_j(\omega)]z}\Big\{\overline{c_{jl}}(\omega, \mu(z)) + \frac{1}{2\beta_j(\omega)}\sum_{l'>N}\int_{-\infty}^{\infty} ds\, e^{-\beta_{l'}|s|-i\beta_l(\omega)s} \\ \times \left[\beta_{l'}(\omega)Q_{jl'}(\omega, \mu(z))\mathrm{sgn}(s) + M_{jl'}(\omega, \mu(z))\right] \overline{C_{l'l}}(\omega, \mu(z+s))\Big\}.\end{aligned} \tag{4.50}$$

Here we recalled definition (4.43), and wrote similarly the matrices Q^ε and M^ε defined in (4.23)-(4.24)

$$Q^\varepsilon(\mu(z)) = Q(\mu(z)) + O(\varepsilon) \quad \text{and} \quad M^\varepsilon(\mu(z)) = M(\mu(z)) + O(\varepsilon). \tag{4.51}$$

Note that the entries in $\boldsymbol{\Upsilon}$ are linear in the random process μ, and so their expectation is zero,

$$\mathbb{E}\left[\boldsymbol{\Upsilon}^{(a)}_{jl}(\omega, \mu(z), z)\right] = \mathbb{E}\left[\boldsymbol{\Upsilon}^{(b)}_{jl}(\omega, \mu(z), z)\right] = 0, \quad j, l = 1, \ldots, N. \tag{4.52}$$

The entries in $\boldsymbol{\gamma}$ are quadratic in $\mu(z)$, and their expectation is not zero.

4.8. The propagator. — Because $\mathbf{a}(\omega, z)$ satisfies the initial conditions (4.35) at $z = 0$, and $\mathbf{b}(\omega, z)$ satisfies the end conditions (4.30), it is convenient to write the solution of (4.44) in terms of the $2N \times 2N$ propagator matrix $\mathbb{P}(\omega, z)$. It satisfies the evolution equation

$$\partial_z\mathbb{P}(\omega, z) = \left[\varepsilon\boldsymbol{\Upsilon}(\omega, \mu(z), z) + \varepsilon^2\boldsymbol{\gamma}(\omega, \mu(z), z) + O(\varepsilon^3)\right]\mathbb{P}(\omega, z), \tag{4.53}$$

for $z > 0$, and the initial condition

$$\mathbb{P}(\omega, 0) = \mathbf{I}_{2N}, \tag{4.54}$$

where $\mathbf{I}_{2N}$ is the $2N \times 2N$ identity matrix. The solution of (4.44) is given by

$$\begin{bmatrix} \mathbf{a}(\omega, z) \\ \mathbf{b}(\omega, z) \end{bmatrix} = \mathbb{P}(\omega, z) \begin{bmatrix} \mathbf{a}(\omega, 0+) \\ \mathbf{b}(\omega, 0+) \end{bmatrix}, \tag{4.55}$$

with $\mathbf{a}(\omega,0+)$ defined in (4.35), and $\mathbf{b}(\omega,0+)$ determined from the boundary identity

$$\left[\begin{array}{c}\mathbf{a}(\omega,\bar{L}^\varepsilon)\\ \mathbf{0}\end{array}\right] = \mathbb{P}(\omega,\bar{L}^\varepsilon)\left[\begin{array}{c}\mathbf{a}(\omega,0+)\\ \mathbf{b}(\omega,0+)\end{array}\right]. \tag{4.56}$$

The special structure of the coupling matrices in (4.53) implies that if $(\mathbf{a},\mathbf{b})$ is a solution of equations (4.44), then so is $(\overline{\mathbf{b}},\overline{\mathbf{a}})$. Thus, we must have

$$\left[\begin{array}{c}\overline{\mathbf{b}}(\omega,z)\\ \overline{\mathbf{a}}(\omega,z)\end{array}\right] = \mathbb{P}(\omega,z)\left[\begin{array}{c}\overline{\mathbf{b}}(\omega,0+)\\ \overline{\mathbf{a}}(\omega,0+)\end{array}\right], \tag{4.57}$$

in conjunction with (4.55), which implies that the propagator has the block form

$$\mathbb{P}(\omega,z) = \left[\begin{array}{cc}\mathbb{P}^{(a)}(\omega,z) & \mathbb{P}^{(b)}(\omega,z)\\ \overline{\mathbb{P}^{(b)}}(\omega,z) & \overline{\mathbb{P}^{(a)}}(\omega,z)\end{array}\right]. \tag{4.58}$$

The blocks $\mathbb{P}^{(a,b)}(\omega,z)\in\mathbb{C}^{N\times N}$ satisfy the initial conditions

$$\mathbb{P}^{(a)}(\omega,0)=\mathbf{I} \quad \text{and} \quad \mathbb{P}^{(b)}(\omega,0)=\mathbf{0}, \tag{4.59}$$

where $\mathbf{I}$ and $\mathbf{0}$ are the $N\times N$ identity and zero matrices, respectively.

4.9. The long range scaling. — Because the right hand side in the evolution equations (4.53) is of order ε, we expect that there is no net scattering effect over distances of order one, meaning that

$$\lim_{\varepsilon\to 0}\mathbb{P}(\omega,z)=\mathbf{I}_{2N}.$$

If we considered ranges of order ε^{-1}, we would have an order one right hand side in the scaled equations (4.53). Still, there would be no net scattering effect in the limit $\varepsilon\to 0$, because the expectation of the leading term is zero. This is a stochastic averaging result given for example in [**15**, Section 6.4]. It takes longer ranges, of order ε^{-2} to see net scattering effects, so we let $z=Z/\varepsilon^2$, with scaled range Z of order one. This means in particular that the limit range of the fluctuations is $\bar{L}^\varepsilon=\bar{L}/\varepsilon^2$.

We denote the propagator in this long range scaling by

$$\mathbb{P}^\varepsilon(\omega,Z)=\mathbb{P}\left(\omega,\frac{Z}{\varepsilon^2}\right), \tag{4.60}$$

and obtain from (4.53) that it satisfies the equations

$$\partial_Z\mathbb{P}^\varepsilon(\omega,Z)=\left[\frac{1}{\varepsilon}\boldsymbol{\Upsilon}\left(\omega,\mu\left(\frac{Z}{\varepsilon^2}\right),\frac{Z}{\varepsilon^2}\right)+\boldsymbol{\gamma}\left(\omega,\mu\left(\frac{Z}{\varepsilon^2}\right),\frac{Z}{\varepsilon^2}\right)+O(\varepsilon)\right]\mathbb{P}^\varepsilon(\omega,Z), \tag{4.61}$$

with initial conditions

$$\mathbb{P}^\varepsilon(\omega,0)=\mathbf{I}_{2N}. \tag{4.62}$$

Recall the block structure (4.58) of the generator. The off-diagonal blocks $\mathbb{P}^{\varepsilon(b)}(\omega, Z)$ satisfy homogeneous initial conditions. They couple the forward and backward propagating waves, and we show in section 4.11 that they are negligible in the $\varepsilon \to 0$ limit if the correlation length is larger than the wavelength. We recall first the theorem that gives the limit of $\mathbb{P}^{\varepsilon}(\omega, Z)$.

4.10. The diffusion approximation. — The system (4.61) belongs to the general class of problems that can be analyzed in the limit $\varepsilon \to 0$ with the diffusion approximation limit theorem. This theorem is stated in [**15**, Section 6.5], and we refer to [**23, 24**] for its proof. We summarize it briefly.

Consider a system of stochastic differential equations of the form

$$\partial_Z \mathcal{X}^{\varepsilon}(Z) = \frac{1}{\varepsilon}\mathcal{F}^{(0)}\left(\mathcal{X}^{\varepsilon}(Z), \mu\left(\frac{Z}{\varepsilon^2}\right), \frac{Z}{\varepsilon^2}\right) + \mathcal{F}^{(1)}\left(\mathcal{X}^{\varepsilon}(Z), \mu\left(\frac{Z}{\varepsilon^2}\right), \frac{Z}{\varepsilon^2}\right), \tag{4.63}$$

for $Z > 0$ and vector or matrix valued $\mathcal{X}^{\varepsilon}(Z)$ with real entries, satisfying the initial conditions

$$\mathcal{X}^{\varepsilon}(0) = \mathcal{X}_o. \tag{4.64}$$

The functions $\mathcal{F}^{(0,1)}(\mathcal{X}, \mu, \tau)$ are at most linearly growing and smooth in $\mathcal{X}$, and the dependence in τ is periodic, or almost periodic. Moreover, $\mathcal{F}^{(0)}(\mathcal{X}, \mu, \tau)$ is centered, meaning that for any fixed $\mathcal{X}$ and τ,

$$\mathbb{E}[\mathcal{F}^{(0)}(\mathcal{X}, \mu, \tau)] = 0.$$

All these assumptions are satisfied in our case: The right hand side in (4.61) is linear in $\mathbb{P}^{\varepsilon}$, the matrices $\boldsymbol{\Upsilon}$ and $\boldsymbol{\gamma}$ are periodic in the last argument, and $\mathbb{E}[\boldsymbol{\Upsilon}] = 0$.

The diffusion approximation theorem states that as $\varepsilon \to 0$, $\mathcal{X}^{\varepsilon}(z)$ converges in distribution to the diffusion Markov process $\mathcal{X}(z)$ with generator $\mathcal{G}$ acting on smooth functions $\varphi(\mathcal{X})$ as

$$\begin{aligned}\mathcal{G}\varphi(\mathcal{X}) = \lim_{T\to\infty} \frac{1}{T}\int_0^T d\tau \int_0^\infty dz\, \mathbb{E}\left[\mathcal{F}^{(0)}(\mathcal{X}, \mu(0), \tau) \cdot \nabla_{\mathcal{X}}\left[\mathcal{F}^{(0)}(\mathcal{X}, \mu(z), \tau + z) \cdot \nabla_{\mathcal{X}}\varphi(\mathcal{X})\right]\right] \\ + \frac{1}{T}\int_0^T d\tau\, \mathbb{E}\left[\mathcal{F}^{(1)}(\mathcal{X}, \mu(0), \tau) \cdot \nabla_{\mathcal{X}}\varphi(\mathcal{X})\right].\end{aligned} \tag{4.65}$$

We can apply it to our problem by letting $\mathcal{X}^{\varepsilon}$ be the matrix in $\mathbb{R}^{4N\times 4N}$ obtained by concatenating the absolute values and phases of the entries in the propagator $\mathbb{P}^{\varepsilon}$.

4.11. The forward scattering approximation. — When we use the diffusion limit theorem described above, we obtain that the limit entries of $\mathbb{P}^{\varepsilon(b)}(z)$ are coupled to the limit entries of $\mathbb{P}^{\varepsilon(a)}(z)$ by coefficients that are proportional to

$$\widehat{\mathcal{R}}_{\mu}(\beta_j + \beta_l) = 2\int_0^\infty dz\, \mathcal{R}_{\mu}(z)\cos[(\beta_j + \beta_l)z],$$

for $j,l=1,\dots,N$. Here $\widehat{\mathcal{R}}_\mu$ is the power spectral density of the process μ, the Fourier transform of the covariance $\mathcal{R}_\mu$. It is evaluated at the sum of the wavenumbers because the phase factors present in the matrices $\boldsymbol{\Upsilon}^{(b)}$ and $\boldsymbol{\gamma}^{(b)}$ are $(\beta_j+\beta_l)z$. The phases in the matrices $\boldsymbol{\Upsilon}^{(a)}$ and $\boldsymbol{\gamma}^{(a)}$ are $(\beta_j-\beta_l)z$, so the limit entries of $\mathbb{P}^{\varepsilon(a)}(z)$ are coupled to each other through $\widehat{\mathcal{R}}_\mu(\beta_j-\beta_l)$, for $j,l=1,\dots,N$.

The forward scattering approximation is based on the assumption that the power spectral density decays fast enough to get

$$\widehat{\mathcal{R}}_\mu(\beta_j+\beta_l)\approx 0\,,\quad \text{for } j,l=1,\dots,N. \tag{4.66}$$

If this is true, $\mathbb{P}^{\varepsilon(a)}$ and $\mathbb{P}^{\varepsilon(b)}$ decouple in the limit. Equivalently, the forward and backward going wave amplitudes are asymptotically decoupled, and due to the boundary conditions $\mathbf{b}(\omega,\bar{L^\varepsilon})=0$, we may neglect the backward going waves.

To illustrate the assumption (4.66), consider the Gaussian covariance

$$\mathcal{R}_\mu(z)=e^{-\frac{z^2}{2\ell^2}}. \tag{4.67}$$

The wavenumbers decrease monotonically in the index j, so assumption (4.66) holds if the power spectral density

$$\widehat{\mathcal{R}}_\mu(\beta)=\sqrt{2\pi}\ell e^{-\frac{\beta^2\ell^2}{2}}.$$

satisfies

$$\widehat{\mathcal{R}}_\mu(\beta)\approx 0,\quad \forall \beta\geq 2\beta_N(\omega).$$

Explicitly, we need that

$$2\beta_N(\omega)=\frac{2\pi}{\mathfrak{D}}\sqrt{2\vartheta(\omega)N}\approx 2k\sqrt{\frac{2\vartheta(\omega)}{N}}\geq\frac{3}{\ell} \tag{4.68}$$

where we recalled definition (3.16) of N and $\vartheta(\omega)$. Thus, the forward scattering approximation is valid when the correlation length is larger than the wavelength

$$\frac{k\ell}{2\pi}=\frac{\ell}{\lambda}\gtrsim\sqrt{N}. \tag{4.69}$$

As before, the symbol $\gtrsim$ stands for larger or equal up to a multiplicative constant of order one.

4.12. The asymptotic limit. — Gathering the results, we can approximate the acoustic pressure field as

$$p\left(t,y,\frac{Z}{\varepsilon^2}\right)\approx\int_{-\infty}^{\infty}\frac{d\omega}{2\pi}\sum_{j=1}^{N}\phi_j(y)a_j^\varepsilon(\omega,Z)e^{i\beta_j(\omega)\frac{Z}{\varepsilon^2}-i\omega t}, \tag{4.70}$$

with mode amplitudes $\{a_j^\varepsilon(\omega, Z)\}_{j=1,\dots,N}$ converging in distribution as $\varepsilon \to 0$ to a complex valued diffusion Markov process

$$a_j^\varepsilon(\omega, Z) \rightharpoonup \frac{\alpha_j(\omega, Z)}{\sqrt{\beta_j(\omega)}}. \tag{4.71}$$

We write the limit process as

$$\alpha_j(\omega, Z) = \mathcal{P}_j^{1/2}(\omega, Z) e^{i\theta_j(\omega, Z)}, \tag{4.72}$$

with phases $\theta_j(\omega, z)$, and scaled powers

$$\mathcal{P}_j(\omega, Z) = |\alpha_j(\omega, Z)|^2, \quad j = 1, \dots, N. \tag{4.73}$$

The scaling by $\sqrt{\beta_j}$ in (4.71) symmetrizes the constant coefficient matrices that appear in the infinitesimal generator $\mathcal{G}$ given by

$$\mathcal{G} = \mathcal{G}_{\mathcal{P}} + \mathcal{G}_\theta. \tag{4.74}$$

The first term is a partial differential operator in the powers

$$\mathcal{G}_{\mathcal{P}} = \sum_{\substack{j,\, l\, =\, 1 \\ j\, \neq\, l}}^{N} \Gamma_{jl}^{(c)}(\omega) \left[\mathcal{P}_l \mathcal{P}_j \left(\frac{\partial}{\partial \mathcal{P}_j} - \frac{\partial}{\partial \mathcal{P}_l} \right) \frac{\partial}{\partial \mathcal{P}_j} + (\mathcal{P}_l - \mathcal{P}_j) \frac{\partial}{\partial \mathcal{P}_j} \right], \tag{4.75}$$

and the second term is a partial differential operator in the phases

$$\begin{aligned} \mathcal{G}_\theta = \frac{1}{4} \sum_{\substack{j,\, l\, =\, 1 \\ j\, \neq\, l}}^{N} \Gamma_{jl}^{(c)}(\omega) \left[\frac{P_j}{P_l} \frac{\partial^2}{\partial \theta_l^2} + \frac{P_l}{P_j} \frac{\partial^2}{\partial \theta_j^2} + 2 \frac{\partial^2}{\partial \theta_j \partial \theta_l} \right] + \frac{1}{2} \sum_{j,l=1}^{N} \Gamma_{jl}(\omega) \frac{\partial^2}{\partial \theta_j \partial \theta_l} \\ + \frac{1}{2} \sum_{\substack{j,\, l\, =\, 1 \\ j\, \neq\, l}}^{N} \Gamma_{jl}^{(s)}(\omega) \frac{\partial}{\partial \theta_j} + \sum_{j=1}^{N} \kappa_j(\omega) \frac{\partial}{\partial \theta_j}. \end{aligned} \tag{4.76}$$

We denote henceforth multiple sums by multiple summation indexes. That is to say

$$\sum_{j,l=1}^{N} \equiv \sum_{j=1}^{N} \sum_{l=1}^{N}.$$

Now let us describe the matrices of coefficients in the generator, which depend on the covariance $\mathcal{R}_\mu$ of the random process μ. The matrix $\Gamma^{(c)}(\omega)$ is symmetric, with rows summing to zero

$$\Gamma_{jj}^{(c)}(\omega) = -\sum_{l \neq j} \Gamma_{jl}^{(c)}(\omega) < 0, \tag{4.77}$$

and non-negative off-diagonal entries

$$\Gamma_{jl}^{(c)}(\omega) = \frac{\mathfrak{D}^2}{4\beta_j(\omega)\beta_l(\omega)} \left[\phi_j'(\mathfrak{D}) \phi_l'(\mathfrak{D}) \right]^2 \widehat{\mathcal{R}}_\mu[\beta_j(\omega) - \beta_l(\omega)], \quad j \neq l. \tag{4.78}$$

This is because $\widehat{\mathcal{R}}_\mu(\beta) \geq 0$ for any $\beta \in \mathbb{R}$, by Bochner's theorem. The matrix $\Gamma(\omega)$ is similar, but all its entries are positive and given by

$$\Gamma_{jl}(\omega) = \frac{\mathfrak{D}^2}{4\beta_j(\omega)\beta_l(\omega)} \left[\phi_j'(\mathfrak{D})\phi_l'(\mathfrak{D})\right]^2 \widehat{\mathcal{R}}_\mu(0) > 0. \tag{4.79}$$

The matrix $\Gamma^{(s)}(\omega)$ has the off-diagonal entries

$$\Gamma^{(s)}_{jl}(\omega) = \frac{\mathfrak{D}^2}{2\beta_j(\omega)\beta_l(\omega)} \left[\phi_j'(\mathfrak{D})\phi_l'(\mathfrak{D})\right]^2 \int_0^\infty dz\, \sin\left[(\beta_j(\omega) - \beta_l(\omega))z\right] \mathcal{R}_\mu(z) \tag{4.80}$$

which may be positive or negative, and its rows sum to zero

$$\Gamma^{(s)}_{jj}(\omega) = -\sum_{l\neq j} \Gamma^{(s)}_{jl}(\omega). \tag{4.81}$$

All the terms in the generator except for the last one in (4.76) are due to the leading order term in the evolution equation for the amplitudes a_j^ε, which is not affected by the evanescent modes. The second order term in the evolution equations gives

$$\lim_{T\to\infty} \int_0^T d\tau\, \mathbb{E}\left[\boldsymbol{\gamma}^a_{j,l}(\omega, \mu(0), \tau)\right] = i\kappa_j(\omega)\delta_{jl}. \tag{4.82}$$

The matrix is diagonal because of the phase $(\beta_j - \beta_l)\tau$, and after a straightforward calculation we obtain that the result is imaginary. Given the expression (4.49) of $\boldsymbol{\gamma}^{(a)}$ we see that

$$\kappa_j(\omega) = \kappa_j^{(a)}(\omega) + \kappa_j^{(e)}(\omega), \tag{4.83}$$

with the first part due to the direct coupling of the propagating modes, and the second due to the coupling via the evanescent modes. We have

$$\begin{aligned} \kappa_j^{(a)}(\omega) &= \mathbb{E}\left[c_{jj}(\omega, \mu(0))\right] \\ &= -\frac{1}{2\beta_j(\omega)} \left\{ 3\left(\frac{\pi j}{\mathfrak{D}}\right)^2 + \frac{1}{\ell^2} \int_0^{\mathfrak{D}} dy \left[y^2\phi_j'(y) + y\phi_j(y)\right] \phi_j'(y) \right\}, \end{aligned} \tag{4.84}$$

and $\kappa_j^{(e)}$ follows similarly.

The asymptotic limit described in this section allows us to analyze imaging and time reversal with remote arrays. Given the generator, we can compute the statistical moments of the wave field in order to understand the loss of coherence due to scattering, and the propagation of energy. Before we do so, we show next that the result in waveguides with randomly fluctuating wave speed is very similar. In fact, the generator of the limit diffusion process is exactly the same. However, the coefficients $\Gamma^{(c)}_{jl}$, $\Gamma^{(o)}_{jl}$, $\Gamma^{(s)}_{jl}$ and κ_j are not the same. Thus, random boundaries and random interior inhomogeneities have different scattering effects, as explained in section 6.

5. Waveguides with random internal inhomogeneities

Consider two dimensional random waveguides with interior inhomogeneities, but flat boundaries. We model the inhomogeneities as random fluctuations of the sound speed, so that

$$\frac{c_o^2}{c^2(y,z)} = 1 + 1_{(0,\bar{L}^\varepsilon)}(z)\,\varepsilon\nu(y,z), \tag{5.1}$$

for $y \in (0,\mathfrak{D})$ and $z \in \mathbb{R}$. The mean zero stationary random function $\nu(y,z)$ is bounded and mixing, with integrable covariance

$$\mathcal{R}_\nu(y,z) = \mathbb{E}\left[\nu(y+y',z+z')\nu(y',z')\right]. \tag{5.2}$$

We normalize the covariance by $\mathcal{R}_\nu(0) = 1$, and consider weak fluctuations with amplitude scaled by $\varepsilon \ll 1$. The fluctuations are isotropic, with correlation length ℓ, and we motivate their confinement to the range interval $(0,\bar{L}^\varepsilon)$ with $\bar{L}^\varepsilon = \bar{L}/\varepsilon^2$ as before.

The Fourier transform $\widehat{p}(\omega,y,z)$ of the pressure field satisfies a similar equation to (4.12) for $z \in (0,\bar{L}^\varepsilon)$,

$$\mathcal{L}^\varepsilon \widehat{p}(\omega,y,z) = 0, \quad y \in (0,\mathfrak{D}), \tag{5.3}$$

with homogeneous Dirichlet boundary conditions

$$\widehat{p}(\omega,0,z) = \widehat{p}(\omega,\mathfrak{D},z) = 0. \tag{5.4}$$

The partial differential operator $\mathcal{L}^\varepsilon$ is the same to leading order, but it has a different $O(\varepsilon)$ part,

$$\mathcal{L}^\varepsilon = \partial_z^2 + \partial_y^2 + k^2 + 1_{(0,\bar{L}^\varepsilon)}(z)\,\varepsilon k^2\nu(y,z). \tag{5.5}$$

The analysis is exactly as before. We decompose $\widehat{p}$ in the waveguide modes, solve for the evanescent part in terms of the propagating amplitudes, and obtain a closed system of equations that looks the same as (4.44). The entries in the matrices $\boldsymbol{\Upsilon}^{(a),(b)}$ are of the form (4.47)-(4.48), but the random matrices C_{jl} have a different expression

$$C_{jl}(\omega,z) = \frac{k^2}{2\beta_j(\omega)\beta_l(\omega)} \int_0^{\mathfrak{D}} dy\,\nu(y,z)\phi_j(y)\phi_l(y). \tag{5.6}$$

The second order matrices $\boldsymbol{\gamma}^{(a),(b)}$ are due only to the coupling via the evanescent modes. The first is given by

$$\boldsymbol{\gamma}_{jl}^{(a)}(\omega,\nu,z) = ie^{i[\beta_l(\omega)-\beta_j(\omega)]z} \sum_{l'>N} \int_{-\infty}^{\infty} ds\, e^{-\beta_{l'}|s|+i\beta_l(\omega)s} \frac{C_{jl'}(\omega,z)C_{ll'}(\omega,z+s)}{2\beta_j(\omega)\beta_l(\omega)\beta_{l'}(\omega)},$$

and the second by

$$\boldsymbol{\gamma}_{jl}^{(b)}(\omega,\nu,z) = -ie^{-i[\beta_l(\omega)-\beta_j(\omega)]z} \sum_{l'>N} \int_{-\infty}^{\infty} ds\, e^{-\beta_{l'}|s|-i\beta_l(\omega)s} \frac{C_{jl'}(\omega,z)C_{ll'}(\omega,z+s)}{2\beta_j(\omega)\beta_l(\omega)\beta_{l'}(\omega)}.$$

5.1. The asymptotic limit. — Since the coupled system of equations has the same form as (4.44), we can write directly the asymptotic approximation of the acoustic pressure

$$p\left(t, y, \frac{Z}{\varepsilon^2}\right) \approx \int_{-\infty}^{\infty} \frac{d\omega}{2\pi} \sum_{j=1}^{N} \phi_j(y) a_j^{\varepsilon}(\omega, Z) e^{i\beta_j(\omega)\frac{Z}{\varepsilon^2} - i\omega t}. \tag{5.7}$$

Here we used the forward scattering approximation justified as before, based on the assumption that the correlation length is large with respect to the wavelength. The mode amplitudes $\{a_j^{\varepsilon}(\omega, Z)\}_{j=1,\ldots,N}$ converge in distribution as $\varepsilon \to 0$ to a complex valued diffusion Markov process

$$a_j^{\varepsilon}(\omega, Z) \rightharpoonup \frac{\alpha_j(\omega, Z)}{\sqrt{\beta_j(\omega)}}, \qquad \alpha_j(\omega, Z) = \mathcal{P}_j^{1/2}(\omega, Z) e^{i\theta_j(\omega, Z)}. \tag{5.8}$$

The infinitesimal generator is given by (4.74)-(4.76), but the matrices of coefficients are different.

The symmetric matrix $\Gamma^{(c)}(\omega)$ has the off-diagonal entries

$$\begin{aligned} \Gamma_{jl}^{(c)}(\omega) = \frac{k^4}{4\beta_j(\omega)\beta_l(\omega)} \int_{-\infty}^{\infty} dz \cos[(\beta_j(\omega) - \beta_l(\omega))z] \\ \times \int_0^{\mathfrak{D}} dy \int_0^{\mathfrak{D}} dy' \mathcal{R}_\nu(y - y', z) \phi_j(y) \phi_l(y) \phi_j(y') \phi_l(y'), \end{aligned} \tag{5.9}$$

and its rows sum to zero. Thus, the diagonal entries are given by

$$\Gamma_{jj}^{(c)}(\omega) = -\sum_{l \neq j} \Gamma_{jl}^{(c)}(\omega) \ < 0. \tag{5.10}$$

Because $\Gamma_{jl}^{(c)}$ are proportional to the power spectral densities of the stationary random processes C_{jl} defined in (5.6), they are non-negative by Bochner's theorem. The symmetric matrix $\Gamma(\omega)$ has the entries

$$\Gamma_{jl}(\omega) = \frac{k^4}{4\beta_j(\omega)\beta_l(\omega)} \int_{-\infty}^{\infty} dz \int_0^{\mathfrak{D}} dy \int_0^{\mathfrak{D}} dy' \, \mathcal{R}_\nu(y - y', z) \phi_j^2(y) \phi_l^2(y'), \tag{5.11}$$

for all $l, j = 1, \ldots, N$. Its diagonal Γ_{jj} is positive, because it is proportional to the power spectral density of C_{jj}, evaluated at zero.

The matrix $\Gamma^{(s)}$ has the off-diagonal entries

$$\begin{aligned} \Gamma_{jl}^{(s)}(\omega) = \frac{k^4}{2\beta_j(\omega)\beta_l(\omega)} \int_0^{\infty} dz \sin[(\beta_j(\omega) - \beta_l(\omega))z] \\ \times \int_0^{\mathfrak{D}} dy \int_0^{\mathfrak{D}} dy' \mathcal{R}_\nu(y - y', z) \phi_j(y) \phi_l(y) \phi_j(y') \phi_l(y'), \end{aligned} \tag{5.12}$$

that may be positive or negative, and its rows sum to zero

$$\Gamma^{(s)}_{jj}(\omega) = -\sum_{l\neq j} \Gamma^{(s)}_{jl}(\omega)\,. \tag{5.13}$$

Finally, the coefficient κ_j in the last term of the generator $\mathcal{G}_\theta$ is due only to the evanescent modes,

$$\kappa_j(\omega) = \kappa^{(e)}_j(\omega). \tag{5.14}$$

Its expression follows from the expectation of $\boldsymbol{\gamma}^{(a)}(\omega,\nu,\tau)$ averaged over the phase τ, as in (4.82).

6. Net scattering effects

In this section we describe the statistics of the moment amplitudes, with emphasis on the first and second moments. They allow us to understand the loss of coherence and the mode decorrelation due to scattering. We also compare the results in the two types of waveguides: with boundary fluctuations and with interior inhomogeneities. But first, we make some general remarks.

Remark 1. — *The coefficients of the partial derivatives in the powers $\mathcal{P}_j$ in the generator $\mathcal{G}$ depend only on $\{\mathcal{P}_j\}_{j=1,\dots,N}$. This means that the scaled mode powers $\{\beta_j|a^\varepsilon_j|^2\}_{j=1,\dots,N}$ converge in distribution as $\varepsilon\to 0$ to the diffusion Markov process $\{|\alpha_j|^2=\mathcal{P}_j\}_{j=1,\dots,N}$ with generator $\mathcal{G}_\mathcal{P}$ given in (4.75).*

Remark 2. — *The evanescent waves influence only the coefficient κ_j in the last term of $\mathcal{G}_\theta$. Since they do not appear in $\mathcal{G}_\mathcal{P}$, they do not change the energy of the propagating modes in the limit $\varepsilon\to 0$. Moreover, since κ_j is in the diagonal part of $\mathcal{G}_\theta$, they do not affect the mode coupling as $\varepsilon\to 0$. The only effect of the evanescent modes is a mode and frequency dependent phase modulation.*

Remark 3. — *The symmetry of the matrix $\Gamma^{(c)}$ of coefficients in $\mathcal{G}_\mathcal{P}$ gives that*

$$\mathcal{G}_\mathcal{P}\Big(\sum_{j=1}^N \mathcal{P}_j\Big) = \sum_{\substack{j,\,l\,=\,1\\ j\,\neq\,l}}^N \Gamma^{(c)}_{jl}(\omega)(\mathcal{P}_l-\mathcal{P}_j) = 0. \tag{6.1}$$

Thus, the energy of the limit diffusion process is conserved. The process $\{\alpha_j\}_{j=1,\dots,N}$ is supported on the sphere in $\mathbb{C}^N$ centered at zero and of radius

$$r_{_\mathcal{P}}(\omega) = \sum_{j=1}^N |\alpha_j(\omega,0)|^2 = \sum_{j=1}^N \beta_j(\omega)|a_{j,o}(\omega)|^2 = \sum_{j=1}^N \frac{|\widehat{F}_j(\omega)|^2}{4\beta_j(\omega)}. \tag{6.2}$$

Here we used the initial conditions (4.35). We will see later that if we let $Z\to\infty$, the process becomes uniformly distributed over this sphere. This is the equipartition limit where the waves forget their initial state, and imaging becomes impossible.

6.1. Single frequency moments. — The results stated in section 4.12 give after a direct calculation that uses the expression of the generator $\mathcal{G}$, that

$$\mathbb{E}\left[a_j^\varepsilon(\omega,Z)\right] \stackrel{\varepsilon\to 0}{\longrightarrow} \frac{\mathbb{E}\left[\alpha_j(\omega,Z)\right]}{\sqrt{\beta_j(\omega)}} = a_{j,o}(\omega) e^{\left[\frac{\Gamma_{jj}^{(c)}(\omega)-\Gamma_{jj}(\omega)}{2}\right]Z + i\left[\frac{\Gamma_{jj}^{(s)}(\omega)}{2}+\kappa_j(\omega)\right]Z}, \tag{6.3}$$

where $a_{j,o}(\omega)$ is the amplitude in the ideal waveguide, given by (3.12). Thus, the mode amplitudes of the coherent (mean) pressure field $\mathbb{E}[p]$ are not the same as in the ideal waveguide. They decay exponentially with Z, because

$$\Gamma_{jj}^{(c)} - \Gamma_{jj} < 0.$$

The mode powers satisfy

$$\mathbb{E}\left[|a_j^\varepsilon(\omega,Z)|^2\right] \stackrel{\varepsilon\to 0}{\longrightarrow} \frac{\mathbb{E}\left[\mathcal{P}_j(\omega,Z)\right]}{\beta_j(\omega)} = \frac{\langle \mathcal{P}_j\rangle(\omega,Z)}{\beta_j(\omega)}, \tag{6.4}$$

where $\langle \mathcal{P}_j\rangle$ is the solution of the initial value problem

$$\begin{aligned}
\partial_Z \langle \mathcal{P}_j\rangle(\omega,Z) &= \sum_{l=1}^N \Gamma_{jl}^{(c)}(\omega)\left[\langle \mathcal{P}_l\rangle(\omega,Z) - \langle \mathcal{P}_j\rangle(\omega,Z)\right], \quad Z>0,\\
\langle \mathcal{P}_j\rangle(\omega,0) &= \beta_j(\omega)|a_{j,o}(\omega)|^2, \qquad j=1,\ldots,N.
\end{aligned}$$

Because the rows of $\Gamma^{(c)}$ sum to zero, we can write the system in vector form

$$\partial_Z \begin{pmatrix} \langle \mathcal{P}_1\rangle(\omega,Z) \\ \vdots \\ \langle \mathcal{P}_N\rangle(\omega,Z) \end{pmatrix} = \Gamma^{(c)}(\omega) \begin{pmatrix} \langle \mathcal{P}_1\rangle(\omega,Z) \\ \vdots \\ \langle \mathcal{P}_N\rangle(\omega,Z) \end{pmatrix}$$

and obtain that

$$\begin{pmatrix} \langle \mathcal{P}_1\rangle(\omega,Z) \\ \vdots \\ \langle \mathcal{P}_N\rangle(\omega,Z) \end{pmatrix} = e^{\Gamma^{(c)}(\omega)Z} \begin{pmatrix} \beta_1(\omega)|a_{1,o}(\omega)|^2 \\ \vdots \\ \beta_N(\omega)|a_{N,o}(\omega)|^2 \end{pmatrix}. \tag{6.5}$$

We already know that $\Gamma_{jl}^{(c)} \geq 0$, for $j \neq l$. If we assume in addition that they are not zero, meaning that the power spectral density of the fluctuations evaluated at $\beta_j - \beta_l$ does not vanish, we can use the Perron-Frobenius theorem to describe the matrix exponential in (6.5). Because $\Gamma_{jl}^{(c)}$ is symmetric, it has real eigenvalues denoted by $\Lambda_j(\omega)$ and orthonormal eigenvectors $\mathbf{u}_j$, for $j=1,\ldots,N$. The Perron-Frobenius theorem states that the largest eigenvalue is simple

$$\Lambda_N(\omega) \leq \ldots \leq \Lambda_2(\omega) < \Lambda_1(\omega),$$

and the components of the leading eigenvector $\mathbf{u}_1$ have the same sign. In our case

$$\Lambda_1(\omega) = 0 \quad \text{and} \quad \mathbf{u}_1 = \frac{1}{\sqrt{N}} \begin{pmatrix} 1 \\ \vdots \\ 1 \end{pmatrix}.$$

Thus, the solution of (6.5) is given by

$$\begin{pmatrix} \langle \mathcal{P}_1 \rangle (\omega, Z) \\ \vdots \\ \langle \mathcal{P}_N \rangle (\omega, Z) \end{pmatrix} = \sum_{j=1}^{N} e^{\Lambda_j(\omega) Z} \, \mathbf{u}_j \mathbf{u}_j^T \begin{pmatrix} \beta_1(\omega) |a_{1,o}(\omega)|^2 \\ \vdots \\ \beta_N(\omega) |a_{N,o}(\omega)|^2 \end{pmatrix}, \tag{6.6}$$

and as Z grows, all the terms in the sum, except the first one decay exponentially to zero. More explicitly,

$$\sup_{j=1,\dots N} \left| \langle \mathcal{P}_j \rangle (\omega, Z) - \frac{r_{\mathcal{P}}(\omega)}{N} \right| \leq O\left(e^{-|\Lambda_2(\omega)| Z} \right), \tag{6.7}$$

so the mode powers converge to the uniform distribution on the sphere of radius $r_{\mathcal{P}}(\omega)$ defined in Remark 3.

Because $\mathbb{E}[\alpha_j]$ decays exponentially with Z, its signal to noise ratio (SNR)

$$\mathrm{SNR}_j(\omega) = \frac{|\mathbb{E}[\alpha_j(\omega, Z)]|}{\sqrt{\langle \mathcal{P}_j \rangle (\omega, Z) - |\mathbb{E}[\alpha_j(\omega, Z)]|^2}} \sim e^{-Z/\mathcal{S}_j(\omega)} \tag{6.8}$$

decays on the scale

$$\mathcal{S}_j(\omega) = \frac{2}{\Gamma_{jj}(\omega) - \Gamma_{jj}^{(c)}(\omega)}. \tag{6.9}$$

We call $\mathcal{S}_j(\omega)$ the *scattering mean free path*. It is the range scale over which the mode loses its coherence, meaning that its mean is dominated by the random fluctuations.

To quantify the fluctuations of the mode powers, we need the fourth order moments

$$\langle \mathcal{P}_{jl} \rangle (\omega, z) = \mathbb{E}\left[\mathcal{P}_j(\omega, Z) \mathcal{P}_l(\omega, Z) \right]. \tag{6.10}$$

They satisfy the differential equations

$$\partial_Z \langle \mathcal{P}_{jj} \rangle (\omega, z) = -2\Gamma_{jj}^{(c)}(\omega) \langle \mathcal{P}_{jj} \rangle (\omega, z) + 4 \sum_{n=1}^{N} \Gamma_{jn}^{(c)}(\omega) \langle \mathcal{P}_{jn} \rangle (\omega, z), \tag{6.11}$$

for $j = l = 1, \dots, N$ and

$$\begin{aligned} \partial_Z \langle \mathcal{P}_{jl} \rangle (\omega, z) &= -2\Gamma_{jl}^{(c)}(\omega) \langle \mathcal{P}_{jl} \rangle (\omega, z) \\ &\quad + \sum_{n=1}^{N} \left[\Gamma_{jn}^{(c)}(\omega) \langle \mathcal{P}_{nl} \rangle (\omega, z) + \Gamma_{ln}^{(c)}(\omega) \langle \mathcal{P}_{jn} \rangle (\omega, z) \right], \end{aligned} \tag{6.12}$$

for $j \neq l$, and the initial conditions

$$\langle \mathcal{P}_{jl} \rangle (\omega, 0) = \beta_j(\omega)\beta_l(\omega)|a_{j,o}(\omega)a_{l,o}(\omega)|^2, \qquad j,l = 1,\ldots,N. \tag{6.13}$$

This linear system can be put in matrix form, and analyzed using the Perron-Frobenius theorem, as before. Again, the simple leading eigenvalue is zero, so as Z grows, the solution tends to the stationary one, lying in the span of the leading eigenvector. The components of this normalized eigenvector are $(1+\delta_{jl})/\sqrt{N(N+1)}$, so we obtain that

$$\langle \mathcal{P}_{jl} \rangle (\omega, Z) \stackrel{Z\to\infty}{\longrightarrow} \begin{cases} \frac{r^2_{\mathcal{P}}(\omega)}{N(N+1)}, & \text{if } j \neq l, \\ \frac{2r^2_{\mathcal{P}}(\omega)}{N(N+1)}, & \text{if } j = l. \end{cases} \tag{6.14}$$

The variance of the mode powers follows from (6.14) and (6.7)

$$\mathrm{var}(\mathcal{P}_j) = \langle \mathcal{P}_{jj} \rangle (\omega, Z) - \left[\langle \mathcal{P}_j \rangle (\omega, Z)\right]^2 \stackrel{Z\to\infty}{\longrightarrow} \frac{r^2_{\mathcal{P}}(\omega)(N-1)}{N^2(N+1)} \approx \frac{r^2_{\mathcal{P}}(\omega)}{N^2}, \tag{6.15}$$

where the approximation is for $N \gg 1$. Thus, the standard deviation $[\mathrm{var}(\mathcal{P}_j)]^{1/2}$ of the powers is approximately the same as their mean $\langle \mathcal{P}_j \rangle$. The fluctuations do not overwhelm the coherent (mean) part, but they are significant. The mode powers are not deterministic. In fact, it is shown in [**15**, Section 20.3.4] that in the limit $Z \to \infty$ and for $N \gg 1$, they are approximately exponential random variables, with mean $r_{\mathcal{P}}(\omega)/N$.

We also get from (6.14) and (6.7) that the covariance satisfies

$$\mathrm{cov}(\mathcal{P}_j, \mathcal{P}_l) = \langle \mathcal{P}_{jl} \rangle (\omega, Z) - \langle \mathcal{P}_j \rangle (\omega, Z) \langle \mathcal{P}_l \rangle (\omega, Z) \stackrel{Z\to\infty}{\longrightarrow} \frac{-r^2_{\mathcal{P}}(\omega)}{N^2(N+1)} \tag{6.16}$$

for $j \neq l$. The correlation of the mode powers is

$$\mathrm{corr}(\mathcal{P}_j, \mathcal{P}_l) = \frac{\mathrm{cov}(\mathcal{P}_j, \mathcal{P}_l)}{\sqrt{\mathrm{var}(\mathcal{P}_j)\mathrm{var}(\mathcal{P}_l)}} \stackrel{Z\to\infty}{\longrightarrow} \frac{-1}{N-1}, \tag{6.17}$$

and if $N \gg 1$, we see that the modes are essentially uncorrelated at long ranges.

Remark 4. — *We can also state the results in terms of the limit propagator* $\mathbb{P}^{(\alpha)}(\omega, Z)$*, the matrix in* $\mathbb{C}^{N\times N}$ *that maps the initial conditions*

$$\alpha_j(\omega, 0) = \sqrt{\beta_j(\omega)}a_{j,o}(\omega) = \frac{\widehat{F}_j(\omega)}{2i\sqrt{\beta_j(\omega)}} \tag{6.18}$$

to the range dependent limit amplitudes

$$\alpha_j(\omega, Z) = \sum_{l=1}^{N} \mathbb{P}^{(\alpha)}_{jl}(\omega, Z)\alpha_l(\omega, 0), \qquad Z > 0. \tag{6.19}$$

We have the convergence in distribution

$$\mathbb{P}^{\varepsilon(a)}(\omega,Z) \overset{\varepsilon\to 0}{\rightharpoonup} \mathfrak{B}^{-\frac{1}{2}}(\omega)\mathbb{P}^{\alpha}(\omega,Z)\mathfrak{B}^{\frac{1}{2}}(\omega), \tag{6.20}$$

where $\mathfrak{B}$ *is the diagonal matrix*

$$\mathfrak{B}(\omega) = diag\,(\beta_1(\omega),\ldots,\beta_N(\omega))\,. \tag{6.21}$$

6.2. Multi frequency moments. — Because the source emits a signal of bandwidth $\mathcal{B}$, we need multi frequency moments of the propagator $\mathbb{P}^{\varepsilon,(a)}(\omega,Z)$, to describe the wave field in the limit $\varepsilon\to 0$. The calculation of these moments amounts to using (4.61) to derive evolution equations for the products

$$\prod_{j=1}^{m}\mathbb{P}^{\varepsilon,(a)}(\omega_j,Z), \quad \text{for } m>1,$$

and then applying the diffusion approximation theorem to get their limit as $\varepsilon\to 0$. We refer to [**15**, Chapters 6,8,20] for details of the calculation.

For the analysis of imaging and time reversal, we need the auto-correlation of $\mathbb{P}^{\varepsilon,(a)}(\omega,Z)$ at two different frequencies, given in [**15**, Proposition 20.7]. The propagator decorrelates at different frequencies, meaning that

$$\mathbb{E}\left[\mathbb{P}^{\varepsilon,(a)}_{jl}(\omega,Z)\overline{\mathbb{P}^{\varepsilon,(a)}_{j'l'}}(\omega',Z)\right] \overset{\varepsilon\to 0}{\longrightarrow} \mathbb{E}\left[\mathbb{P}^{(\alpha)}_{jl}(\omega,Z)\right]\mathbb{E}\left[\overline{\mathbb{P}^{(\alpha)}_{j'l'}}(\omega',Z)\right], \quad \omega\neq\omega'. \tag{6.22}$$

The mean propagator is

$$\mathbb{E}\left[\mathbb{P}^{(\alpha)}_{jl}(\omega,Z)\right] = \delta_{jl}\,e^{-\frac{Z}{s_j(\omega)}+i\frac{Z}{\zeta_j(\omega)}}, \tag{6.23}$$

where we let

$$\zeta_j(\omega) = \left[\frac{\Gamma^{(s)}_{jj}(\omega)}{2}+\kappa_j(\omega)\right]^{-1}. \tag{6.24}$$

There is correlation over frequency offsets of order ε^2, and the second moments are

$$\begin{aligned}\mathbb{E}\left[\mathbb{P}^{\varepsilon,(a)}_{jl}(\omega,Z)\overline{\mathbb{P}^{\varepsilon,(a)}_{j'l'}}(\omega-\varepsilon^2 h,Z)\right] \overset{\varepsilon\to 0}{\longrightarrow} \delta_{jj'}\delta_{ll'}\frac{\beta_l(\omega)}{\beta_j(\omega)}\widehat{\mathcal{W}}^{(l)}_j(\omega,h,Z)e^{-ih\beta_j'(\omega)Z}\\ +(1-\delta_{jj'})\delta_{jl}\delta_{j'l'}e^{\mathcal{K}_{jj'}(\omega)Z}.\end{aligned} \tag{6.25}$$

Here we introduced the coefficients

$$\mathcal{K}_{jj'}(\omega) = \frac{\Gamma^{(c)}_{jj}(\omega)+\Gamma^{(c)}_{j'j'}(\omega)-\Gamma_{jj}(\omega)-\Gamma_{j'j'}(\omega)+2\Gamma_{jj'}(\omega)}{2}+i\left[\frac{1}{\zeta_j(\omega)}-\frac{1}{\zeta_{j'}(\omega)}\right], \tag{6.26}$$

and we let

$$\widehat{\mathcal{W}}^{(l)}_j(\omega,h,Z) = \int_{-\infty}^{\infty}d\tau\,\mathcal{W}^{(l)}_j(\omega,\tau,Z)e^{ih\tau} \tag{6.27}$$

be the Fourier transform of the mean Wigner distribution $\mathcal{W}_j^{(l)}(\omega,\tau,Z)$. It solves the transport equations

$$\left[\partial_Z + \beta_j'(\omega)\partial_\tau\right]\mathcal{W}_j^{(l)}(\omega,\tau,Z) = \sum_{\substack{n=1\\ n\neq j}}^{N}\Gamma_{jn}^{(c)}(\omega)\left[\mathcal{W}_n^{(l)}(\omega,\tau,Z) - \mathcal{W}_j^{(l)}(\omega,\tau,Z)\right] \tag{6.28}$$

for $Z>0$, with initial conditions

$$\mathcal{W}_j^{(l)}(\omega,\tau,0) = \delta_{jl}\delta(\tau). \tag{6.29}$$

To compare with the results of the previous section, let us rewrite the second moments in terms of the amplitudes

$$\begin{aligned}\mathbb{E}\left[a_j^\varepsilon(\omega,Z)\overline{a_{j'}}^\varepsilon(\omega-\varepsilon^2 h,Z)\right] \xrightarrow{\varepsilon\to 0} \delta_{jj'}\sum_{l=1}^{N}\widehat{\mathcal{W}}_j^{(l)}(\omega,h,Z)e^{-ih\beta_j'(\omega)Z}\frac{\beta_l(\omega)}{\beta_j(\omega)}|a_{l,o}(\omega)|^2\\ +(1-\delta_{jj'})e^{\mathcal{K}_{jj'}(\omega)Z}a_{j,o}(\omega)\overline{a_{j',o}(\omega)}.\end{aligned} \tag{6.30}$$

We note that when $j\neq j'$ the right hand side decays exponentially with Z, because the real part of $\mathcal{K}_{jj'}$ is negative. The covariance is

$$\begin{aligned}\operatorname{cov}\left[a_j^\varepsilon, a_{j'}^\varepsilon\right] &= \mathbb{E}\left[a_j^\varepsilon(\omega,Z)\overline{a_{j'}}^\varepsilon(\omega-\varepsilon^2 h,Z)\right] - \mathbb{E}\left[a_j^\varepsilon(\omega,Z)\right]\mathbb{E}\left[\overline{a_{j'}}^\varepsilon(\omega,Z)\right]\\ &\xrightarrow{\varepsilon\to 0}\frac{\mathbb{E}[\alpha_j(\omega,Z)]\mathbb{E}[\overline{\alpha_{j'}}(\omega,Z)]}{\sqrt{\beta_j(\omega)\beta_{j'}(\omega)}}\left[e^{2\Gamma_{jj'}(\omega)Z}-1\right],\end{aligned} \tag{6.31}$$

with expectations given by (6.3), and the correlation of a_j^ε and $a_{j'}^\varepsilon$ decays exponentially with Z, meaning that the mode amplitudes decorrelate at long ranges. We already saw in the previous section that the mode powers decorrelate in the limit $Z\to\infty$.

In the case $j=j'$, and for a frequency offset $h=0$, we recover the mean power result (6.4), with

$$\langle\mathcal{P}_j\rangle(\omega,Z) = \sum_{l=1}^{N}\widehat{\mathcal{W}}_j^{(l)}(\omega,0,Z)|\alpha_l(\omega,0)|^2, \tag{6.32}$$

and $\alpha_l(\omega,0)$ given by (6.18). For a non-zero frequency offset, $\widehat{\mathcal{W}}_j^{(l)}(\omega,h,Z)$ satisfies the linear system of differential equations

$$\left[\partial_Z - ih\beta_j'(\omega)\right]\widehat{\mathcal{W}}_j^{(l)}(\omega,h,Z) = \sum_{n=1}^{N}\Gamma_{jn}^{(c)}(\omega)\widehat{\mathcal{W}}_n^{(l)}(\omega,h,Z), \quad Z>0, \tag{6.33}$$

with initial conditions

$$\widehat{\mathcal{W}}_j^{(l)}(\omega,h,0) = \delta_{jl}. \tag{6.34}$$

The solution is given by the exponential of the matrix $ih\mathfrak{B}' + \Gamma^{(c)}$,

$$\widehat{\mathcal{W}}_j^{(l)}(\omega, h, Z) = \mathbf{e}_j \cdot \exp\left\{\left[ih\mathfrak{B}' + \Gamma^{(c)}\right] Z\right\} \mathbf{e}_l, \tag{6.35}$$

where $\mathfrak{B}'$ is the diagonal matrix with entries β_j' and $\{\mathbf{e}_j\}_{j=1,\ldots,N}$ is the canonical basis in $\mathbb{R}^N$. We can write $\widehat{\mathcal{W}}_j^{(l)}$ as the sum of the coherent part, which decays exponentially with Z, and a remainder

$$\widehat{\mathcal{W}}_j^{(l)}(\omega, h, Z) = \delta_{jl} e^{ih\beta_l'(\omega)Z + \Gamma_{ll}^{(c)}(\omega)Z} + \widehat{W}_j^{(l)}(\omega, h, Z). \tag{6.36}$$

The remainder satisfies the homogeneous initial conditions

$$\widehat{W}_j^{(l)}(\omega, h, 0) = 0, \tag{6.37}$$

and evolution equations driven by the coherent part

$$\begin{aligned}\left[\partial_Z - ih\beta_j'(\omega)\right] \widehat{W}_j^{(l)}(\omega, h, Z) = \sum_{n=1}^{N} \Gamma_{jn}^{(c)}(\omega) \widehat{W}_n^{(l)}(\omega, h, Z) \\ + \Gamma_{jl}^{(c)}(\omega) e^{ih\beta_l'(\omega)Z + \Gamma_{ll}^{(c)}(\omega)Z}.\end{aligned} \tag{6.38}$$

Equivalently, in the time domain, the Wigner transform is given by

$$\mathcal{W}_j^{(l)}(\omega, \tau, Z) = \delta_{jl} e^{\Gamma_{ll}^{(c)}(\omega)Z} \delta\left(\tau - \beta_l'(\omega)Z\right) + W_j^{(l)}(\omega, \tau, Z), \tag{6.39}$$

where the coherent terms propagates the singularity along the characteristic $\tau = \beta_l' Z$, but its weight decays exponentially in Z. The remainder $W_j^{(l)}$ is a continuous density that does not decay exponentially in range, so using equation (6.30) we obtain that

$$\lim_{\varepsilon \to 0} \mathbb{E}\left[a_j^{\varepsilon}(\omega, Z) \overline{a_j}^{\varepsilon}(\omega - \varepsilon^2 h, Z)\right] \approx e^{-ih\beta_j'(\omega)Z} \sum_{l=1}^{N} \widehat{W}_j^{(l)}(\omega, h, Z) \frac{\beta_l(\omega) |a_{l,o}(\omega)|^2}{\beta_j(\omega)} \tag{6.40}$$

for large Z.

6.3. Pulse propagation. — We described in section 3.2 the signal received at the array at range $Z_{\mathcal{A}}/\varepsilon^2$, in homogeneous waveguides. Now we look at the signal received in random waveguides.

We obtain from equation (4.70) that

$$\begin{aligned}p\left(t, y, \frac{Z_{\mathcal{A}}}{\varepsilon^2}\right) \approx \sum_{j,l=1}^{N} \phi_j(y) \int_0^{\mathfrak{D}} \frac{dy'}{\Delta_y} \phi_l(y') \rho\left(\frac{y' - y^\star}{\Delta_y}\right) \\ \times \int_{-\infty}^{\infty} \frac{d\omega}{2\pi\mathcal{B}} \widehat{f}\left(\frac{\omega - \omega_o}{\mathcal{B}}\right) \mathbb{P}_{jl}^{\varepsilon,(a)}(\omega, Z_{\mathcal{A}}) e^{i\beta_j(\omega)\frac{Z_{\mathcal{A}}}{\varepsilon^2} - i\omega t},\end{aligned} \tag{6.41}$$

where we used the initial conditions (4.35) and the source model (2.12). We analyze the signal (6.41) in the narrowband and broadband regimes defined by equations (2.16) and (2.19).

In the narrowband case we let

$$\omega = \omega_o + \varepsilon^2 w$$

and evaluate equation (6.42) at time $t = T/\varepsilon^2$. We obtain that

$$p\left(t=\frac{T}{\varepsilon^2}, y, \frac{Z_{\mathcal{A}}}{\varepsilon^2}\right) \approx \sum_{j,l=1}^{N} \phi_j(y)\, \mathfrak{f}_{jl}^{\varepsilon}(T) \int_0^{\mathfrak{D}} \frac{dy'}{\Delta_y} \phi_l(y') \rho\left(\frac{y'-y^\star}{\Delta_y}\right), \tag{6.42}$$

where the signals

$$\mathfrak{f}_{jl}^{\varepsilon}(T) = \frac{e^{i[\beta_j(\omega_o) Z_{\mathcal{A}} - \omega_o T]/\varepsilon^2}}{2i\beta_j(\omega_o)} \mathfrak{F}_{jl}^{\varepsilon}(T) \tag{6.43}$$

have the random factor

$$\mathfrak{F}_{jl}^{\varepsilon}(T) = \int_{-\infty}^{\infty} \frac{dw}{2\pi\Omega_{\mathcal{B}}}\, \widehat{f}\left(\frac{w}{\Omega_{\mathcal{B}}}\right) \mathbb{P}_{jl}^{\varepsilon,(a)}(\omega_o + \varepsilon^2 w, Z_{\mathcal{A}}) e^{iw[\beta_j'(\omega_o) Z_{\mathcal{A}} - T]}. \tag{6.44}$$

If the kernel $\mathbb{P}^{\varepsilon,(a)}$ where the identity matrix, we would recover the result in the ideal waveguide. In our case the kernel is random, with moments described by equations (6.23) and (6.25). The mean of $\mathfrak{F}_{jl}^{\varepsilon}$ satisfies

$$\mathbb{E}\left[\mathfrak{F}_{jl}^{\varepsilon}(T)\right] \stackrel{\varepsilon\to 0}{\longrightarrow} \delta_{jl}\, f\left[\Omega_{\mathcal{B}}\left(T - \beta_j'(\omega_o) Z_{\mathcal{A}}\right)\right] e^{-\frac{Z_{\mathcal{A}}}{\mathcal{S}_j(\omega_o)} + i\frac{Z_{\mathcal{A}}}{\zeta_j(\omega_o)}}, \tag{6.45}$$

so the coherent signal $\mathbb{E}[p]$ is similar to that in the ideal waveguide, except that the contribution of each mode is exponentially damped on the range scale of the scattering mean free path $\mathcal{S}_j(\omega_o)$. There is also a mode dependent phase modulation. It is obvious from the second moments (6.25) that the standard deviation of p exceeds its mean for large $Z_{\mathcal{A}}$, meaning that the random fluctuations of the narrowband signals received at the array overwhelm its coherent part. The array data is basically incoherent at long ranges.

In the broadband regime we change variables in (6.41) as

$$\omega = \omega_o + \varepsilon w,$$

and obtain

$$p\left(t=\frac{T}{\varepsilon^2}, y, \frac{Z_{\mathcal{A}}}{\varepsilon^2}\right) \approx \sum_{j,l=1}^{N} \phi_j(y)\, \mathfrak{f}_{jl}^{\varepsilon}(T) \int_0^{\mathfrak{D}} \frac{dy'}{\Delta_y} \phi_l(y') \rho\left(\frac{y'-y^\star}{\Delta_y}\right). \tag{6.46}$$

Here $\mathfrak{f}_{jl}^{\varepsilon}(T)$ has the same form as in (6.43), but the random factor is

$$\mathfrak{F}_{jl}^{\varepsilon}(T) = \int_{-\infty}^{\infty} \frac{dw}{2\pi\Omega_{\mathcal{B}}}\, \widehat{f}\left(\frac{w}{\Omega_{\mathcal{B}}}\right) \widehat{\mathfrak{d}}_j\left(\frac{w}{\Omega_{\mathcal{B}}}\right) \mathbb{P}_{jl}^{\varepsilon,(a)}(\omega_o + \varepsilon w, Z_{\mathcal{A}}) e^{iw[\beta_j'(\omega_o) Z_{\mathcal{A}} - T]/\varepsilon}, \tag{6.47}$$

with dispersion kernel $\mathfrak{d}_j$ defined in equation (3.24). We have a fast phase in (6.47), which vanishes when T equals the travel time of the j-th mode

$$T = T_j = \beta_j'(\omega_o) Z_{\mathcal{A}}. \tag{6.48}$$

Let us observe the signal in a time window centered at T_j and of width of order ε, similar to that of the emitted pulse. Explicitly, let

$$T = T_j + \varepsilon s, \tag{6.49}$$

and obtain from (6.47) that

$$\mathfrak{F}^{\varepsilon}_{jl}(T_j + \varepsilon s) = \int_{-\infty}^{\infty} \frac{dw}{2\pi\Omega_{\mathcal{B}}} \widehat{f}\left(\frac{w}{\Omega_{\mathcal{B}}}\right) \widehat{\mathfrak{d}}_j\left(\frac{w}{\Omega_{\mathcal{B}}}\right) \mathbb{P}^{\varepsilon,(a)}_{jl}(\omega_o + \varepsilon w, Z_{\mathcal{A}}) e^{-iws}. \tag{6.50}$$

We can compute the mean and variance of this signal as we did above, but note the following. Because the propagator decorrelates rapidly, over frequency offsets of order ε^2, the right hand side in (6.50) is essentially the superposition of uncorrelated random variables, and we expect it to be close to its mean by the law of large numbers. We refer to [**15**, Section 20.4.3] for details on the proof and cite the result from there.

As $\varepsilon \to 0$, we have the convergence in distribution

$$\mathfrak{F}^{\varepsilon}_{jl}(T_j + \varepsilon s) \rightharpoonup \delta_{jl}\, e^{\frac{\Gamma^{(c)}_{jj}(\omega_o) Z_{\mathcal{A}}}{2} + i\frac{Z_{\mathcal{A}}}{\zeta_j(\omega_o)} + iB_j(Z_{\mathcal{A}})} f \star \mathfrak{d}_j\left(\Omega_{\mathcal{B}}\, s\right), \tag{6.51}$$

where B_j is Brownian motion with variance

$$\mathbb{E}\left[B_j(Z_{\mathcal{A}})\right] = \Gamma_{jj}(\omega_o) Z_{\mathcal{A}}. \tag{6.52}$$

This is a *pulse stabilization* result, because it says that when we observe the wave around the expected travel time T_j, in a time window comparable to the emitted pulse width, it is deterministic except for the Brownian motion in the phase. Furthermore, the pulse shape which is affected by dispersion is the same as in the ideal waveguide. The essential difference is that the pulse amplitude decays exponentially in $Z_{\mathcal{A}}$, on the scale

$$\mathcal{S}^{\mathcal{P}}_j = \frac{2}{|\Gamma^{(c)}_{jj}(\omega_o)|}.$$

As the waves travel in the waveguide, the energy is transferred from the coherent part which arrives first, to the incoherent part that arrives after it over a longer time interval than the pulse width. See Figure 4 for an illustration.

6.4. Comparative study of the net scattering effects. — We have now seen that the coherent field decays exponentially with range on the mode dependent scale $\mathcal{S}_j(\omega_o)$, the *scattering mean free path*. Definition (6.9) shows that $1/\mathcal{S}_j$ is given by the sum of two terms

$$\frac{1}{\mathcal{S}^{\mathcal{P}}_j(\omega_o)} := -\frac{\Gamma^{(c)}_{jj}(\omega_o)}{2} \tag{6.53}$$

and

$$\frac{1}{\mathcal{S}_j^\theta(\omega_o)} := \frac{\Gamma_{jj}(\omega_o)}{2}. \tag{6.54}$$

The first term (6.53) is defined by the power diffusion coefficients in the generator $\mathcal{G}_\mathcal{P}$, and we denote by $\mathcal{S}_j^\mathcal{P}$ the range scale over which the modes exchange energy. We know that each mode is associated to a direction of propagation of a plane wave, so we call $\mathcal{S}_j^\theta$ the *transport mean free path*. Classically, this is defined as the distance beyond which the wave loses its initial direction due to scattering [**26**].

The second term (6.54) is defined by the phase diffusion coefficients in the generator $\mathcal{G}_\theta$. They are also the variances of the Brownian motions B_j appearing in the phase of the coherent front (6.51). We denote by $\mathcal{S}_j^\theta$ the range scale over which the random phase of the mode amplitudes become significant, thus giving the exponential damping of their expectation. For example, when taking the expectation of (6.51), we get

$$\mathbb{E}\left[e^{iB_j(Z_\mathcal{A})}\right] = \int_\infty^\infty \frac{du}{\sqrt{2\pi\Gamma_{jj}(\omega_o)Z_\mathcal{A}}} \exp\left[iu - \frac{u^2}{2\Gamma_{jj}(\omega_o)Z_\mathcal{A}}\right] = e^{-\Gamma_{jj}(\omega_o)Z_\mathcal{A}/2}.$$

We wish to compare the scattering and transport mean free paths in waveguides with random boundaries vs. waveguides with internal inhomogeneities. These scales are different because the diffusion matrices Γ and $\Gamma^{(c)}$ have different expressions, given by (4.78)-(4.79) and (5.9)-(5.11), respectively. The details of the estimation can be found in [**1**]. We recall here the results for the scaling regime

$$\sqrt{N} \lesssim \frac{\ell}{\lambda_o} \ll N. \tag{6.55}$$

The first inequality is the assumption (4.69) made in the forward scattering approximation. The second inequality says that the wavelength is large in comparison with the waveguide depth $\mathfrak{D}$, so that there are many propagating modes.

In both types of waveguides $\mathcal{S}_j$ decreases monotonically with the mode index. This is intuitive, because the high order modes bounce more often at the boundary and thus take long paths from the source to the array. The cumulative scattering effects build up over the longer paths, and the damping rate of the expectation of the mode amplitudes is larger.

In the waveguides with random boundary, and for the first modes, we have

$$\mathcal{S}_1^\mathcal{P}(\omega_o) \sim \mathcal{S}_1(\omega) \sim \mathfrak{D}\sqrt{\frac{\ell}{\lambda_o}} \gtrsim \mathfrak{D}\sqrt{N}, \tag{6.56}$$

where the symbol $\sim$ indicates that the scales are of the same order. For the last modes the scattering mean free path satisfies

$$\mathcal{S}_N(\omega_o) \sim \mathfrak{D}\frac{\lambda_o}{N^2\ell} \lesssim \mathfrak{D}N^{-5/2}, \tag{6.57}$$

but the transport mean free path has a different behavior. It is given by

$$\mathcal{S}_N^{\mathcal{P}}(\omega_o) \sim \mathfrak{D}\frac{\ell}{N^3\lambda_o} \gtrsim \mathcal{S}_N(\omega_o), \tag{6.58}$$

when

$$\ell \sim \sqrt{N}\lambda_o \gg \lambda_o,$$

and it is much longer than the scattering mean free path in high frequency regimes

$$\mathcal{S}_N^{\mathcal{P}}(\omega_o) \gg \mathcal{S}_N(\omega_o), \quad \ell \gg \sqrt{N}\lambda_o. \tag{6.59}$$

This is particular to the waveguides with random boundaries, and it can be understood as follows. When $\ell \gg \lambda_o$, the high order modes strike the boundary many times over a range of the order of the correlation length, at almost the same angle of incidence. At each strike, the amplitude gains a random phase, and because the phases are statistically correlated they accumulate, thus giving a large diffusion coefficient Γ_{jj}, for $j \sim N$. The deviation of the direction of the waves due to the boundary fluctuations is typically small from one strike to another, and there is less energy exchanged between the high order modes. This is why $\mathcal{S}_j^{\mathcal{P}} \gg \mathcal{S}_j$ for $j \sim N$.

In the waveguides with interior inhomogeneities, and for the first modes we have

$$\mathcal{S}_1^{\mathcal{P}}(\omega_o) \sim \mathcal{S}_1(\omega_o) \sim \mathfrak{D}\frac{\lambda_o}{N\ell} \lesssim \mathfrak{D}N^{-3/2}, \tag{6.60}$$

and for the last modes

$$\mathcal{S}_N^{\mathcal{P}}(\omega_o) \sim \mathcal{S}_N(\omega_o) \sim \mathfrak{D}\frac{\lambda_o}{N^2\ell} \lesssim \mathfrak{D}N^{-5/2}. \tag{6.61}$$

Thus, we see that the first modes are much more affected by the interior inhomogeneities than the random boundaries. This is important for imaging, because it says that when the boundary scattering effects dominate, we can use first mode pass filters to obtain reliable results up to long ranges, satisfying

$$\mathfrak{D} \ll Z_{\mathcal{A}} \lesssim D\sqrt{N}.$$

Such filters are useless in waveguides with interior inhomogeneities, because even the first modes lose their coherence at ranges

$$Z_{\mathcal{A}} \lesssim \mathfrak{D}N^{-3/2} \ll \mathfrak{D}.$$

The high order modes have the same scattering mean free path in both types of waveguides. However, the transport mean free path is different. The main mechanism for the loss of coherence in the waveguides with random inhomogeneities is due to the exchange of energy between the modes. The scattering and transport mean free paths are similar for all the modes in such waveguides.

It remains to compare the *equipartition distance*

$$\mathcal{S}^E(\omega_o) := \frac{1}{|\Lambda_2(\omega)|}, \tag{6.62}$$

defined in terms of the second eigenvalue Λ_2 of the matrix $\Gamma^{(c)}$. As shown in equation (6.7), it is the range scale over which the power becomes uniformly distributed over the modes, independent of the initial excitation. This means that with arrays at ranges $Z_{\mathcal{A}} > \mathcal{S}^E$ it is not possible to determine the cross-range location of the source.

We do not have a theoretical estimate of the equipartition distance, but we calculated it numerically in [**1**] for the case of Gaussian autocorrelations $\mathcal{R}_\mu$ and $\mathcal{R}_\nu$. The result is that in waveguides with random boundaries

$$\mathcal{S}^E(\omega_o) \sim \mathcal{S}_1(\omega_o), \tag{6.63}$$

meaning that once all the modes have lost coherence, it is no longer possible to determine the cross-range of the source, no matter what imaging method we use.

In waveguides with random inhomogeneities we get

$$\mathcal{S}^E(\omega_o) \gg \mathcal{S}_1(\omega_o). \tag{6.64}$$

This shows that once the modes lose their coherence, it is useful to use incoherent imaging methods to estimate source locations at ranges $Z_{\mathcal{A}} \in (\mathcal{S}_1, \mathcal{S}^E)$.

7. Model of the array data

We denote by $p_{\mathcal{A}}(t, y)$ the pressure wave measured at the sensors of the array supported in the interval

$$\mathcal{A} = [y_m, y_M] \subset [0, \mathfrak{D}],$$

at range

$$z_{\mathcal{A}} = \frac{Z_{\mathcal{A}}}{\varepsilon^2}.$$

The length $|\mathcal{A}| = y_M - y_m$ of the interval is called the *aperture*. The array has *full aperture* when $|\mathcal{A}| = \mathfrak{D}$, and *partial aperture* when $|\mathcal{A}| < \mathfrak{D}$. We assume for convenience that the sensors are spaced sufficiently close together to make the continuum array approximation. This means that when computing sums over the locations of the sensors we can replace them by integrals over $y \in \mathcal{A}$.

The data is

$$p_{\mathcal{A}}(t, y) = 1_{\mathcal{A}}(y)\, \chi\left(\frac{\varepsilon^2 t}{T}\right) p\left(t, y, \frac{Z_{\mathcal{A}}}{\varepsilon^2}\right), \tag{7.1}$$

with p given by (4.70). The recordings are over a finite time interval modeled with the window function χ of dimensionless arguments and support of order one. The scaling by T/ε^2 of the argument of χ reflects that the sensors record over a sufficiently long interval so that at least some of the modes reach the array. We allow an arbitrary shape of the window, and we normalize it by

$$\chi(0) = 1. \tag{7.2}$$

The Fourier transform of the data is

$$\widehat{p}_{\mathcal{A}}(\omega,y)=1_{\mathcal{A}}(y)\int_{-\infty}^{\infty}\frac{du}{2\pi}\,\widehat{\chi}(u)\,\widehat{p}\left(\omega-\frac{\varepsilon^2 u}{T},y,\frac{Z_{\mathcal{A}}}{\varepsilon^2}\right), \tag{7.3}$$

and from (4.70), with the mode amplitudes written in terms of the propagator,

$$\widehat{p}\left(\omega,y,\frac{Z_{\mathcal{A}}}{\varepsilon^2}\right)\approx\sum_{j,l=1}^{N}\phi_j(y)\mathbb{P}_{jl}^{\varepsilon,(a)}\left(\omega,Z_{\mathcal{A}}\right)a_{l,o}(\omega)e^{i\beta_j(\omega)\frac{Z_{\mathcal{A}}}{\varepsilon^2}}. \tag{7.4}$$

The initial amplitudes are

$$a_{l,o}(\omega)=\frac{1}{2i\beta_l(\omega)}\int_0^{\mathfrak{D}}dy'\widehat{F}(\omega,y')\phi_l(y'), \tag{7.5}$$

and with the source model (2.12) we have

$$\widehat{F}(\omega,y)=\frac{1}{\Delta_y}\rho\left(\frac{y-y^\star}{\Delta_y}\right)\frac{1}{\mathcal{B}}\widehat{f}\left(\frac{\omega-\omega_o}{\mathcal{B}}\right). \tag{7.6}$$

Gathering the results,

$$\begin{aligned}\widehat{p}_{\mathcal{A}}(\omega,y)\approx 1_{\mathcal{A}}(y)\int_0^{\mathfrak{D}}\frac{dy'}{\Delta_y}\rho\left(\frac{y'-y^\star}{\Delta_y}\right)\sum_{j,l=1}^{N}\frac{\phi_l(y')\phi_j(y)}{2i\beta_l(\omega_o)}\int_{-\infty}^{\infty}\frac{du}{2\pi}\,\widehat{\chi}(u)\,e^{-i\beta_j'(\omega_o)\frac{uZ_{\mathcal{A}}}{T}}\\ \times\frac{1}{\mathcal{B}}\widehat{f}\left(\frac{\omega-\omega_o}{\mathcal{B}}-\frac{\varepsilon^2 u}{\mathcal{B}T}\right)\mathbb{P}_{jl}^{\varepsilon,(a)}\left(\omega-\frac{\varepsilon^2 u}{T},Z_{\mathcal{A}}\right)e^{i\beta_j(\omega)\frac{Z_{\mathcal{A}}}{\varepsilon^2}},\end{aligned} \tag{7.7}$$

where the approximate sign means equality up to a residual term that vanishes in the limit $\varepsilon\to 0$. Since we consider bandwidths that are much smaller than ω_o, we can approximate the wavenumber in the denominator by its value at the central frequency.

If we had an ideal waveguide, the propagator would be just the identity matrix, and (7.4) would simplify as

$$\widehat{p}_o\left(\omega,y,\frac{Z_{\mathcal{A}}}{\varepsilon^2}\right)\approx\sum_{j=1}^{N}\phi_j(y)a_{j,o}(\omega)e^{i\beta_j(\omega)\frac{Z_{\mathcal{A}}}{\varepsilon^2}}. \tag{7.8}$$

Here the approximation is because we neglect the evanescent waves.

8. Time reversal

Time reversal is an experiment that uses an active array of sensors to record the data $p_{\mathcal{A}}$ and then re-emit its time reversed version in the same medium. The waves are expected to refocus back at the source by the time reversibility of the wave equation. Here we study mathematically the time reversal process in order to understand the role played by cumulative scattering in random waveguides.

The time reversed recordings are

$$p_{\mathcal{A}}^{\rm TR}(t,y) = p_{\mathcal{A}}\left(\frac{T}{\varepsilon^2} - t, y\right), \tag{8.1}$$

and in the Fourier domain

$$\widehat{p}_{\mathcal{A}}^{\rm TR}(\omega,y) = \overline{\widehat{p}_{\mathcal{A}}}(\omega,y) e^{i\omega\frac{T}{\varepsilon^2}}, \tag{8.2}$$

where we recall that the bar denotes complex conjugation. The array emits the signal $p_{\mathcal{A}}^{\rm TR}$ and we observe the resulting wave field denoted by $\mathcal{O}(t,y,Z/\varepsilon^2)$. Its Fourier transform is similar to (7.4), with the source $\widehat{F}(\omega,y)$ replaced by (8.2). The waves are moving backward, so we should be careful with the propagator.

Let us denote by $\mathbb{P}^{\varepsilon,(a)}(\omega,Z_o,Z)$ the propagator between the ranges Z_o/ε^2 and Z/ε^2, with $Z > Z_o$. Up to now Z_o was zero, and we suppressed it in the arguments. We have

$$\mathbf{a}^{\varepsilon}(\omega,Z) = \mathbb{P}^{\varepsilon,(a)}(\omega,Z,Z_o)\mathbf{a}^{\varepsilon}(\omega,Z_o),$$

and because the energy is conserved in the limit $\varepsilon \to 0$, the propagator must satisfy

$$[\mathbb{P}^{\varepsilon,(a)}]^* \mathbb{P}^{\varepsilon,(a)} \approx \mathbf{I}.$$

Here the index $\star$ denotes the conjugate transpose, and the approximation means that there is a residual that tends to zero as $\varepsilon \to 0$. Therefore we obtain that

$$\mathbf{a}^{\varepsilon}(\omega,Z_o) \approx \left[\mathbb{P}^{\varepsilon,(a)}(\omega,Z_2,Z_1)\right]^{\star} \mathbf{a}^{\varepsilon}(\omega,Z).$$

We need the backward going waves. Recalling the structure (4.58) of $\mathbb{P}^{\varepsilon}$, in particular its second block on the diagonal, we see that the backpropagation should be done with the complex conjugate of the matrix above, which is the transpose of $\mathbb{P}^{\varepsilon,(a)}$.

It remains to calculate the amplitudes of the backward going emerging wave at the array. We decompose the wave in forward and backward going parts as in section 4.4, and then impose the source condition that is at now at the array range $Z_{\mathcal{A}}/\varepsilon^2$ instead of zero. We find the amplitudes

$$b_j(\omega,Z_{\mathcal{A}}) = \frac{e^{i\beta_j(\omega)\frac{Z_{\mathcal{A}}}{\varepsilon^2}}}{2i\beta_j(\omega)} \int_0^{\mathfrak{D}} dy\, \widehat{p}_{\mathcal{A}}^{\rm TR}(\omega,y)\, \phi_j(y),$$

and their propagation to range $Z < Z_{\mathcal{A}}$ is

$$b_j(\omega,Z) = \sum_{l=1}^{N} \mathbb{P}_{lj}^{\varepsilon,(a)}(\omega,Z_{\mathcal{A}},Z) b_l(\omega,Z_{\mathcal{A}}).$$

The observed wave field is given by

$$\mathcal{O}\left(t,y,\frac{Z}{\varepsilon^2}\right) \approx \sum_{j=1}^{N} \phi_j(y) \int_{-\infty}^{\infty} \frac{d\omega}{2\pi}\, b_j(\omega,Z) e^{-i\beta_j(\omega)\frac{Z}{\varepsilon^2} - i\omega t}, \tag{8.3}$$

and more explicitly

$$\mathcal{O}\left(t,y,\frac{Z}{\varepsilon^2}\right) \approx \int_0^{\mathfrak{D}} \frac{dy'}{\Delta_y}\rho\left(\frac{y'-y^\star}{\Delta_y}\right) \sum_{j,l,j',l'=1}^{N} \mathfrak{M}_{j'l}\,\frac{\phi_{l'}(y')\phi_j(y)}{4\beta_l(\omega_o)\beta_{l'}(\omega_o)}$$
$$\times \int_{-\infty}^{\infty}\frac{du}{2\pi}\,\overline{\widehat{\chi}}(u)\,e^{iu\beta'_{j'}(\omega_o)\frac{Z_{\mathcal{A}}}{T}} \int_{-\infty}^{\infty}\frac{d\omega}{2\pi\mathcal{B}}\,\overline{\widehat{f}}\left(\frac{\omega-\omega_o}{\mathcal{B}}-\frac{\varepsilon^2 u}{\mathcal{B}T}\right)e^{i\omega\left(\frac{T}{\varepsilon^2}-t\right)}$$
$$\times\ \mathbb{P}^{\varepsilon,(a)}_{lj}(\omega,Z_{\mathcal{A}}-Z)\overline{\mathbb{P}^{\varepsilon,(a)}_{j'l'}}\left(\omega-\frac{\varepsilon^2 u}{T},Z_{\mathcal{A}}\right)e^{i[\beta_l(\omega)-\beta_{j'}(\omega)]\frac{Z_{\mathcal{A}}}{\varepsilon^2}-i\beta_j(\omega)\frac{Z}{\varepsilon^2}}. \tag{8.4}$$

Here we denote by $\mathfrak{M}_{jl}$ the matrix that couples the modes for arrays with partial apertures

$$\mathfrak{M}_{jl} = \int_0^{\mathfrak{D}} dy\, 1_{\mathcal{A}}(y)\,\phi_j(y)\phi_l(y). \tag{8.5}$$

It equals the identity for arrays with full aperture.

The time reversal function is defined by (8.4) observed at time $t = T/\varepsilon^2$ and at the range of the source,

$$\mathcal{J}^{\mathrm{TR}}(y) = \mathcal{O}\left(\frac{T}{\varepsilon^2},y,0\right). \tag{8.6}$$

We write it as

$$\mathcal{J}^{\mathrm{TR}}(y) \approx \int_0^{\mathfrak{D}} \frac{dy'}{\Delta_y}\rho\left(\frac{y'-y^\star}{\Delta_y}\right)\Psi^{\mathrm{TR}}(y',y), \tag{8.7}$$

in terms of the *point spread kernel* Ψ^{TR}. The model of the kernel is

$$\Psi^{\mathrm{TR}}(y',y) = \sum_{j,l,j',l'=1}^{N} \mathfrak{M}_{j'l}\,\frac{\phi_{l'}(y')\phi_j(y)}{4\beta_l(\omega_o)\beta_{l'}(\omega_o)} \int_{-\infty}^{\infty}\frac{du}{2\pi}\,\overline{\widehat{\chi}}(u)\,e^{iu\beta'_{j'}(\omega_o)\frac{Z_{\mathcal{A}}}{T}}$$
$$\times \int_{-\infty}^{\infty}\frac{d\omega}{2\pi\mathcal{B}}\,\overline{\widehat{f}}\left(\frac{\omega-\omega_o}{\mathcal{B}}-\frac{\varepsilon^2 u}{\mathcal{B}T}\right)e^{i[\beta_l(\omega)-\beta_{j'}(\omega)]\frac{Z_{\mathcal{A}}}{\varepsilon^2}}$$
$$\times\ \mathbb{P}^{\varepsilon,(a)}_{lj}(\omega,Z_{\mathcal{A}})\overline{\mathbb{P}^{\varepsilon,(a)}_{j'l'}}\left(\omega-\frac{\varepsilon^2 u}{T},Z_{\mathcal{A}}\right). \tag{8.8}$$

Ideally, it should be the Dirac distribution $\delta(y'-y)$, but we cannot achieve it. Our goal is to understand the behavior of the kernel, and quantify its focusing around the expected peak at $y'=y$. We present below the resolution analysis of Ψ^{TR} for broadband sources. The narrowband case is treated in detail in [**15**, Section 20.9].

8.1. Resolution analysis for broadband signals. — In the broadband case, we can change variables in the frequency integral in (8.8)

$$\omega = \omega_o + \varepsilon w, \quad |w| \le \pi\Omega_{\mathcal{B}},$$

and assuming a differentiable $\widehat{f}$, we obtain the point spread function

$$\Psi^{\rm TR}(y',y) \approx \sum_{j,l,j',l'=1}^{N} \mathfrak{M}_{j'l} \frac{\phi_{l'}(y')\phi_j(y)}{4\beta_l(\omega_o)\beta_{l'}(\omega_o)}\, e^{i[\beta_l(\omega_o)-\beta_{j'}(\omega_o)]\frac{Z_{\mathcal{A}}}{\varepsilon^2}}$$
$$\times \int_{-\infty}^{\infty} \frac{dw}{2\pi\Omega_{\mathcal{B}}}\, \overline{\widehat{f}}\left(\frac{w}{\Omega_{\mathcal{B}}}\right) \widehat{\mathfrak{d}}_j\left(\frac{w}{\Omega_{\mathcal{B}}}\right) \overline{\widehat{\mathfrak{d}}_{j'}}\left(\frac{w}{\Omega_{\mathcal{B}}}\right) e^{iw[\beta_l'(\omega_o)-\beta_{j'}'(\omega_o)]\frac{Z_{\mathcal{A}}}{\varepsilon}}$$
$$\times \int_{-\infty}^{\infty} \frac{du}{2\pi}\, \overline{\widehat{\chi}}(u)\, e^{i\beta_{j'}'(\omega_o)\frac{uZ_{\mathcal{A}}}{T}}\, \mathbb{P}_{lj}^{\varepsilon,(a)}(\omega_o+\varepsilon w, Z_{\mathcal{A}}) \overline{\mathbb{P}_{j'l'}^{\varepsilon,(a)}}\left(\omega_o+\varepsilon w - \frac{\varepsilon^2 u}{T}, Z_{\mathcal{A}}\right), \tag{8.9}$$

where $\mathfrak{d}_j$ is the dispersion kernel (3.24). To analyze resolution, we need the mean and variance of $\Psi^{\rm TR}$. The variance is small, of order ε^2, because the decorrelation frequency is of order ε^2. Thus, the point spread function is close to its mean in the neighborhood of its peak,

$$\Psi^{\rm TR}(y',y) \approx \mathbb{E}[\Psi^{\rm TR}(y',y)].$$

We say that the time reversal process is *statistically stable*, because its point spread function is essentially deterministic.

The cross-range resolution r_y is the offset $|y'-y|$ that bounds the essential support of $\mathbb{E}[\Psi^{\rm TR}]$. That is to say, $\mathbb{E}[\Psi^{\rm TR}(y,y')]$ is large when $|y'-y| \le r_y$. In practice, by large we mean that $\mathbb{E}[\Psi^{\rm TR}]$ is greater than the standard deviation of the fluctuations by a user defined threshold factor.

Intuitively, we expect that the best point spread function is given by full aperture arrays. This is because such arrays capture all the propagating waves that arrive in the time measurement window. We will see that this is indeed the case in ideal waveguides. Surprisingly, in random waveguides we can achieve the same resolution even with small apertures. This is the *super resolution* property of time reversal.

To highlight the effect of scattering on the time reversal process, we compare $\mathbb{E}[\Psi^{\rm TR}]$ with the point spread function $\Psi_o^{\rm TR}$ in ideal waveguides. It is obtained from (8.9) by replacing the propagators with the identity matrix. Explicitly, we have

$$\Psi_o^{\rm TR}(y',y) \approx \sum_{j,j'=1}^{N} \mathfrak{M}_{j'j} \frac{\phi_{j'}(y')\phi_j(y)}{4\beta_j(\omega_o)\beta_{j'}(\omega_o)}\, \chi\left(\frac{\beta_{j'}'(\omega_o)Z_{\mathcal{A}}}{T}\right) e^{i[\beta_j(\omega_o)-\beta_{j'}(\omega_o)]\frac{Z_{\mathcal{A}}}{\varepsilon^2}}$$
$$\times \int_{-\infty}^{\infty} \frac{dw}{2\pi\Omega_{\mathcal{B}}} \overline{\widehat{f}}\left(\frac{w}{\Omega_{\mathcal{B}}}\right) \widehat{\mathfrak{d}}_j\left(\frac{w}{\Omega_{\mathcal{B}}}\right) \overline{\widehat{\mathfrak{d}}_{j'}}\left(\frac{w}{\Omega_{\mathcal{B}}}\right) e^{iw[\beta_j'(\omega_o)-\beta_{j'}'(\omega_o)]\frac{Z_{\mathcal{A}}}{\varepsilon}}. \tag{8.10}$$

The expressions (8.4) and (8.10) simplify in the full aperture case, where $\mathfrak{M}_{jl} = \delta_{jl}$. We have

$$\Psi_{\mathrm{F}}^{\mathrm{TR}}(y',y) \approx \sum_{j,l,l'=1}^{N} \frac{\phi_{l'}(y')\phi_j(y)}{4\beta_l(\omega_o)\beta_{l'}(\omega_o)} \int_{-\infty}^{\infty} \frac{dw}{2\pi\Omega_{\mathcal{B}}}\, \overline{\widehat{f}}\left(\frac{w}{\Omega_{\mathcal{B}}}\right)$$

$$\times \int_{-\infty}^{\infty} \frac{du}{2\pi}\overline{\widehat{\chi}}(u)\, e^{i\beta_l'(\omega_o)\frac{uZ_{\mathcal{A}}}{T}} \mathbb{P}_{lj}^{\varepsilon,(a)}(\omega_o+\varepsilon w, Z_{\mathcal{A}})\overline{\mathbb{P}_{ll'}^{\varepsilon,(a)}}\left(\omega_o+\varepsilon w - \frac{\varepsilon^2 u}{T}, Z_{\mathcal{A}}\right) \tag{8.11}$$

in random waveguides, and

$$\Psi_{o,\mathrm{F}}^{\mathrm{TR}}(y',y) \approx \frac{f(0)}{4}\sum_{j=1}^{N} \frac{\phi_j(y')\phi_j(y)}{\beta_j^2(\omega_o)}\, \chi\left(\frac{\beta_j'(\omega_o)Z_{\mathcal{A}}}{T}\right). \tag{8.12}$$

in ideal waveguides. The index F reminds us that we have full aperture arrays.

8.1.1. The mean point spread function. — We use the second moments (6.25) to analyze the expectation of Ψ^{TR}. We obtain after straightforward calculations that its is given by the sum of two terms

$$\mathbb{E}\left[\Psi^{\mathrm{TR}}(y',y)\right] \approx \langle\Psi_1\rangle(y',y) + \langle\Psi_2\rangle(y',y). \tag{8.13}$$

The first term comes from the second moment $\mathbb{E}[\mathbb{P}_{lj}^{\varepsilon,(a)}\overline{\mathbb{P}_{lj}^{\varepsilon,(a)}}]$, given by the Wigner transform,

$$\langle\Psi_1\rangle(y',y) = \frac{f(0)}{4}\sum_{j,l=1}^{N} \mathfrak{M}_{ll}\, \frac{\phi_j(y')\phi_j(y)}{\beta_l^2(\omega_o)} \int_{-\infty}^{\infty} \frac{du}{2\pi}\, \overline{\widehat{\chi}}(u)\widehat{\mathcal{W}}_l^{(j)}\left(\omega_o, \frac{u}{T}, Z_{\mathcal{A}}\right). \tag{8.14}$$

The dispersion kernels disappear because $|\widehat{\mathfrak{d}}_j|^2 = 1$. The second term is due to the moments $\mathbb{E}[\mathbb{P}_{jj}^{\varepsilon,(a)}\overline{\mathbb{P}_{j'j'}^{\varepsilon,(a)}}]$,

$$\langle\Psi_2\rangle(y',y) = \sum_{\substack{j,\,j'=1\\ j\neq j'}}^{N} \mathfrak{M}_{j'j}\frac{\phi_{j'}(y')\phi_j(y)}{4\beta_j(\omega_o)\beta_{j'}(\omega_o)} e^{i[\beta_j(\omega_o)-\beta_{j'}(\omega_o)]\frac{Z_{\mathcal{A}}}{\varepsilon^2} - \mathcal{K}_{jj'}(\omega_o)Z_{\mathcal{A}}}$$

$$\times [f\star\mathfrak{d}_j\star\mathfrak{d}_{j'}]\left(\frac{[\beta_{j'}'(\omega_o)-\beta_j'(\omega_o)]Z_{\mathcal{A}}}{\varepsilon}\right)\chi\left(\frac{\beta_{j'}'Z_{\mathcal{A}}}{T}\right), \tag{8.15}$$

and it does not contribute in (8.13), because the pulse has compact support.

Recalling the expression (6.36) of the Wigner transform, with continuous density $W_l^{(j)}$, we obtain that

$$\int_{-\infty}^{\infty} \frac{du}{2\pi}\,\overline{\widehat{\chi}}(u)\,\widehat{\mathcal{W}}_l^{(j)}\left(\omega, \frac{u}{T}, Z_{\mathcal{A}}\right) = \delta_{jl}\,\chi\left(\frac{\beta_j'(\omega_o)Z_{\mathcal{A}}}{T}\right) e^{-\frac{2Z_{\mathcal{A}}}{s_j^P(\omega_o)}}$$

$$+ \int_{-\infty}^{\infty} d\tau\,\chi\left(\frac{\tau}{T}\right) W_l^{(j)}(\omega_o,\tau,Z_{\mathcal{A}}). \tag{8.16}$$

Here we used the definition of the transport mean free path $\mathcal{S}_j^{\mathcal{P}}$ and rewrote the integral over u as a convolution of the Wigner density and the time reversed window χ. The expectation of the point spread function becomes

$$\mathbb{E}\left[\Psi^{\rm TR}(y',y)\right] \approx \frac{f(0)}{4}\sum_{j=1}^{N}\mathfrak{M}_{jj}\frac{\phi_j(y')\phi_j(y)}{\beta_j^2(\omega_o)}e^{-\frac{2Z_{\mathcal{A}}}{\mathcal{S}_j^{\mathcal{P}}(\omega_o)}}\chi\left(\frac{\beta_j'(\omega_o)Z_{\mathcal{A}}}{T}\right)+$$

$$\frac{f(0)}{4}\sum_{j,l=1}^{N}\mathfrak{M}_{ll}\frac{\phi_j(y')\phi_j(y)}{\beta_l^2(\omega_o)}\int_{-\infty}^{\infty}d\tau\,\chi\left(\frac{\tau}{T}\right)W_l^{(j)}\left(\omega_o,\tau,Z_{\mathcal{A}}\right). \tag{8.17}$$

The first term sums the product of the eigenfunctions with positive weights that decay with the mode index. The weights are positive because

$$\mathfrak{M}_{jj} = \int_0^{\mathfrak{D}} dy\, 1_{\mathcal{A}}(y)\phi_j^2(y) > 0, \tag{8.18}$$

and they decay because the transport mean free path $\mathcal{S}_j^{\mathcal{P}}$ decreases monotonically with the index j. All the weights decrease exponentially in $Z_{\mathcal{A}}$, so at long ranges $Z_{\mathcal{A}} > S_1^{\mathcal{P}}$, the mean point spread function is given by the second term in (8.17).

It is impossible to calculate analytically the integral of the Wigner density over the recording window. But if we let $Z_{\mathcal{A}}$ grow, the density becomes independent of j and l, and (8.17) simplifies to

$$\mathbb{E}\left[\Psi^{\rm TR}(y',y)\right] \sim \sum_{j=1}^{N_T}\phi_j(y)\phi_{j'}(y), \qquad Z_{\mathcal{A}} > \mathcal{S}^E(\omega_o). \tag{8.19}$$

Here we let $N_T \leq N$ be the number of modes for which $W_l^{(j)}$ peaks in the recording window, and use $\sim$ to denote approximate, up to a multiplicative constant. We refer to [**15**, Section 20.6.2] for the analysis of $W_j^{(l)}$ at large ranges. It is shown there that

$$W_j^{(l)}(\omega_o,\tau,Z_{\mathcal{A}}) \overset{Z_{\mathcal{A}}\gg\mathcal{S}^E}{\sim} \frac{1}{N\sqrt{2\pi\sigma^2 Z_{\mathcal{A}}}}\exp\left[-\frac{(\tau-\langle\beta'\rangle Z_{\mathcal{A}})^2}{2\sigma^2 Z_{\mathcal{A}}}\right]$$

where $\langle\beta'\rangle$ is the average group speed

$$\langle\beta'\rangle = \frac{1}{N}\sum_{j=1}^{N}\beta_j'(\omega_o),$$

and σ^2 is similar to

$$\sigma^2 \sim \frac{2\mathcal{S}^E(\omega_o)}{N}\sum_{j=1}^{N}\left[\beta_j'(\omega_o)-\langle\beta'\rangle\right]^2.$$

Thus, all the modes contribute in the sum if

$$T > \langle\beta'\rangle Z_{\mathcal{A}} + 3\sqrt{\sigma^2 Z_{\mathcal{A}}}.$$

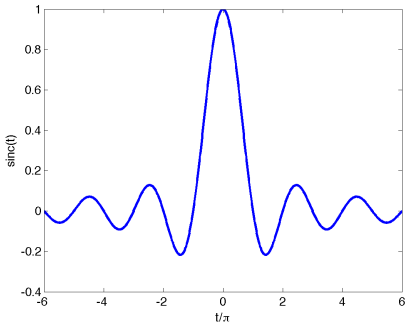

FIGURE 2. Plot of the function $\mathrm{sinc}(t)$ for $t \in [-6\pi, 6\pi]$. The argument t is scaled by π in the abscissa.

To see what this means, let us suppose that $N_T = N \gg 1$, and use the definition (3.3) of the eigenfunctions and the approximation

$$\frac{\pi}{\mathfrak{D}} \approx \frac{k_o}{N}.$$

We can estimate the sum in the right hand side of (8.19) as

$$\begin{aligned}
\sum_{j=1}^{N} \phi_j(y)\phi_{j'}(y) &= \frac{2}{\mathfrak{D}} \sum_{j=1}^{N} \sin\left(\frac{\pi j y}{\mathfrak{D}}\right) \sin\left(\frac{\pi j y'}{\mathfrak{D}}\right) \\
&\approx \frac{k_o}{N} \sum_{j=1}^{N} \sin\left(\frac{k_o j y}{N}\right) \sin\left(\frac{k_o j y'}{N}\right) \\
&\approx k_o \int_0^1 du\, \sin(k_o u y) \sin(k_o u y') \\
&= \frac{k_o}{2} \left\{ \mathrm{sinc}\left[k_o(y-y')\right] - \mathrm{sinc}\left[k_o(y+y')\right] \right\} \qquad (8.20)
\end{aligned}$$

The sinc function is equal to one when its argument is zero and it decays away from it, as illustrated in Figure 2. Because y and y' are positive, we can neglect the second term in (8.20) and conclude from (8.19) that

$$\mathbb{E}\left[\Psi^{\mathrm{TR}}(y', y)\right] \sim \frac{k_o}{2} \mathrm{sinc}\left[k_o(y-y')\right], \qquad Z_{\mathcal{A}} > \mathcal{S}^E. \qquad (8.21)$$

The kernel is large for

$$|y - y'| \le r_y := \frac{\pi}{k_o} = \frac{\lambda_o}{2}, \qquad (8.22)$$

and the resolution is the ideal Abbe diffraction limit independent of the aperture of the array!

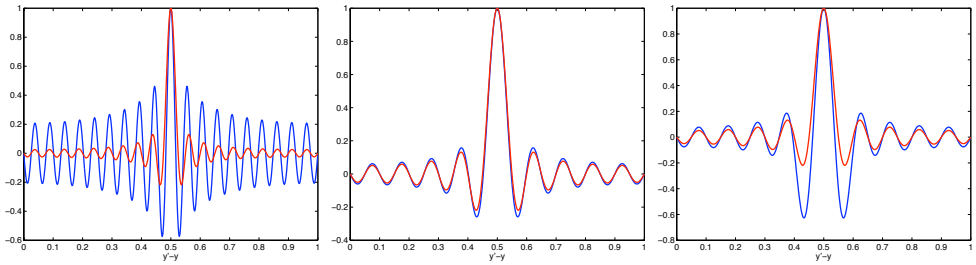

FIGURE 3. The point spread functions $\Psi_o^{\rm TR}(y,y')$ (in blue) and $\Psi^{\rm TR}(y,y')$ (in red). From left to right: full aperture and $N_T = N$; full aperture and $N_T = N/2$; 5% aperture and $N_T = N/2$. Each plot is normalized to have a maximum equal to one.

8.1.2. The point spread function in ideal waveguides. — Because of the large phases in the integral of the expression (8.10) of the point spread function, we see that only the terms $j' = j$ contribute. We obtain that

$$\Psi_o^{\rm TR}(y',y) \approx \frac{f(0)}{4} \sum_{j=1}^{N} \mathfrak{M}_{jj} \frac{\phi_j(y)\phi_j(y')}{\beta_j^2(\omega_o)} \chi\left(\frac{\beta_j'(\omega_o) Z_{\mathcal{A}}}{T}\right), \tag{8.23}$$

and even simpler,

$$\Psi_o^{\rm TR}(y',y) \sim \sum_{j=1}^{N_T} \mathfrak{M}_{jj} \frac{\phi_j(y)\phi_j(y')}{\beta_j^2(\omega_o)}, \tag{8.24}$$

where N_T is the number of modes that arrive in the recording window.

To illustrate the difference between $\Psi_o^{\rm TR}$ and $\mathbb{E}[\Psi^{\rm TR}]$, we plot in Figure 3 the right hand sides of equations (8.24) and (8.19), for a waveguide with $N = 40$ propagating modes, and an array with aperture

$$\mathcal{A} = [0, |\mathcal{A}|],$$

so that

$$\mathfrak{M}_{jj} = \int_0^{|\mathcal{A}|} dy\, \phi_j^2(y) = \frac{|\mathcal{A}|}{\mathfrak{D}} \left[1 - \operatorname{sinc}\left(\frac{2\pi j |\mathcal{A}|}{\mathfrak{D}}\right)\right].$$

The left plot is for $N_T = N$ and for $|\mathcal{A}| = \mathfrak{D}$. We see that both functions peak at $y = y'$, but $\Psi_o^{\rm TR}$ has large sidelobes. This is because of the weights β_j^{-2} in (8.24) that are very large when $j = N$. The middle plot is again for a full aperture, but with $N_T = N/2$. Here the weights are comparable for all the recorded modes, and the point spread functions look similar. The resolution is about half of that in the left plot. The right plot is for $N_T = N/2$ and an aperture equal to 5% of the waveguide depth, $|\mathcal{A}| = 0.05\mathfrak{D}$. We note that the point spread function $\Psi_o^{\rm TR}$ is affected by the partial aperture, it has large sidelobes.

9. Imaging

The goal of the imaging process is to transform the data $p_{\mathcal{A}}(t, y)$ into a function $\mathcal{J}(y, Z)$ that has two properties:

- $\mathcal{J}(y, Z)$ is large when (y, Z) is in the support of the unknown source, and small otherwise. This allows us to estimate the location of the source from the peaks of $\mathcal{J}(y, Z)$ in the search domain.
- $\mathcal{J}(y, Z)$ is statistically stable in the vicinity of its peaks

  $$\mathbb{E}[\mathcal{J}(y, Z)] \approx \mathcal{J}(y, Z).$$

  This gives robust estimates of the source location.

A typical coherent imaging method forms $\mathcal{J}(y, Z)$ by superposing the recordings $p_{\mathcal{A}}$ over the array aperture, after synchronizing them relative to the search points (y, Z). The synchronization uses a mathematical model of wave propagation to relate the search points to arrival times of the waves at the array. In waveguides the synchronization is tricky, because the modes travel at different group speeds and the signal is affected by dispersion. The best way to do it, is to backpropagate the time reversed recordings in our model of the waveguide. The synthetic backpropagation is done analytically or numerically, and it is mathematically equivalent to that in time reversal if we have perfect knowledge of the waveguide. This is not possible in random waveguides. Thus, we backpropagate in a surrogate waveguide with straight boundaries and constant wave speed c_o.

We analyze coherent imaging in section 9.1. We show that it can work for broadband sources if we complement it with a low order mode pass filter. That is to say, if we keep only the modes with scattering mean free path $\mathcal{S}_j > Z_{\mathcal{A}}$. This is possible in waveguides with random boundaries, but not in those with random inhomogeneities, where $\mathcal{S}_j$ is very small for all the modes. The array data in such waveguides is basically incoherent.

A natural idea for imaging at long ranges is to work with cross-correlations of the data. It has been exploited successfully in a variety of contexts, and we describe in section 9.2 how it can be implemented for our problem.

To illustrate the points, we refer to numerical results described in in section 10.

9.1. Coherent imaging. — Recall from section 8 the amplitudes of the emerging backward wave at the array

$$b_j(\omega, Z_{\mathcal{A}}) = \frac{e^{i\beta_j(\omega)\frac{Z_{\mathcal{A}}}{\varepsilon^2}}}{2i\beta_j(\omega)} \int_0^{\mathfrak{D}} dy\, \widehat{p}^{\,\mathrm{TR}}_{\mathcal{A}}(\omega, y)\, \phi_j(y).$$

We use them as initial conditions for the wave equation in the surrogate ideal waveguide, and obtain the following model of the backpropagated wave field

$$\mathcal{O}\left(t, y, \frac{Z}{\varepsilon^2}\right) \approx \sum_{j=1}^{N} \phi_j(y) \int_{-\infty}^{\infty} \frac{d\omega}{2\pi}\, b_j(\omega, Z_{\mathcal{A}}) e^{-i\beta_j(\omega)\frac{Z}{\varepsilon^2} - i\omega t}. \tag{9.1}$$

Similar to what we did for time reversal, we define the imaging function by

$$\mathcal{J}(y, Z) = \mathcal{O}\left(t = \frac{T}{\varepsilon^2}, y, \frac{Z}{\varepsilon^2}\right). \tag{9.2}$$

If the coherent imaging method is to be useful, we expect it to work best in broadband regimes. Recall that the waves decorrelate over frequency offsets of order ε^2, so the broadband should help with the statistical stability. We consider henceforth the broadband regime defined by (2.19). We also take for simplicity an array with full aperture, where the coupling matrix $\mathfrak{M}$ equals the identity.

We obtain from definitions (9.1)-(9.2) and the expression of $\widehat{p}^{\,\mathrm{TR}}_{\mathcal{A}}$ that

$$\mathcal{J}_{\mathrm{F}}(y, Z) = \int_0^{\mathfrak{D}} \frac{dy'}{\Delta_y} \rho\left(\frac{y' - y^\star}{\Delta_y}\right) \Psi_{\mathrm{F}}(y, y', Z), \tag{9.3}$$

where the index F reminds us that we have full aperture and Ψ_{F} is the point spread function

$$\begin{aligned} \Psi_{\mathrm{F}}(y, y', Z) = &\sum_{j,l=1}^{N} \frac{\phi_l(y')\phi_j(y)}{4\beta_j(\omega_o)\beta_l(\omega_o)} e^{-i\beta_j(\omega_o)\frac{Z}{\varepsilon^2}} \\ &\times \int_{-\infty}^{\infty} \frac{dw}{2\pi\Omega_{\mathcal{B}}}\, \overline{\widehat{f}}\left(\frac{w}{\Omega_{\mathcal{B}}}\right) e^{-iw\beta_j'(\omega_o)\frac{Z}{\varepsilon} - iw^2\beta_j''(\omega_o)\frac{Z}{2}} \\ &\times \int_{-\infty}^{\infty} \frac{du}{2\pi}\, \overline{\widehat{\chi}}(u)\, e^{iu\beta_j'(\omega_o)\frac{Z_{\mathcal{A}}}{T}} \overline{\mathbb{P}^{\varepsilon,(a)}_{jl}}\left(\omega_o + \varepsilon w - \frac{\varepsilon^2 u}{T}, Z_{\mathcal{A}}\right). \end{aligned} \tag{9.4}$$

We analyze next its mean and variance.

9.1.1. The mean point spread function for full aperture arrays. — We take the expectation of (9.4) and use the moment formula (6.23) to obtain

$$\begin{aligned} \mathbb{E}\left[\Psi_{\mathrm{F}}(y, y', Z)\right] \approx &\sum_{j=1}^{N} \frac{\phi_j(y')\phi_j(y)}{4\beta_j^2(\omega_o)} e^{-i\beta_j(\omega_o)\frac{Z}{\varepsilon^2} - \frac{Z_{\mathcal{A}}}{\mathcal{S}_j(\omega_o)} - i\frac{Z_{\mathcal{A}}}{\zeta_j(\omega_o)}} \chi\left(\frac{\beta_j'(\omega_o) Z_{\mathcal{A}}}{T}\right) \\ &\times \int_{-\infty}^{\infty} \frac{dw}{2\pi\Omega_{\mathcal{B}}}\, \overline{\widehat{f}}\left(\frac{w}{\Omega_{\mathcal{B}}}\right) e^{-iw\beta_j'(\omega_o)\frac{Z}{\varepsilon} - iw^2\beta_j''(\omega_o)\frac{Z}{2}}. \end{aligned} \tag{9.5}$$

Range focusing: Because the signal f has $O(1)$ support, it is clear that (9.9) is large only when $Z = O(\varepsilon)$. From this argument we expect the range resolution

$$z = \frac{Z}{\varepsilon^2} \sim \frac{c_o}{\varepsilon\Omega_B} = \frac{c_o}{\mathcal{B}}. \tag{9.6}$$

But in (9.9) we also sum over terms that oscillate rapidly due to the large phase $\beta_j Z/\varepsilon^2$. If enough modes contribute to the sum, the range resolution improves to $Z = O(\varepsilon^2)$, i.e.,

$$z = \frac{Z}{\varepsilon^2} \sim \lambda_o. \tag{9.7}$$

The recording window captures $N_T \leq N$ modes, but the contribution of each mode is weighted by $\exp(-Z_{\mathcal{A}}/\mathcal{S}_j)$. Suppose that $Z_{\mathcal{A}} < \mathcal{S}_j$ for $j = 1, \ldots, N_{\mathcal{S}} \leq N$. Then, the number of modes that contribute to the sum in (9.9) is

$$\mathfrak{N} = \min\{N_T, N_{\mathcal{S}}\}. \tag{9.8}$$

We need a large enough $\mathfrak{N}$ to get the improved range resolution (9.7).

Cross-range focusing: Let us evaluate the mean point spread function at the range $Z = 0$ of the source, and obtain

$$\mathbb{E}\left[\Psi_{\mathrm{F}}(y, y', 0)\right] \approx \frac{f(0)}{4} \sum_{j=1}^{N_T} \frac{\phi_j(y')\phi_j(y)}{\beta_j^2(\omega_o)} \exp\left\{-\frac{Z_{\mathcal{A}}}{\mathcal{S}_j(\omega_o)} - i\frac{Z_{\mathcal{A}}}{\zeta_j(\omega_o)}\right\}. \tag{9.9}$$

This is similar to the time reversal point spread function (8.12) in ideal waveguides, but the mode contributions have phase modulations on the range scale ζ_j, and exponentially decaying weights on the scale $\mathcal{S}_j$. In regimes with

$$\zeta_j(\omega_o) \sim \mathcal{S}_j(\omega_o) > Z_{\mathcal{A}}, \quad j = 1, \ldots, \mathfrak{N},$$

the behavior of (9.9) is similar to that of $\Psi^{\mathrm{TR}}_{o,\mathrm{F}}$ with $N_T = \mathfrak{N}$. See the middle plot in Figure (3) for an example of the point spread function. The phase modulation plays a role when

$$\zeta_j(\omega_o) < Z_{\mathcal{A}} < \mathcal{S}_j(\omega_o), \quad j = 1, \ldots, \mathfrak{N}.$$

The point spread function may not be focused at $y = y'$ unless we weight optimally the modes. That is to say, instead of backpropagating like in (9.1), we can multiply each mode amplitude b_j by a weight to be determined with optimization, given a figure of merit that measures the quality of the image.

9.1.2. Statistical stability of the point spread function. — The mean point spread function is focused at $y = y'$ and $Z = 0$, but the imaging method is useful only if the SNR at the peak is large, where

$$\mathrm{SNR} = \frac{\left|\mathbb{E}\left[\Psi_F(y, y, 0)\right]\right|}{\left\{\mathbb{E}\left[\left|\Psi_{\mathrm{F}}(y, y, 0)\right|^2\right] - \left|\mathbb{E}\left[\Psi_{\mathrm{F}}(y, y, 0)\right]\right|^2\right\}^{1/2}}.$$

The variance is

$$\begin{aligned}\text{var}\left[\Psi_{\rm F}(y,y,0)\right] \approx \sum_{j,l,j',l'=1}^{N} & \frac{\phi_j(y)\phi_l(y)\phi_{j'}(y)\phi_{l'}(y)}{16\beta_j(\omega_o)\beta_l(\omega_o)\beta_{j'}(\omega_o)\beta_{l'}(\omega_o)} \int_{-\infty}^{\infty}\frac{du}{2\pi}\int_{-\infty}^{\infty}\frac{du'}{2\pi}\widehat{\chi}(u')\overline{\widehat{\chi}}(u) \\ & \times e^{i[u\beta_j'(\omega_o)-u'\beta_{j'}'(\omega_o)]\frac{Z_{\mathcal{A}}}{T}}\int_{-\infty}^{\infty}\frac{dw}{2\pi\Omega_{\mathcal{B}}}\int_{-\infty}^{\infty}\frac{dw'}{2\pi\Omega_{\mathcal{B}}}\overline{\widehat{f}}\left(\frac{w}{\Omega_{\mathcal{B}}}\right)\widehat{f}\left(\frac{w'}{\Omega_{\mathcal{B}}}\right) \\ & \times\Bigg\{\mathbb{E}\left[\mathbb{P}_{jl}^{\varepsilon,(a)}\left(\omega_o+\varepsilon w'-\frac{\varepsilon^2u'}{T},Z_{\mathcal{A}}\right)\overline{\mathbb{P}_{j'l'}^{\varepsilon,(a)}}\left(\omega_o+\varepsilon w-\frac{\varepsilon^2u}{T},Z_{\mathcal{A}}\right)\right] \\ & -\delta_{jl}\delta_{j'l'}e^{-Z_{\mathcal{A}}\left[\frac{1}{\overline{s}_{j'}(\omega_o)}+\frac{1}{\overline{s}_j(\omega_o)}\right]+iZ_{\mathcal{A}}\left[\frac{1}{\zeta_{j'}(\omega_o)}-\frac{1}{\zeta_j(\omega_o)}\right]}\Bigg\}, \end{aligned} \tag{9.10}$$

where we used the expectations (6.23). We know that the propagator decorrelates for frequency offsets that exceed $O(\varepsilon^2)$. Thus, only the frequencies satisfying $|w-w'| = O(\varepsilon)$ contribute in (9.10), and we let

$$w-w' = \varepsilon\widetilde{w}, \quad |\widetilde{w}| \le \widetilde{\Omega} = O(1).$$

Using the second moments (6.25), and the expression (6.36) of the Wigner transform, we obtain that the variance is given by the sum of two terms

$$\text{var}\left[\Psi_{\rm F}(y,y,0)\right] \approx \mathfrak{T}_1 + \mathfrak{T}_2. \tag{9.11}$$

The first term is determined by the continuous density of the Wigner transform,

$$\begin{aligned}\mathfrak{T}_1 = \frac{\varepsilon\widetilde{\Omega}\|f\|^2}{16\pi\Omega_{\mathcal{B}}}\sum_{j,l=1}^{N}\frac{\phi_j^2(y)\phi_l^2(y)}{\beta_j^2(\omega_o)\beta_l^2(\omega_o)}\int_{-\infty}^{\infty}\chi^2\left(\frac{\tau}{T}\right)W_j^{(l)}(\omega_o,\tau,Z_{\mathcal{A}}) \\ \times\,\text{sinc}\left\{\widetilde{\Omega}\left[\beta_j'(\omega_o)Z_{\mathcal{A}}-\tau\right]\right\}.\end{aligned} \tag{9.12}$$

Here we let

$$\|f\|^2 = \int_{-\infty}^{\infty}\frac{du}{2\pi}|\widehat{f}(u)|^2,$$

and obtained the right hand side in (9.12) after standard manipulations. The second term is due to the diagonal (coherent) terms that decay exponentially with range,

$$\begin{aligned}\mathfrak{T}_2 = \frac{\varepsilon\widetilde{\Omega}\|f\|^2}{32\pi\Omega_{\mathcal{B}}}\sum_{j,l=1}^{N}\frac{\phi_j^2(y)\phi_l^2(y)}{\beta_j^2(\omega_o)\beta_l^2(\omega_o)}\chi\left(\frac{\beta_j'(\omega_o)Z_{\mathcal{A}}}{T}\right)\chi\left(\frac{\beta_l'(\omega_o)Z_{\mathcal{A}}}{T}\right) \\ \times\Big\{(1-\delta_{j,l})e^{-\frac{Z_{\mathcal{A}}}{\overline{s}_{j'}(\omega_o)}-\frac{Z_{\mathcal{A}}}{\overline{s}_j(\omega_o)}+i\left[\frac{Z_{\mathcal{A}}}{\zeta_{j'}(\omega_o)}-\frac{Z_{\mathcal{A}}}{\zeta_j(\omega_o)}\right]}\left[e^{\Gamma_{jl}(\omega_o)Z_{\mathcal{A}}}-1\right] \\ +\delta_{j,l}\left[e^{-\frac{2Z_{\mathcal{A}}}{\mathcal{S}_j^{\mathcal{P}}(\omega_o)}}-e^{-\frac{2Z_{\mathcal{A}}}{\overline{s}_j(\omega_o)}}\right]\Big\}.\end{aligned} \tag{9.13}$$

The second term dominates the first at shorter ranges, but as $Z_{\mathcal{A}}$ increases, the first term becomes the larger one. In any case, we can see that the variance is proportional

to εN_T, if $N_T \ll N$. The integral of the Wigner transform is close to the identity matrix for smaller ranges, but it becomes a full matrix with entries of order $1/N$ as we approach the equipartition regime. Only the modes that arrive in the support of the measurement window contribute to the sums in (9.12) and (9.13), and we have $\beta_j \sim k$ if $N_T \ll N$. The variance is larger for $N_T \sim N$.

The peak value of the mean point spread function is of the order of the first term in (9.9), and the SNR estimate is

$$\text{SNR} \sim \frac{\varepsilon^{-1/2}\mathfrak{N}}{\sqrt{N_T}} e^{-\frac{Z_{\mathcal{A}}}{\mathcal{S}_1(\omega_o)}}, \tag{9.14}$$

where we assumed

$$\mathcal{S}_j(\omega_o) \sim \mathcal{S}_1(\omega_o), \quad j = 1, \ldots, \mathfrak{N}.$$

It shows that the imaging method is useless if $Z_{\mathcal{A}} > \mathcal{S}_1$. Coherent imaging works only when $Z_{\mathcal{A}} < \mathcal{S}_j$ for $j = 1, \ldots, N_{\mathcal{S}}$, and $N_{\mathcal{S}}$ sufficiently large. The number $\mathfrak{N} = \min\{N_T, N_{\mathcal{S}}\}$ of coherent modes that contribute in the point spread function determines its resolution. The SNR decreases with N_T, so we should have $N_T \approx \mathfrak{N}$. The quality of the image may be improved by weighting the contribution of the modes. The weights can be determined by optimizing a measure of quality of the image.

9.2. Imaging with cross-correlations. — The idea of imaging with cross-correlations of the data has been used successfully in the coherent interferometric (CINT) imaging approach introduced and analyzed in [**7, 8, 5**]. The point is that when net scattering is significant, it is better to work with the square of the wave field, i.e., with the energy resolved locally in time and over directions of arrival. Because the second moments of the mode amplitudes do not tend to zero as the range increases, we can obtain statistically stable imaging methods when we backpropagate the cross-correlations of the recordings $p_{\mathcal{A}}(t, y)$.

Let us write the data projected on the span of the eigenfunctions

$$\widehat{D}_j(\omega) = \int_0^{\mathfrak{D}} dy\, \widehat{p}_{\mathcal{A}}(\omega, y)\phi_j(y),$$

for frequencies $\omega = \omega_o + \varepsilon w$ and $|w| \leq \pi\Omega_{\mathcal{B}}$. We assume for simplicity that the array has full aperture, and obtain from (7.7) that

$$\begin{aligned}\widehat{D}_j(\omega) \approx \int_0^{\mathfrak{D}} \frac{dy}{\Delta_y} \rho\left(\frac{y - y^\star}{\Delta_y}\right) \frac{1}{\varepsilon\Omega_{\mathcal{B}}} \widehat{f}\left(\frac{w}{\Omega_{\mathcal{B}}}\right) \widehat{\mathfrak{d}}_j\left(\frac{w}{\Omega_{\mathcal{B}}}\right) e^{i\beta_j(\omega_o)\frac{Z_{\mathcal{A}}}{\varepsilon^2} + iw\beta_j'(\omega_o)\frac{Z_{\mathcal{A}}}{\varepsilon}} \\ \times \int_{-\infty}^{\infty} \frac{du}{2\pi} \widehat{\chi}(u)\, e^{-i\beta_j'(\omega_o)\frac{uZ_{\mathcal{A}}}{T}} \sum_{l=1}^{N} \frac{\phi_l(y)}{2i\beta_l(\omega_o)} \mathbb{P}_{jl}^{\varepsilon,(a)}\left(\omega_o + \varepsilon w - \frac{\varepsilon^2 u}{T}, Z_{\mathcal{A}}\right).\end{aligned} \tag{9.15}$$

We wish to image by backpropagating the mode dependent energy resolved locally in time

$$\mathfrak{E}_j(\tau) = \int_{-\infty}^{\infty} \frac{d\omega}{2\pi} \int_{-\infty}^{\infty} \frac{d(\varepsilon\widetilde{w})}{2\pi} \widehat{D}_j\left(\omega + \varepsilon^2 \frac{\widetilde{w}}{2}\right) \overline{\widehat{D}_j}\left(\omega - \varepsilon^2 \frac{\widetilde{w}}{2}\right) e^{-i\widetilde{w}\tau}. \tag{9.16}$$

Here we scale the offset $\widetilde{w}$ by ε because we know that the propagator decorrelates over frequency intervals exceeding ε^2. We saw that the modes decorrelate due to scattering, so we consider one mode at a time. This implies that we work with waves traveling in the same direction.

To understand how to extract the source location from (9.16), we calculate its expectation. We rewrite (9.16) as

$$\mathfrak{E}_j(\tau) \approx \int_0^{\mathfrak{D}} \frac{dy}{\Delta_y} \rho\left(\frac{y - y^\star}{\Delta_y}\right) \int_0^{\mathfrak{D}} \frac{dy'}{\Delta_y} \rho\left(\frac{y' - y^\star}{\Delta_y}\right) \Psi_j(y, y', \tau), \tag{9.17}$$

with kernel Ψ_j following obviously from (9.15). Its expectation is given by

$$\mathbb{E}\left[\Psi_j(y, y', \tau)\right] \approx \frac{\|f\|^2}{4\Omega_{\mathcal{B}}} \chi^2\left(\frac{\beta_j'(\omega_o) Z_{\mathcal{A}}}{T}\right) \sum_{l=1}^{N} \frac{\phi_l(y)\phi_l(y')}{\beta_l^2(\omega_o)} \mathcal{W}_j^{(l)}\left(\omega_o, \tau, Z_{\mathcal{A}}\right), \tag{9.18}$$

where we used the second moments (6.25).

Because we are in the broadband regime and the waves decorrelate over frequency offsets of order ε^2, the variance of $\mathfrak{E}_j(\tau)$ is small in the vicinity of its peak. Thus, we can analyze the imaging method by looking at the expectation of the kernel.

9.2.1. Range estimation. — The information about the range of the source is encoded in the τ peak location of the right hand side in (9.18). The problem is that we do not know the transport speed of $\mathcal{W}_j^{(l)}$. It is not the same as the mode group speed $\beta_j'(\omega_o)$, unless $Z_{\mathcal{A}}$ is smaller than the transport mean free path $\mathcal{S}_j^{\mathcal{P}}$. We are interested in longer ranges, where coherent imaging does not work. Recall from the discussion in section 8.1.1 that in the very long range limit, beyond the equipartition distance, the transport speed is $\langle\beta'\rangle$, the average of the mode group speeds. But we already know that we cannot image beyond the equipartition distance, because the waves forget the initial conditions. The interesting regime for imaging is

$$\mathcal{S}_j^{\mathcal{P}}(\omega_o) < Z_{\mathcal{A}} < \mathcal{S}^E(\omega_o),$$

where the speed needs to be estimated from the transport equations (6.28).

The matrix $\Gamma^{(c)}$ of coefficients in the transport equations is determined by the power spectral density of the autocorrelation of the fluctuations, evaluated at differences of the wave numbers. If we know the autocorrelation, i.e., $\Gamma^{(c)}$, we can relate the τ peak location of $\mathfrak{E}_j(\tau)$ to the range of the source. If we do not know it, we can try to estimate both the source range and the autocorrelation of the fluctuations. This was proposed and analyzed in [**22, 6**] for a point source, i.e., $\Delta_y \ll \mathfrak{D}$, where (9.16) and

(9.19) give

$$\begin{aligned}\mathbb{E}\left[\mathfrak{E}_j(\tau)\right] &\approx \mathbb{E}\left[\Psi_j(y^\star, y^\star, \tau)\right] \\ &\approx \frac{\|f\|^2}{4\Omega_{\mathcal{B}}}\chi^2\left(\frac{\beta_j'(\omega_o)Z_{\mathcal{A}}}{T}\right)\sum_{l=1}^{N}\frac{\phi_l^2(y^\star)}{\beta_l^2(\omega_o)}\mathcal{W}_j^{(l)}\left(\omega_o, \tau, Z_{\mathcal{A}}\right). \end{aligned} \tag{9.19}$$

We do not know the weights $\phi_l^2(y^\star)$, because we do not know $y^\star$. However, we are interested only in the τ peak location of this expression, which is not really affected by the weights. The estimation in [**22, 6**] computes

$$\mathcal{E}_j(t) = \frac{\mathfrak{E}_j\left[t + \beta_j'(\omega_o)(Z_{\mathcal{A}} - Z)\right]}{\max_\tau |\mathfrak{E}_j(\tau)|}, \tag{9.20}$$

and compares it with

$$\mathcal{E}_{j,M}(t) = \frac{\mathfrak{E}_{j,M}\left[t + \beta_j'(\omega_o)(Z_{\mathcal{A}} - Z)\right]}{\max_\tau |\mathfrak{E}_{j,M}(\tau)|}, \tag{9.21}$$

for a search range offset Z of the source. The offset by the deterministic travel time $\beta_j'(Z_{\mathcal{A}} - Z)$ allows us to observe the deviation from zero of the t peak location of $\mathcal{E}_j(t)$. The search model $\mathfrak{E}_{j,M}(\tau)$ is given by

$$\mathfrak{E}_{j,M}(\tau) = \sum_{l=1}^{N}\frac{1}{\beta_l^2(\omega_o)}\mathcal{W}_{j,M}^{(l)}\left(\omega_o, \tau, Z_{\mathcal{A}}\right), \tag{9.22}$$

and the Wigner transform $\mathcal{W}_{j,M}^{(l)}$ solves the transport equations (6.28), with the model matrix of coefficients $\Gamma_M^{(c)}$.

We compute $\Gamma_M^{(c)}$ using definition (4.78) for waveguides with random boundaries and (5.9) for waveguides with internal inhomogeneities. These definitions require a model of the correlation $\mathcal{R}_\mu(z)$ or $\mathcal{R}_\nu(y, z)$ of the fluctuations. If we know the model, we should use it. If not, it turns out that the estimation is quite robust with respect to the model. In [**22, 6**] we considered waveguides with interior inhomogeneities and used the correlation

$$\mathcal{R}_\nu(y, z) = \mathcal{R}\left(\frac{y}{\ell}, \frac{z}{\ell}\right),$$

with different choices of $\mathcal{R}$. The correlation length ℓ is determined at the same time as the range of the source. The results show that the range estimation is independent of the particular choice of $\mathcal{R}$. We refer to section 10 for an illustration with numerical simulations. More detailed simulations are in [**22, 6**].

9.2.2. Cross-range estimation. — Once we have estimated the range of the source and the model $\Gamma_M^{(c)}$, we can seek the cross-range. Take for example the integral over τ in (9.17) and use that

$$\widehat{\mathcal{W}}_j^{(l)}(\omega_o, 0, Z_{\mathcal{A}}) = \int_{-\infty}^{\infty} d\tau \mathcal{W}_j^{(l)}(\omega_o, \tau, Z_{\mathcal{A}}) = \mathbf{e}_j \cdot e^{\Gamma^{(c)}(\omega_o)Z_{\mathcal{A}}}\mathbf{e}_l, \tag{9.23}$$

to obtain

$$\int d\tau\, \mathbb{E}[\Psi_j(y,y',\tau)] \sim \sum_{l=1}^{N} \frac{\phi_l(y)\phi_l(y')}{\beta_l^2(\omega_o)}\, \mathbf{e}_j \cdot e^{\Gamma^{(c)}(\omega_o) Z_{\mathcal{A}}} \mathbf{e}_l, \quad j = 1, \ldots, N_T. \tag{9.24}$$

Here we let $\sim$ denoting approximate up to a multiplicative constant, as before, and we take into account the finite size of the recording window by limiting the mode index $j \leq N_T$.

We know that (9.23) becomes independent of l when $Z_{\mathcal{A}}$ approaches the equipartition distance, so we can write

$$\int d\tau\, \mathbb{E}[\mathfrak{E}_j(\tau)] \sim \sum_{l=1}^{N} \frac{\phi_l(y)\phi_l(y')}{\beta_l^2(\omega_o)}, \quad Z_{\mathcal{A}} \gtrsim \mathcal{S}^E. \tag{9.25}$$

This is like the time reversal point spread function $\Psi^{\rm TR}_{o,\rm F}$ in ideal waveguides, and it peaks at $y \approx y'$. Therefore, we get that

$$\int d\tau\, \mathbb{E}[\mathfrak{E}_j(\tau)] \sim \int_0^{\mathfrak{D}} \int_0^{\mathfrak{D}} \frac{dy}{\Delta_y} \rho\left(\frac{y-y^\star}{\Delta_y}\right) \int_0^{\mathfrak{D}} \frac{dy'}{\Delta_y} \rho\left(\frac{y'-y^\star}{\Delta_y}\right) \Psi^{\rm TR}_{o,\rm F}(y,y'), \tag{9.26}$$

and if we have a point-like source at $y^\star$,

$$\int d\tau\, \mathbb{E}[\mathfrak{E}_j(\tau)] \sim \Psi^{\rm TR}_{o,\rm F}(y^\star, y^\star), \quad \Delta_y \ll \mathfrak{D}. \tag{9.27}$$

Obviously, this is independent on where $y^\star$ lies in $(0, \mathfrak{D})$, so we cannot estimate the source location. As we said before, in the equipartition regime the waves forget their initial conditions and imaging is no longer possible.

If $Z_{\mathcal{A}} < \mathcal{S}^E$, we can estimate the source location from the kernel (9.24), by comparing it with its mathematical model

$$\sum_{l=1}^{N} \frac{\phi_l^2(y)}{\beta_l^2(\omega_o)}\, \mathbf{e}_j \cdot e^{\Gamma^{(c)}_M(\omega_o) Z_{\mathcal{A}}} \mathbf{e}_l, \quad j = 1, \ldots, N_T,$$

with $\Gamma^{(c)}_M$ computed previously. We refer to [**22, 6**] for more details of the cross-range estimation.

10. Numerical results

We recall a few a few numerical simulations from [**6**], for two dimensional waveguides with interior inhomogeneities. The wave field $p(t,y,z)$ is simulated by solving the wave equation in a medium with wave speed fluctuations modeled as in (5.1), and with Gaussian correlation

$$\mathcal{R}_\nu(y,z) = e^{-\frac{y^2+z^2}{2\ell^2}}.$$

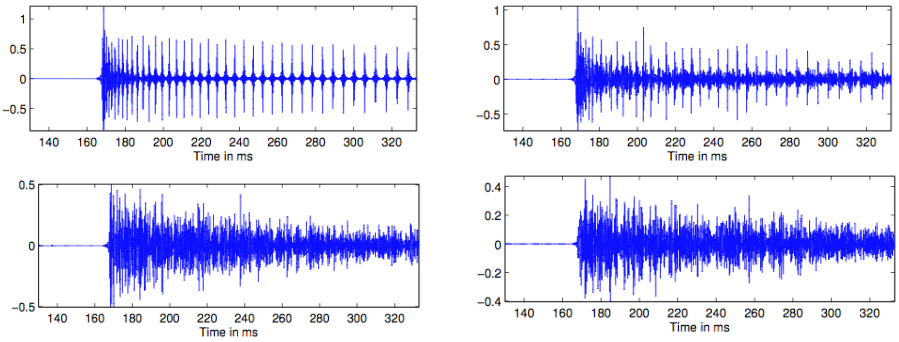

FIGURE 4. The acoustic pressure computed at the receiver location $y = \mathfrak{D}/2$ for (clockwise from top left): $\varepsilon = 0$, $\varepsilon = 1\%$, $\varepsilon = 2\%$ and $\varepsilon = 3\%$.

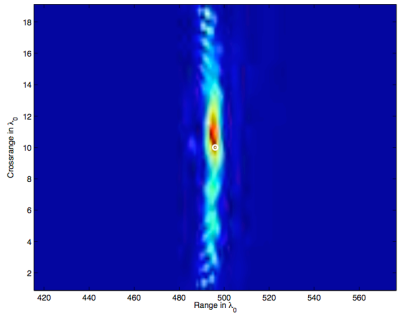

FIGURE 5. The coherent imaging function $\mathcal{J}_{\mathrm{F}}(y, z)$ for $\varepsilon = 1\%$.

We generate the process $\nu(y, z)$ numerically using random Fourier series [**10**]. The correlation length is $\ell = \lambda_o/2$ and the perturbation parameter ε ranges between[(3)] $0\% - 3\%$.

The simulations are for a point source at $y^\star = \mathfrak{D}/2$, emitting a pulse with extra wide bandwidth of $1.5 - 4.5$kHz. It is larger than the bandwidth considered in our model (2.19), but the analysis can be extended easily to this case.

The central wavelength in the simulations is $\lambda_o = 0.5$m, calculated at the constant sund speed $c_o = 1.5$km/s in water. The depth of the waveguide is $\mathfrak{D} = 20\lambda_o$, so that $N(\omega_o) = 40$. The array is at range $z_{\mathcal{A}} = 500\lambda_o$.

We plot in Figure 4 the computed signal at the receiver location $y = \mathfrak{D}/2$, for three different strengths ε of the fluctuations. We see a clean train of pulses in the ideal waveguide ($\varepsilon = 0$). The scattering effects are significant for $\varepsilon > 0$, as predicted by the theory, and the signal looks almost like noise when $\varepsilon \geq 2\%$.

[(3)] If we look carefully at the scaling in the model of the fluctuations in [**6**], we see that the increase of ε may be related to an increase in the net scattering effects in our model.

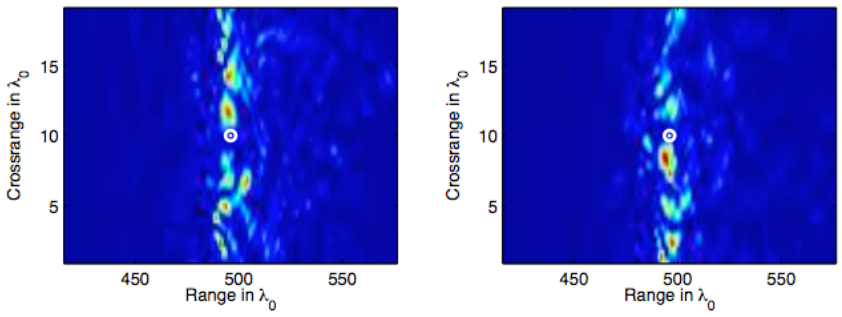

FIGURE 6. Coherent function $\mathcal{J}_{\rm F}\,(y,z)$ for $\varepsilon = 2\%$ and two realizations of the fluctuations. The true source location is shown with a white circle.

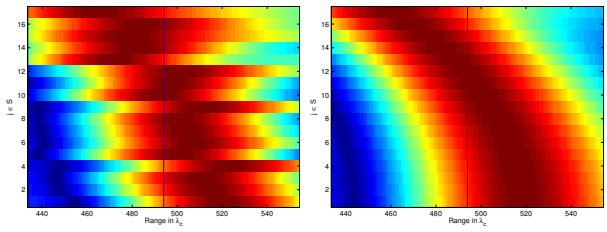

FIGURE 7. Computed $\mathcal{E}_j(t)$ and model $\mathcal{E}_M(t)$ plotted as a function of $Z_{\mathcal{A}} - t/\beta_j'$ in the abscissa and j in the ordinate. The model is computed with the true autocorrelation and source range location. Because the transport speed varies with the mode index, the peak locations change with j.

In Figures 5 and 6 we plot the coherent imaging function (9.3) for $\varepsilon = 1\%$ and 2%, respectively. The source is in the middle of the domain and the method locates it when $\varepsilon = 1\%$, because the net scattering effects are not so strong. However, we see from the results in 6 that when the scattering is stronger, the image changes unpredictably with the realization of the fluctuations of the wave speed. This is an illustration of the lack of statistical stability of the imaging function (9.4).

To illustrate the ideas of the incoherent range estimation, we plot in Figures 7 and 8 the calculated $\mathcal{E}_j(t)$ and model $\mathcal{E}_{j,M}(t)$. The model uses a Gaussian autocorrelation with correlation length that is determined in the range estimation. The calculated $\mathcal{E}_j(t)$ is noisy due to scattering and numerical error (left plot in Figure 7). But still, it compares well with the model computed with the correct correlation length and source range (right plot in Figure 7). If we have the wrong range and/or the wrong correlation, the model changes as shown in Figure 8. The location of the peaks is different.

We refer to [**6**] for many more simulations and detailed range and cross-range estimation results.

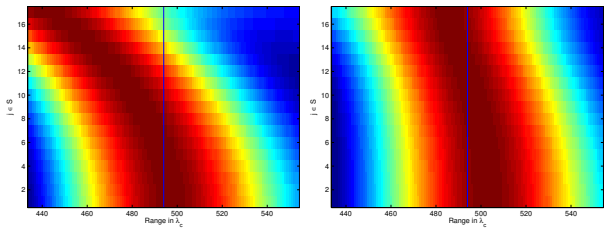

FIGURE 8. Model $\mathcal{E}_M(t)$ as a function of $Z_{\mathcal{A}} - t/\beta_j'$ in the abscissa and j in the ordinate. In the left picture we evaluate the model at the search range $Z_{\mathcal{A}} - 20\lambda_o$ and in the right picture we use a correlation length that is half the true one.

Acknowledgments

These lecture notes describe results obtained in collaboration with: Ricardo Alonso and Josselin Garnier for wave propagation in waveguides with random boundaries [**1**], Leila Issa for the incoherent imaging algorithm based on a model of transport of energy in waveguides [**22, 6**], and Chrysoula Tsogka for the numerical simulations of wave propagation in [**6**]. We also use extensively the studies [**19, 11, 15**].

The work of L. Borcea was partially supported by the AFSOR Grant FA9550-12-1-0117, the ONR Grant N00014-12-1-0256, and by the NSF Grants DMS-0907746, DMS-0934594.

References

[1] R. Alonso, L. Borcea, and J. Garnier. Wave propagation in waveguides with random boundaries. *Commun. Math. Sci.*, 11:233–267, 2012.

[2] G. Bal and L. Ryzhik. Time reversal and refocusing in random media. *SIAM Journal on Applied Mathematics*, 63(5):1475–1498, 2003.

[3] P. Blomgren, G. Papanicolaou, and H. Zhao. Super-resolution in time-reversal acoustics. *Journal of the Acoustical Society of America*, 111:230, 2002.

[4] L. Borcea and J. Garnier. Paraxial coupling of propagating modes in three-dimensional waveguides with random boundaries. *arXiv preprint arXiv:1211.0468*, 2012.

[5] L. Borcea, J. Garnier, G. Papanicolaou, and C. Tsogka. Enhanced statistical stability in coherent interferometric imaging. *Inverse Problems*, 27:085003, 2011.

[6] L. Borcea, L. Issa, and C. Tsogka. Source localization in random acoustic waveguides. *SIAM Multiscale Modeling Simulations*, 8:1981–2022, 2010.

[7] L. Borcea, G. Papanicolaou, and C. Tsogka. Interferometric array imaging in clutter. *Inverse Problems*, 21:1419–1460, 2005.

[8] L. Borcea, G. Papanicolaou, and C. Tsogka. Adaptive interferometric imaging in clutter and optimal illumination. *Inverse Problems*, 22:1405–1436, 2006.

[9] M. Born and E. Wolf. *Principles of optics: Electromagnetic theory of propagation, interference and diffraction of light*. Cambridge University Press, 7 edition, 1999.

[10] L. Devroye. *Non-uniform random variate generation*. Springer, 1986.

[11] L. B. Dozier and F. D. Tappert. Statistics of normal mode amplitudes in a random ocean. *Journal of the Acoustical Society of America*, 63:533–547, 1978.

[12] M. Fink. Time reversed acoustics. *Physics Today*, 50:34, 1997.

[13] M. Fink. Time-reversed acoustics. *Scientific American*, 281(5):91–97, 1999.

[14] S. M. Flatté and F. D. Tappert. Calculation of the effect of internal waves on oceanic sound transmission. *Journal of the Acoustical Society of America*, 58:1151, 1975.

[15] J.P. Fouque, J. Garnier, G. Papanicolaou, and K. Sølna. *Wave propagation and time reversal in randomly layered media*. Springer, New York, 2007.

[16] J. Garnier and K. Sølna. Effective transport equations and enhanced backscattering in random waveguides. *SIAM J. Appl. Math.*, 68:1574–1599, 2008.

[17] C. Gomez. Wave propagation in shallow-water acoustic random waveguides. *Commun. Math. Sci.*, 9:81–125, 2011.

[18] C. Gomez. Wave propagation in shallow-water acoustic waveguides with rough boundaries. *arXiv preprint arXiv:0911.5646 [math AP]*, 2012.

[19] W. Kohler and G. Papanicolaou. *Wave Propagation and Underwater Acoustics, J. B. Keller and J. S. Papadakis, eds.*, volume 70 of *Lecture Notes in Physics*, chapter Wave propagation in randomly inhomogeneous ocean. Springer Verlag, Berlin, 1977.

[20] W.A. Kuperman, W.S Hodkiss, H.C. Song, T. Akal, C. Ferla, and D.R. Jackson. Experimental demonstration of an acoustic time-reversal mirror. *Journal of the Acoustical Society of America*, 103:25–40, 1998.

[21] H. J. Kushner. *Approximation and weak convergence methods for random processes*. MIT Press, Cambridge, 1984.

[22] Issa L. *Source localization in cluttered acoustic waveguides*. PhD thesis, Rice University, 2010.

[23] G. Papanicolaou and W. Kohler. Asymptotic theory of mixing stochastic differential equations. *Commun. Pure Appl. Math.*, 27:641–668, 1974.

[24] G. Papanicolaou and W. Kohler. Asymptotic analysis of deterministic and stochastic equations with rapidly varying components. *Commun. Math. Phys.*, 45:217–232, 1975.

[25] G. Papanicolaou, L. Ryzhik, and K. Sølna. Self-averaging from lateral diversity in the itô-schrödinger equation. *Multiscale Modeling & Simulation*, 6(2):468–492, 2007.

[26] M.C.W. van Rossum and Th.M. Nieuwenhuizen. Multiple scattering of classical waves:microscopy, mesoscopy, and diffusion. *Rev. Mod. Phys.*, 71:313–371, 1999.

[27] J. Weidmann. *Spectral theory of ordinary differential operators*. Lecture Notes in Mathematics 1258. Springer-Verlag, Heidelberg, 1987.

Liliana Borcea, Computational and Applied Mathematics, Rice University, MS 134, Houston, TX 77005-1892 • *E-mail :* borcea@rice.edu